Automatic Control of the 30 MWe SEGS VI Parabolic Trough Plant

by

THORSTEN A. STUETZLE

A thesis submitted in partial fulfillment of
the requirements for the degree of

MASTER OF SCIENCE
(MECHANICAL ENGINEERING)

at the

UNIVERSITY OF WISCONSIN-MADISON

2002

Abstract

A solar electric generating system (SEGS) can be divided into two major subsystems (Lippke, 1995): a solar collector field and a conventional Clausius-Rankine cycle with a turbine-generator. For the 30 MWe SEGS VI Parabolic Trough Collector Plant, one task of a skilled plant operator is to maintain a specified set point of the collector outlet temperature by adjusting the volume flow rate of the heat transfer fluid circulating through the collectors. The collector outlet temperature is mainly affected by changes in the sun intensity, by the collector inlet temperature and by the volume flow rate of the heat transfer fluid. For the development of next generation SEGS plants and in order to obtain a control algorithm that approximates an operator's behaviour, a linear model predictive controller is developed for use in a plant model. The plant model, which is discussed first in this work, consists of a model for the parabolic trough collector field and a model for the power plant. The plant model's usefulness is evaluated through a comparison between predicted and measured data. The performance of the controller is evaluated on four different days in 1998. The influence of the control on the gross output of the plant is examined as well.

Acknowledgements

I am very grateful to my advisors, Professor William A. Beckman and Professor John W. Mitchell, for their guidance and encouragement of my research efforts. In addition, I would like to thank Professor Sandy Klein for his help with EES during this project.

I am grateful to Professor James B. Rawlings from the Department of Chemical Engineering who introduced me to Professor Beckman and this project when I attended his course on model predictive control.

I would like to thank Professor Heisel, Ms. Peik-Stenzel and Dr. Michaelis from the University of Stuttgart. Their efforts gave me the opportunity to study at the Department of Mechanical Engineering at the University of Wisconsin-Madison. Thanks to the German Academic Exchange Service (DAAD) for the financial support during that time. In addition, I would like to thank Professor Zeitz from the University of Stuttgart for providing great support to students of Engineering Cybernetics who are studying abroad.

The thesis work was sponsored by Sandia National Laboratories, a multi-program laboratory operated by Sandia Corporation, a Lockheed Martin Company, for the United States Department of Energy under Contract DE-AC04-94AL85000. A special thank you to Scott Jones of Sandia National Laboratories for his assistance during this project.

Many thanks to Professor Tim Shedd, Professor Greg Nellis, and the graduate students and staff of the Solar Lab for their friendship and help during my stay here.

I would like to thank the international students from the Madison 2001 mailing list for friendship and joint leisure time activities.

Finally, many thanks to my parents who could always be counted on as a source of caring and support, even from a distance of about 4000 miles.

Table of Contents

List of Figures

Chapter 1

Introduction

A solar electric generating system (SEGS), shown in Figure 1.1, refers to a class of solar energy systems that use parabolic troughs in order to produce electricity from sunlight (Pilkington, 1996).

Figure 1.1: Areal View of a SEGS Plant

The parabolic troughs are long parallel rows of curved glass mirrors focusing the sun's energy on an absorber pipe located along its focal line (Figure 1.2). These collectors track the sun by rotating around a north-south axis.

Figure 1.2: Parabolic Trough Collector of a SEGS Plant

The heat transfer fluid (HTF), an oil, is circulated through the pipes. Under normal operation the heated HTF leaves the collectors with a specified collector outlet temperature and is pumped to a central power plant area. There, the HTF is passed through several heat exchangers where its energy is transferred to the power plant's working fluid, which is water or steam (Figure 1.3). The heated steam is used in turn to drive a turbine generator to produce electricity. The facility discussed in this work is the 30 MWe SEGS VI plant, constructed in 1988 by Luz International Ltd., and is located in the Mojave desert of southern California.

A skilled operator controls the parabolic trough collector outlet temperature. One of his tasks is to maintain a specified set point for the collector outlet temperature by adjusting the volume flow rate of the HTF within upper and lower bounds. The collector outlet temperature is mainly affected by changes in the sun intensity, by the collector inlet

temperature and by the volume flow rate of the HTF. The ambient temperature and the wind speed also influence the outlet temperature but their influence is small.

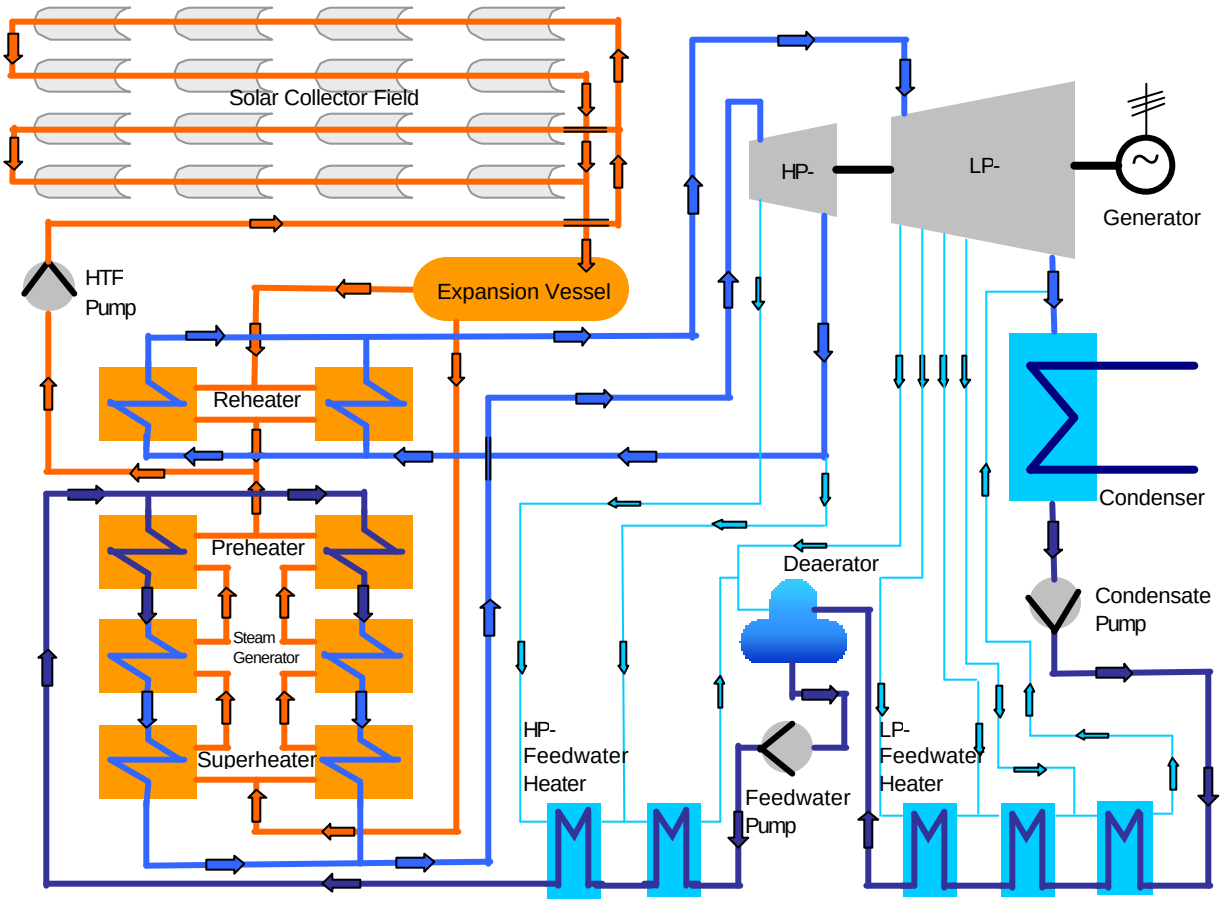

Figure 1.3: Flow Diagram of the 30 MWe SEGS VI Plant

Knowledge of the sun's daily path, observation of clouds and many years of experience and training give the operator the ability to accomplish his task. But there are limitations on the performance of a human controller. Thus, for the development of next generation SEGS plants, it is reasonable to look at automatic controls. In addition, a control algorithm that approximates an operator's behavior can be included in simulation models of SEGS plants.

Automatic control of the HTF in a parabolic trough collector through proportional control has been previously addressed (Schindwolf, 1980). In this study, a linear model predictive controller is developed for the SEGS VI plant. The essential idea behind model predictive control (MPC) is to optimize forecasts of process behavior. The forecasting is accomplished with a process model. Therefore, the model is the essential element of a MPC controller (Rawlings, 2000). The control strategy considers constraints on both the collector outlet temperature and the volume flow rate of the HTF.

In this work, the control performance is evaluated through simulations. Consequently it is very important to obtain an accurate model of the plant on which the controller can be tested.

The following three chapters deal with the modeling of the plant. From Figure 1.3, it can be seen that the plant consists of two cycles: the cycle of the HTF through the collector field, indicated by the orange color, and the power plant cycle, indicated by the blue colors. In Chapter 2, a trough collector field model is presented. In Chapter 3, a model for the power plant is proposed. Chapter 4 shows simulation results with the combined model and predicted and measured data are compared in order to evaluate the model.

Finally, in the last chapter, the model predictive control concept is introduced with a simplified plant model. The control performance is evaluated through simulations with the complex plant model from Chapter 4 and compared to the performance of a human controller. The influence of the control on the gross output of the plant is examined as well.

Chapter 2

Trough Collector Field Model

2.1 Introduction

The 30 MWe SEGS VI plant is located in the Mojave desert of southern California. The layout of the plant is shown in Figure 2.1.

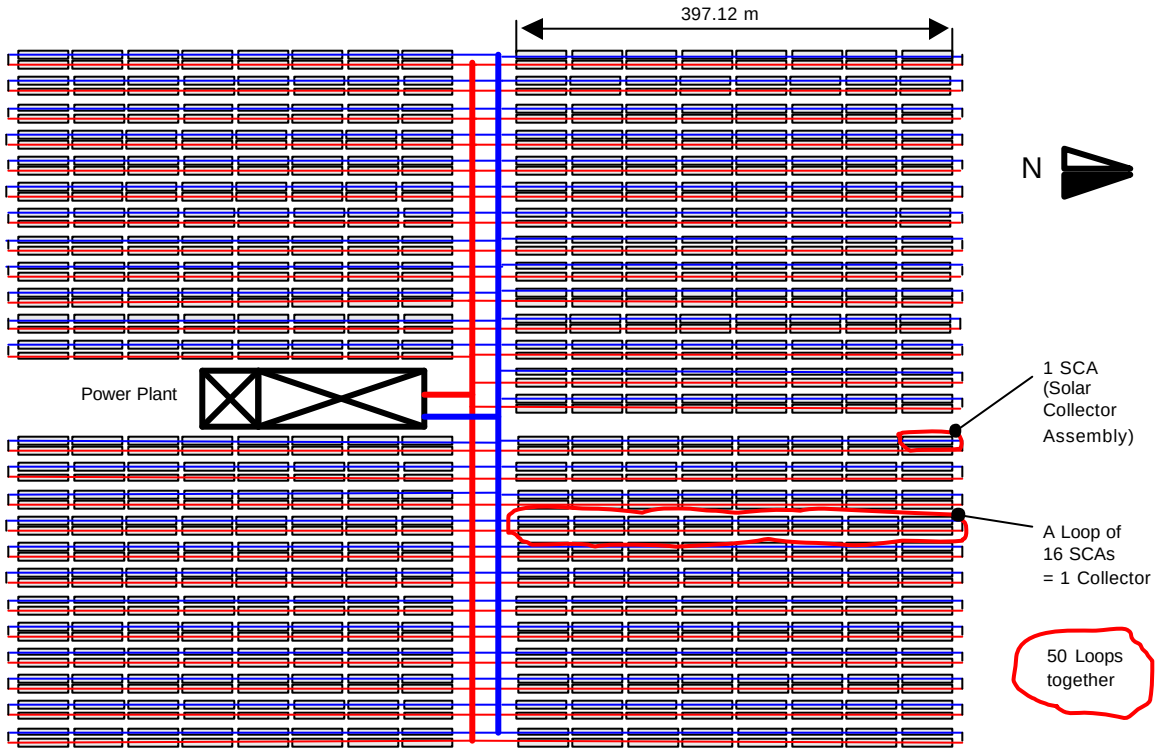

Figure 2.1: Layout of the SEGS VI plant

The Figure 2.1 shows the power plant with the solar trough collector field. The solar trough collector field can be divided into four quadrants. There are three quadrants with 12 solar trough collectors each and one quadrant with 14 solar trough collectors: for a total of 50 solar

trough collectors. One of these 50 collectors is formed by a loop of 16 solar collector assemblies (SCA). The cold heat transfer fluid (HTF) flows into the collector loop at one end, indicated by the blue color in the Figure, is heated up by the absorbed energy of the sun and leaves the collector at the other end, indicated by the red color. The hot HTF of every collector merges in a central header, which is connected to the power plant. In the power plant, the heat energy of the merged hot HTF is used to heat a working fluid, which is water or steam. After transferring its thermal energy to the power plant, the cold HTF leaves the power plant in a central header that feeds the 50 collectors in the field with the cold fluid. There are flow balance valves between the collector loops and the headers. The total length of one collector is two times 397.12 m. The collectors are single-axis tracking and aligned on a north-south line, thus tracking the sun from east to west.

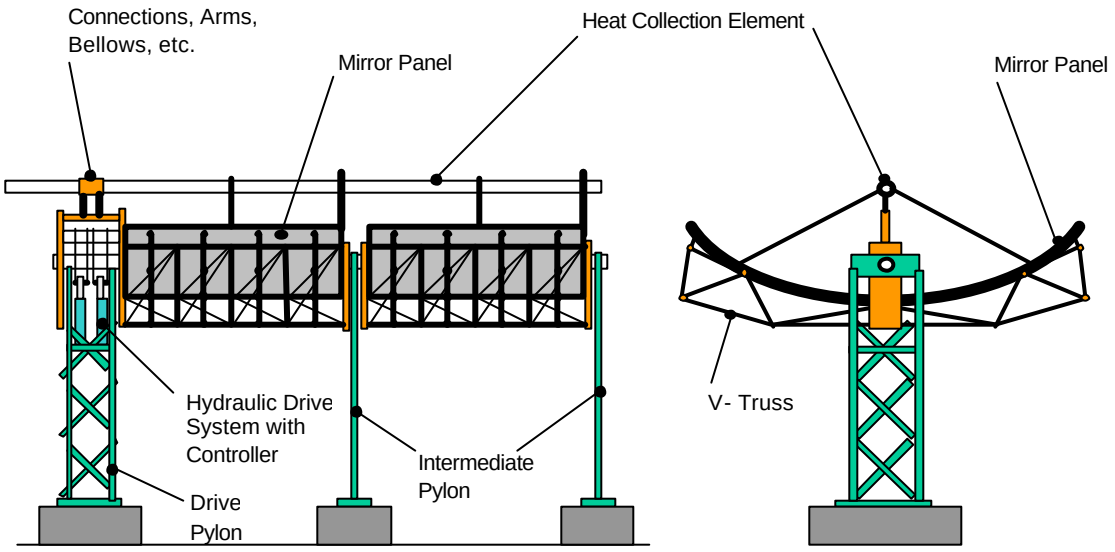

Figure 2.2: Solar Collector Assembly

The structure of a part of one SCA is given in Figure 2.2 (Pilkington 1996). The entire SCA consists of six mirror panels. In Figure 2.2 only two of them are shown. All the SCAs are

controlled by a main process computer, the Field Supervisory Controller (FSC). There is one drive pylon in the center of each SCA with the FSC controlled hydraulic drive system. The six mirror panels are held up either by the central drive pylon, intermediate pylons or by shared pylons between two SCAs or by an end pylon when it is the last SCA in a row. The length of an entire collector mirror is the length of one mirror panel times the number of mirror panels in a single collector. The collector mirror length is $Length = 753.6 \text{ m}$. The low-iron glass parabolic mirrors reflect the solar radiation to the heat collection element (HCE) that is mounted on the SCA through arms.

The HCE, shown in Figure 2.3, is a cermet-coated, stainless-steel absorber tube, surrounded by a partially evacuated glass envelope. The HTF flows in the absorber tube.

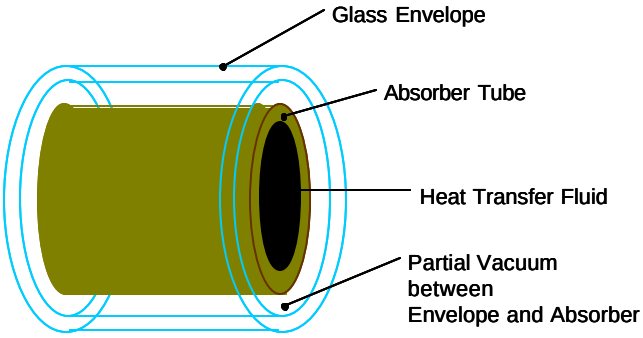

Figure 2.3: Schematic of a Heat Collection Element

Not shown in Figure 2.3 are bellows between different parts of the HCE to allow differential expansion between the glass and the stainless steel. There are flexible metallic hoses, between the SCAs themselves and between the collector loops and the headers.

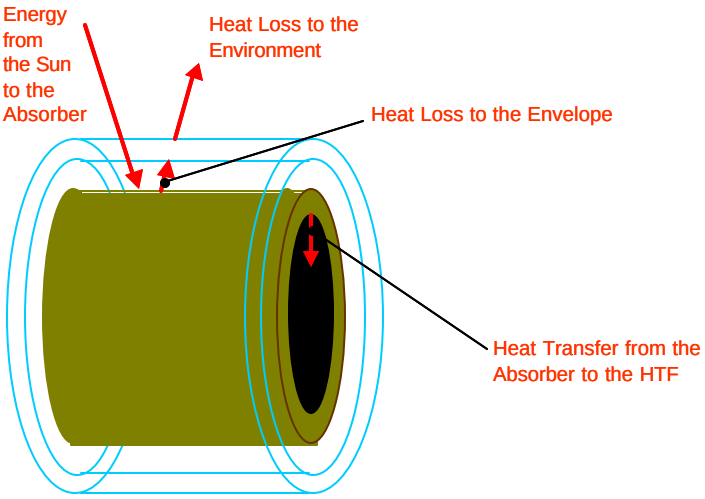

Figure 2.4: Heat Transfer at the HCE

The heat transfer between the different parts of the HCE is shown in Figure 2.4. The sun's energy, reflected by the mirrors, falls on the absorber after passing through the glass envelope. This absorbed solar energy is not fully transmitted to the HTF. There are heat losses from the absorber to the glass envelope. The glass envelope in turn is loosing heat to the environment.

These energy considerations lead to the development of the collector model. Differential equations for the temperatures of the HCE, the absorber and the glass envelope are established. The differential equations are coupled through relations for the heat transfer between the different parts of the HCE. Heat transfer between the absorber and the HTF, between the absorber and the envelope, and between the envelope and the environment is considered. Finally, the estimation of the absorbed solar energy from the direct normal solar radiation after optical losses is discussed.

2.2 Modeling of the Collector

2.2.1 Partial Differential Equations for Temperatures

The modeling of the collector, as shown in Figure 2.5, starts by an energy balance for the HTF, which leads to a partial differential equation for the HTF temperature. The distance along the collector is indicated by z. The equation for the HTF heat change over time t on an element of length Δz at position z is:

$$\frac{\partial}{\partial t}\left(\Delta Q_{HTF}(z,t)\right) = \dot{Q}_{HTF}(z,t) - \dot{Q}_{HTF}(z+\Delta z,t) + q_{gained}(z,t)\Delta z\,. \tag{2.1}$$

In equation (2.1), q_{gained} is the heat transfer per length between the absorber and the HTF.

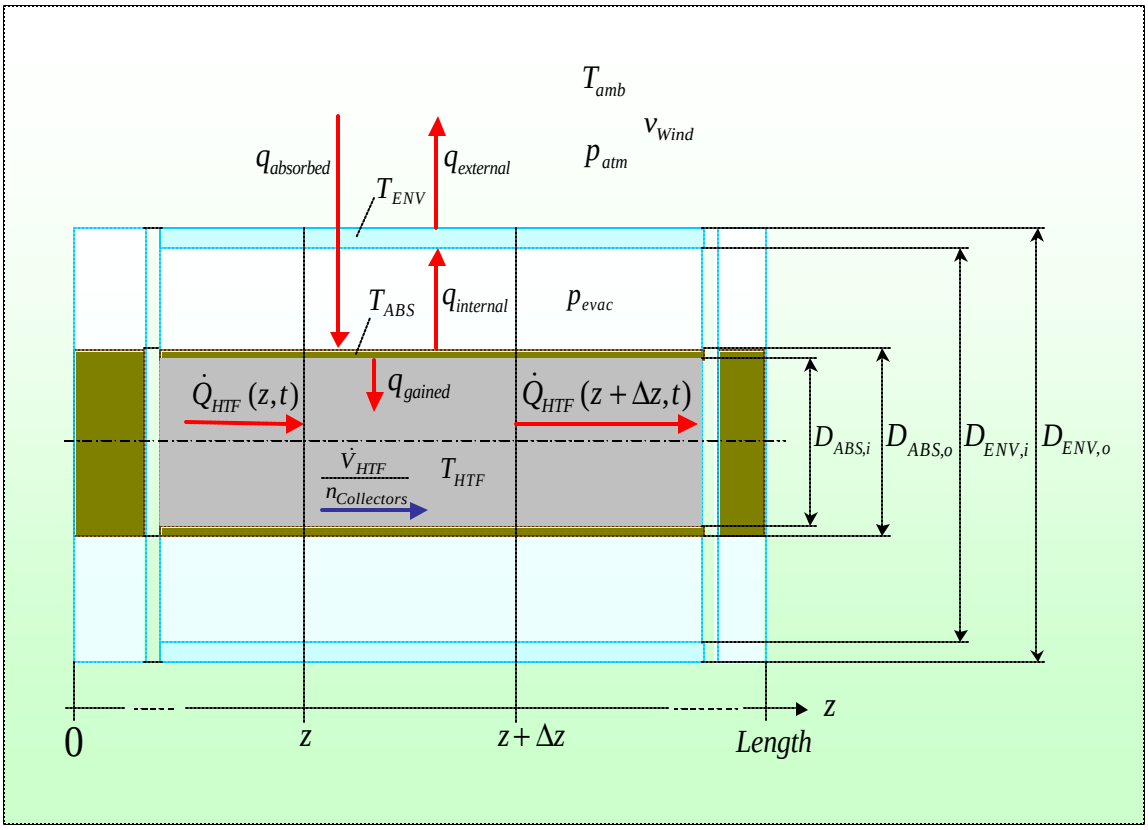

Figure 2.5: Schemata of the HCE

From thermodynamics, it follows that

$$\Delta Q_{HTF}(z,t) = r_{HTF} c_{HTF} A_{ABS,i} \Delta z T_{HTF}(z,t) \tag{2.2}$$

with r_{HTF}, c_{HTF}, T_{HTF} as the HTF density, specific heat and temperature where the first two depend on the latter. The cross-sectional area of the inside tube of the absorber is $A_{ABS,i}$. A list with all the collector dimensions is given in Appendix A. It also follows from thermodynamics

$$\begin{aligned} \dot{Q}_{HTF}(z,t) &= \frac{dQ_{HTF}(z,t)}{dt} \\ &= r_{HTF} c_{HTF} \frac{\dot{V}_{HTF}(t)}{n_{Collectors}} T_{HTF}(z,t) \end{aligned} . \tag{2.3}$$

Notice the overall HTF volume flow rate, $\dot{V}_{HTF}$, depends only on the time t since the fluid is considered to be incompressible. The number of collectors is $n_{Collectors}$. From Figure 2.1 it is known that $n_{Collectors} = 50$. After inserting equation (2.2) and (2.3) into equation (2.1), it follows that

$$\begin{aligned} r_{HTF} c_{HTF} A_{ABS,i} \Delta z \frac{\partial T_{HTF}(z,t)}{\partial t} = {} & r_{HTF} c_{HTF} \frac{\dot{V}_{HTF}(t)}{n_{Collectors}} T_{HTF}(z,t) \\ & - r_{HTF} c_{HTF} \frac{\dot{V}_{HTF}(t)}{n_{Collectors}} T_{HTF}(z+\Delta z,t) \\ & + q_{gained}(z,t)\Delta z. \end{aligned} \tag{2.4}$$

From the definition of the derivative it follows

$$\frac{\partial T_{HTF}(z,t)}{\partial z} = \lim_{\Delta z \to 0} \frac{T_{HTF}(z,t) - T_{HTF}(z+\Delta z,t)}{\Delta z}. \tag{2.5}$$

Dividing equation (2.4) by Δz, letting $\Delta z \to 0$ and considering equation (2.5), yields the following partial differential equation for the HTF temperature:

$$r_{HTF} c_{HTF} A_{ABS,i} \frac{\partial T_{HTF}(z,t)}{\partial t} = -r_{HTF} c_{HTF} \frac{\dot{V}_{HTF}(t)}{n_{Collectors}} \frac{\partial T_{HTF}(z,t)}{\partial z} + q_{gained}(z,t). \tag{2.6}$$

The boundary condition for equation (2.6) is

$$T_{HTF}(0,t) = T_{HTF,inlet}(t) \tag{2.7}$$

with $T_{HTF,inlet}$ as the HTF collector field inlet temperature. The initial condition for equation (2.6) is

$$T_{HTF}(z,0) = T_{HTF,init}(z). \tag{2.8}$$

In analogy to equation (2.1), the differential equation for the absorber temperature, T_{ABS}, is obtained

$$\frac{\partial}{\partial t}\left(\Delta Q_{ABS}(z,t)\right) = \left(q_{absorbed}(t) - q_{internal}(z,t) - q_{gained}(z,t)\right)\Delta z. \tag{2.9}$$

Here, $q_{internal}$ is the heat transfer per length between the absorber and the glass envelope. The absorbed solar energy is $q_{absorbed}$. From thermodynamics it is known that

$$\Delta Q_{ABS}(z,t) = r_{ABS} c_{ABS} A_{ABS} \Delta z T_{ABS}(z,t) \tag{2.10}$$

with r_{ABS}, c_{ABS}, T_{ABS} as the absorber density, specific heat and temperature. The cross-sectional area of the absorber is A_{ABS}. Substituting equation (2.10) into equation (2.9) yields after a division by Δz

$$r_{ABS} c_{ABS} A_{ABS} \frac{\partial T_{ABS}(z,t)}{\partial t} = q_{absorbed}(t) - q_{internal}(z,t) - q_{gained}(z,t). \tag{2.11}$$

The initial condition for equation (2.11) is

$$T_{ABS}(z,0) = T_{ABS,init}(z). \tag{2.12}$$

The glass envelope is assumed to have no radial temperature gradients. The differential equation for the envelope temperature is gained through considerations similar to those used to obtain the differential equation for the absorber temperature (2.11):

$$r_{ENV} c_{ENV} A_{ENV} \frac{\partial T_{ENV}(z,t)}{\partial t} = q_{internal}(z,t) - q_{external}(z,t) \tag{2.13}$$

with r_{ENV}, c_{ENV}, T_{ENV} as the envelope density, specific heat and temperature. The heat transfer per length between the envelope and the environment is $q_{external}$. The initial condition for equation (2.13) is

$$T_{ENV}(z,0) = T_{ENV,init}(z). \tag{2.14}$$

The interacting dynamic of the temperatures given through the differential equations (2.6), (2.11) and (2.13) is determined by the heat transfer between the HTF, the absorber and the envelope. It follows a discussion of equations to estimate the occurring heat transfer.

2.2.2 Heat Transfer between the Absorber and the HTF

Considering convection for internal flow, the heat transfer, q_{gained}, is calculated through the Dittus-Boelter equation for fully developed (hydrodynamically and thermally) turbulent flow in a smooth circular tube (Incropera & De Witt, 2002). Hence, the local Nusselt number, $Nu_{D_{ABS,i}}$ is given by

$$Nu_{D_{ABS,i}} = 0.023 Re_{D_{ABS,i}}^{4/5} Pr_{HTF}^{n} \tag{2.15}$$

where n = 0.4 for heating ($T_{ABS} > T_{HTF}$) and 0.3 for cooling ($T_{ABS} < T_{HTF}$).

The Reynolds number, $Re_{D_{ABS,i}}$, for flow in a circular tube, is given by

$$\mathrm{Re}_{D_{ABS,i}} = \frac{4\, r_{HTF} \dot{V}_{HTF}}{p D_{ABS,i} m_{HTF} n_{Collectors}} \tag{2.16}$$

with m_{HTF} as the viscosity of the HTF. The Prandtl number, Pr_{HTF}, is determined by

$$Pr_{HTF} = \frac{n_{HTF}}{a_{HTF}} \tag{2.17}$$

with the kinematic viscosity of the HTF, n_{HTF}, defined by

$$n_{HTF} = \frac{m_{HTF}}{r_{HTF}} \tag{2.18}$$

and the thermal diffusivity of the HTF, a_{HTF}, which is given through

$$a_{HTF} = \frac{k_{HTF}}{r_{HTF} c_{HTF}}. \tag{2.19}$$

Within equation (2.19), k_{HTF} is the thermal conductivity of the HTF. The heat transfer coefficient, $h_{ABS,HTF}$, is calculated by using the local Nusselt number, $Nu_{D_{ABS,i}}$, through

$$h_{ABS,HTF} = \frac{Nu_{D_{ABS,i}} k_{HTF}}{D_{ABS,i}}, \tag{2.20}$$

where $D_{ABS,i}$ is the inside diameter of the absorber tube and $D_{ABS,i} = 0.066$ m. The HTF properties c_{HTF}, k_{HTF}, m_{HTF} and r_{HTF} are functions of the HTF temperature, T_{HTF}. Finally the heat transfer between the absorber and the HTF, q_{gained}, is calculated as

$$q_{gained} = h_{ABS,HTF} A_{ABS,surf,i} \left(T_{ABS} - T_{HTF}\right) \tag{2.21}$$

with the inner surface area per length of the absorber, $A_{ABS,surf,i}$,

$$A_{ABS,surf,i} = p\, D_{ABS,i}. \tag{2.22}$$

2.2.3 Heat Transfer between the Absorber and the Glass Envelope

The heat transfer between the absorber and the glass envelope, $q_{internal}$, is calculated from convection and radiation

$$q_{internal} = q_{internal,convection} + q_{internal,radiation}. \tag{2.23}$$

Assuming only partial evacuation of the annulus between the absorber and the glass envelope, the occurring free convection is estimated through relations for a free convection flow in the annular space between long, horizontal, concentric cylinders (Incropera & De Witt, 2002). Since the glass envelope is usually cooler than the absorber ($T_{ABS} > T_{ENV}$), the air ascends along the absorber and descends along the glass envelope. The convection heat transfer, $q_{internal,convection}$, may be expressed as

$$q_{internal,convection} = \frac{2p\, k_{\mathrm{eff},Air}}{\ln(D_{ENV,i} / D_{ABS,o})}(T_{ABS} - T_{ENV}) \tag{2.24}$$

where $D_{ENV,i}$ is the inside diameter of the glass envelope ($D_{ENV,i} = 0.112$ m) and $D_{ABS,o}$ is the outside diameter of the absorber ($D_{ABS,o} = 0.07$ m). The effective thermal conductivity, $k_{\mathrm{eff},Air}$, is the thermal conductivity that the stationary air should have to transfer the same amount of heat as moving air. A suggested correlation for $k_{\mathrm{eff},Air}$ is

$$\frac{k_{\mathrm{eff},Air}}{k_{Air}} = 0.386\left(\frac{Pr_{Air}}{0.861 + Pr_{Air}}\right)^{1/4} (Ra_c^*)^{1/4} \tag{2.25}$$

where

$$Ra_c^* = \frac{\left[\ln(D_{ENV,i}/D_{ABS,o})\right]^4}{L^3(D_{ABS,o}^{-3/5}+D_{ENV,i}^{-3/5})^5} Ra_L \,. \tag{2.26}$$

In equation (2.25), Pr_{Air}, is the Prandtl number of air in the annulus. The thermal conductivity of air is k_{Air}. In equation (2.26), L, is the effective length and is given for the annulus through

$$L = 0.5\left(D_{ENV,i} - D_{ABS,o}\right). \tag{2.27}$$

The Rayleigh Number of air, Ra_L, is defined as

$$Ra_L = \frac{g\beta_{Air}(T_{ABS}-T_{ENV})L^3}{\alpha_{Air}\nu_{Air}} \tag{2.28}$$

with g as the gravitational acceleration ($g = 9.81\,\mathrm{m\,s^{-2}}$), the volumetric thermal expansion coefficient of air, β_{Air}, and the thermal diffusivity of air, α_{Air}, calculated as

$$\alpha_{Air} = \frac{k_{Air}}{\rho_{Air} c_{p,Air}} \,. \tag{2.29}$$

Here, ρ_{Air} is the density of air in the annulus and $c_{p,Air}$ is the specific heat of air. The kinematic viscosity of air, ν_{Air}, is given by

$$\nu_{Air} = \frac{\mu_{Air}}{\rho_{Air}} \tag{2.30}$$

with the viscosity of air, μ_{Air}. The properties of air in the annulus, α_{Air}, β_{Air}, $c_{p,Air}$, k_{Air}, μ_{Air}, ν_{Air}, Pr_{Air} and ρ_{Air} are dependent on the mean temperature in the annulus

$$\overline{T}_{Annulus} = 0.5\left(T_{ABS} + T_{ENV}\right). \tag{2.31}$$

In addition, the density r_{Air} depends on the evacuation pressure in the annulus, p_{evac}. A value of $p_{evac} = 7\,\text{kPa}$ is used in the model. This value was chosen such that the calculated collector outlet temperature fits the measured collector outlet temperature best.

The heat transfer through radiation between long, concentric cylinders, $q_{internal,radiation}$, may be expressed as (Incropera & De Witt, 2002)

$$q_{internal,radiation} = \frac{s\, A_{ABS,surf,o}\left(T_{ABS}^4 - T_{ENV}^4\right)}{\frac{1}{e_{ABS}} + \frac{1-e_{ENV}}{e_{ENV}}\left(\frac{D_{ABS,o}}{D_{ENV,i}}\right)}. \tag{2.32}$$

In equation (2.32), s is the Stefan-Boltzmann constant and has the numerical value

$$s = 5.670\times10^{-8}\,\text{W/m}^2\cdot\text{K}^4.$$

The outer surface area per length of the absorber, $A_{ABS,surf,o}$, is given by

$$A_{ABS,surf,o} = p\, D_{ABS,o}. \tag{2.33}$$

The emissivity of the absorber is e_{ABS} and the emissivity of the glass envelope is e_{ENV} with $e_{ENV} = 0.9$ as measured by SANDIA. The emissivity of the absorber, e_{ABS}, increases with the absorber temperature, T_{ABS}. SANDIA provides a linear function for e_{ABS} from their measurements:

$$e_{ABS} = 0.000327\cdot T_{ABS} - 0.065971. \tag{2.34}$$

If $e_{ABS} < 0.05$ then the value is set to $e_{ABS} = 0.05$ (Figure 2.6).

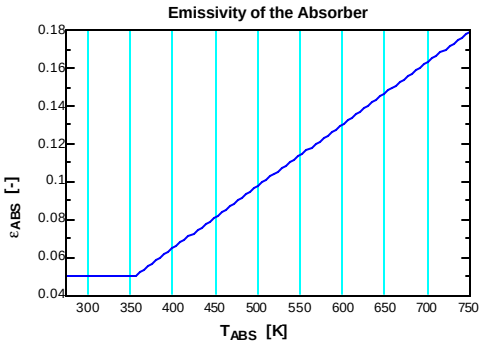

Figure 2.6: Emissivity of the Absorber vs. Absorber Temperature

2.2.4 Heat Transfer between the Glass Envelope and the Environment

The heat transfer between the envelope and the environment is assumed to be due to convection and radiation

$$q_{external} = q_{external,convection} + q_{external,radiation} . \tag{2.35}$$

The environmental air flows around the envelope with a wind speed, v_{Wind}. The fluid motion is assumed to be normal to the axis of the envelope's circular cylinder. The heat transfer due to convection, $q_{external,convection}$, is estimated through a correlation suggested for a circular cylinder in cross flow (Incropera & De Witt, 2002).

Considering overall average conditions, the calculation starts by using the following correlation for the Nusselt Number, $\overline{Nu}_{D_{ENV,o}}$:

$$\overline{Nu}_{D_{ENV,o}} = 0.3 + \frac{0.62 Re_{D_{ENV,o}}^{1/2} Pr_{Air,amb}^{1/3}}{\left[1+(0.4/Pr_{Air,amb})^{2/3}\right]^{1/4}} \left[1+\left(\frac{Re_{D_{ENV,o}}}{282{,}000}\right)^{5/8}\right]^{4/5} \tag{2.36}$$

For the circular glass envelope cylinder, the Reynolds Number, $Re_{D_{ENV,o}}$, is defined as

$$Re_{D_{ENV,o}} = \frac{r_{Air,amb} v_{Wind} D_{ENV,o}}{m_{Air,amb}} \tag{2.37}$$

with $r_{Air,amb}$ as the density of the ambient air, $D_{ENV,o}$ as the outside diameter of the glass envelope ($D_{ENV,o} = 0.115\,\text{m}$) and $m_{Air,amb}$ as the viscosity of the ambient air. The Prandtl number of the ambient air is $Pr_{Air,amb}$. The convection heat transfer coefficient, $\bar{h}_{ENV,Environment}$, is then given through

$$\bar{h}_{ENV,Environment} = \frac{\overline{Nu}_{D_{ENV,o}} k_{Air,amb}}{D_{ENV,o}}. \tag{2.38}$$

The thermal conductivity of the ambient air, $k_{Air,amb}$, and the other properties of the air, $m_{Air,amb}$, $Pr_{Air,amb}$ and $r_{Air,amb}$ are dependent on the mean ambient temperature

$$\overline{T}_{amb} = 0.5\left(T_{ENV} + T_{amb}\right), \tag{2.39}$$

where T_{amb} is the ambient temperature of the environment. In addition, $r_{Air,amb}$ depends on the atmospheric pressure, p_{atm}. Finally, the heat transfer to the environment due to convection is

$$q_{external,convection} = \bar{h}_{ENV,Environment} A_{ENV,surf,o}\left(T_{ENV} - T_{amb}\right) \tag{2.40}$$

with the outer surface area per length of the glass envelope, $A_{ENV,surf,o}$, calculated through

$$A_{ENV,surf,o} = p D_{ENV,o}. \tag{2.41}$$

The heat transfer to the environment due to radiation, $q_{external,radiation}$, may be expressed as (Incropera & De Witt, 2002)

$$q_{external,radiation} = e_{ENV} s A_{ENV,surf,o}\left(T_{ENV}^4 - T_{amb}^4\right) \tag{2.42}$$

with e_{ENV} as the emissivity of the glass envelope. This relationship describes the radiation of a small convex object, the glass envelope, in a large cavity, the environment.

The sun's energy is the energy source that acts on the absorber and induces the heat transfer discussed above. It governs the amount of energy finally transferred to the HTF and thus to the power plant for the generation of electricity. Thus, it is necessary to estimate the amount of absorbed solar energy, $q_{absorbed}$.

2.2.5 Absorbed Solar Energy

The following discussion is based on (Duffie & Beckman, 1991) and (Iqbal, 1983). The sun is a completely gaseous body. Gravitational forces retain its constituent hot gases. The sun's physical structure is complex and may be considered to be composed of several regions, where the innermost region, the core, is the hottest and densest part. Above the core is the interior, which contains practically all of the sun's mass. The core and the interior are considered as a continuous fusion reactor, the source of almost all the sun's energy. This energy is propagated to the outer regions. The sun's surface, the photosphere, is the source of most solar radiation arriving at the earth's atmosphere.

The intensity of solar radiation outside of the earth's atmosphere is nearly fixed about 1.37 kW/m^2 for the mean distance between the earth and the sun of one astronomical unit, 1 AU = 1.496×10^{11} m. It varies with the earth-sun distance over the year in the range of $\pm 3\%$. The earth is at its closest point to the sun (perihelion; $\approx$ 0.983 AU) on approximately 3 January and at its farthest point (aphelion; $\approx$ 1.017 AU) on approximately 4 July. The mean distance is approached at approximately 4 April and 5 October. The amount of solar radiation

reaching the earth's atmosphere is inversely proportional to the square of its distance from the sun.

When solar radiation enters the earth's atmosphere, a part of the incident energy is removed by scattering in the atmosphere due to interaction of the radiation with air molecules, water (vapor and droplets), and dust. Another part of the incident energy is removed in the earth's atmosphere by absorption of radiation in the solar energy spectrum due to ozone in the ultraviolet and to water vapor and carbon dioxide in bands in the infrared. The scattered radiation is called diffuse radiation. A portion of this diffuse radiation goes back to space and a portion reaches the ground. The remaining part of the solar radiation that enters the earth's atmosphere, the radiation arriving on the ground directly in line from the solar disk without having been scattered by the atmosphere or having been absorbed, is called beam radiation. Beam radiation incident on a plane normal to the radiation is called the direct normal radiation. The total solar radiation or global radiation, that is, the sum of the diffuse and beam solar radiation on a surface, is important for the design of flat-plate collectors or for the calculations of heating and cooling loads in architecture. For concentrating systems like the solar trough collector field only the beam radiation or direct normal radiation is used.

The direct normal radiation, G_{bn}, can be measured by using a Normal Incidence Pyrheliometer (NIP). The NIP is an instrument for measuring solar radiation from the sun and from a small portion of the sky around the sun at normal incidence.

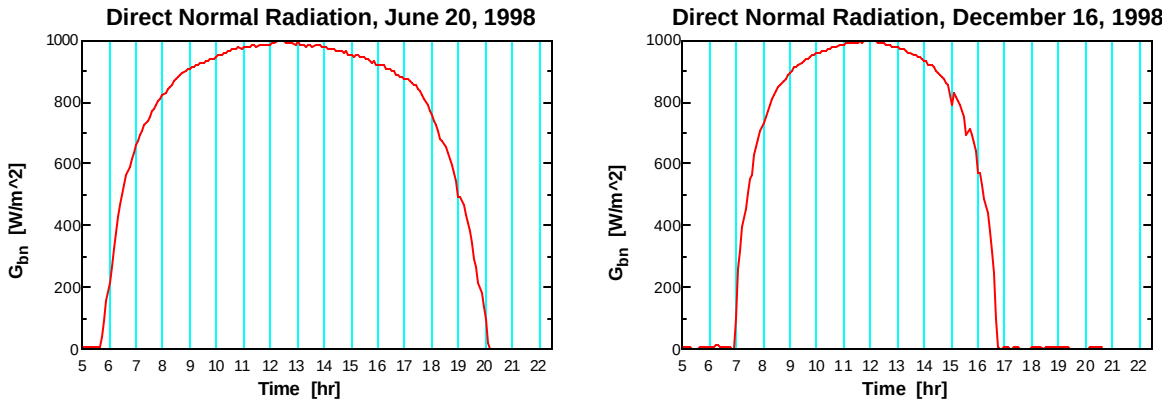

Figure 2.7: Direct normal radiation vs. time for June 20, 1998 (left hand figure) and for December 16, 1998 (right hand figure)

Figure 2.7 shows the direct normal radiation vs. time for a day measured with a NIP at SEGS VI. The left hand figure shows the measurement for a clear (no clouds) spring/summer day, June 20, 1998 and the right hand figure shows the beam radiation during a clear fall/winter day, December 16, 1998.

Notice the direct normal radiation is not constant between sunrise and sunset because the effects of the atmosphere in scattering and absorbing radiation are variable with time as atmospheric conditions and air mass change.

In order to maximize the energy from the solar beam radiation through the concentrating trough collectors, the surface normal of a collector has to be collinear to the vector of the incoming solar beam radiation. The angle of incidence, q, is the angle between the beam radiation on a surface and the normal to that surface. Throughout the sun's daily path between sunrise and sunset, the sun changes its solar position in the sky. Consequently, during a day, the vector of the incoming solar beam radiation changes its direction as well. To minimize the angle of incidence, the solar collectors must track the sun by moving in

prescribed ways. The best way to track the sun is by rotating the collector's surface about two axis. As can be seen in Figure 2.1, the solar collector troughs of SEGS VI are tracking the sun by rotating around a single axis, which is the horizontal north-south axis. Due to this constraint movability, only the component of the solar beam radiation vector, which is collinear to the normal of the single-axis-tracking collector surface, remains to heat the absorber, as shown in Figure 2.8. This component of the solar beam radiation vector may be found by multiplying the amount of solar beam radiation with the cosine of the angle of incidence. Therefore a relationship for the angle of incidence is needed, which is given by (Duffie & Beckman, 1991)

$$\cos q = \left(\cos^2 q_z + \cos^2 d \sin^2 w\right)^{1/2}. \qquad (2.43)$$

On the right hand side of this equation, there are three angles, q_z, d and w, which describe the position of the sun for its daily path and will be explained in the following (Figure 2.9, (Iqbal, 1983)).

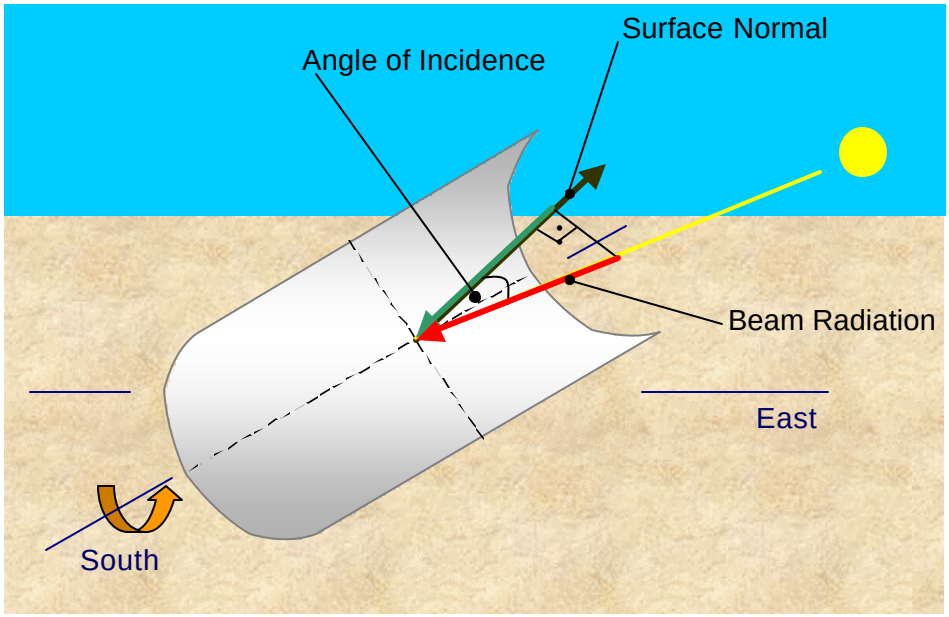

Figure 2.8: North-South Tracking

In Figure 2.9, a celestial sphere is drawn with the earth as the center. In the celestial sphere, the celestial poles are the points at which the earth's extended polar axis cuts the celestial sphere. Similarly, the celestial equator is an outward projection of the earth's equatorial plane on the celestial sphere. At any given time, the collector on the earth's surface has a corresponding position in the celestial sphere called the collector's zenith: this is the point of intersection with the celestial sphere of a normal to the earth's surface at the collector's position. The collector's horizon is a great circle in the celestial sphere described by a plane, which passes through the center of the earth normal to the line joining the center of the earth and the zenith.

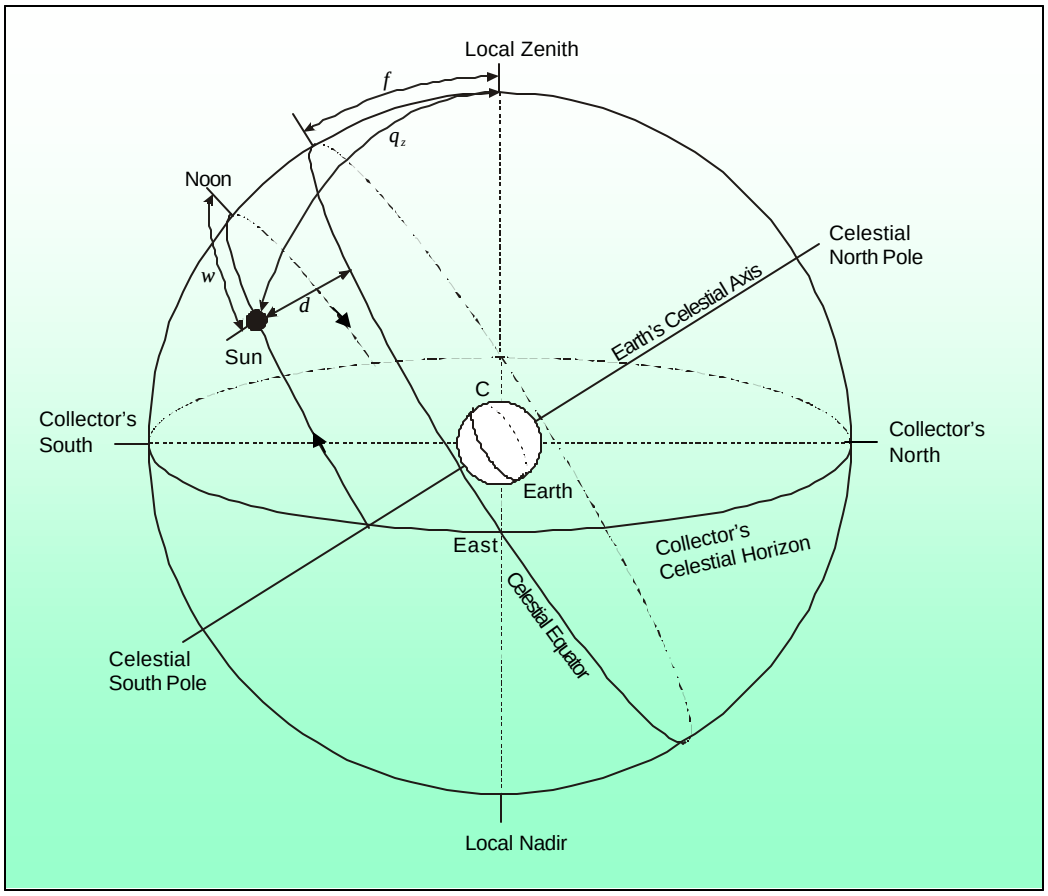

Figure 2.9: Celestial sphere and sun's coordinates relative to collector on earth at point C

The zenith angle, q_z, is the angle between the vertical (the local zenith) and the line to the sun, that is the angle of incidence of beam radiation, q, on a horizontal surface. The angle is within a range of $0° \le q_z \le 90°$. Since the trough collectors are tracking surfaces, they are horizontal only at solar noon and thus the zenith angle is equal to the angle of incidence of beam radiation only at solar noon.

The declination, d, is the angular position of the sun at solar noon (i.e., when the sun is on the local meridian) with respect to the plane of the equator, north positive; the declination angle is within a range of $-23.45° \le d \le 23.45°$. It reaches its minimum value at the winter solstice (21/22 December) and its maximum value at the summer solstice (21/22 June). The angle is zero at the vernal equinox (20/21 March) and at the autumnal equinox (22/23 September). In 24 h, the maximum change in declination (which occurs at the equinoxes) is less than $\frac{1}{2}°$. See also Figure 2.10 where the solar declination is described by drawing a celestial sphere with the earth at the center and the sun revolving around the earth in a year. Several expressions giving the approximate value of solar declination have been suggested.

Spencer presented the following expression for d, in degrees (Spencer, as quoted by Iqbal, 1983):

$$\begin{aligned} d = {} & (0.006918 - 0.399912\cos\Gamma + 0.070257\sin\Gamma \\ & - 0.006758\cos(2\Gamma) + 0.000907\sin(2\Gamma) \\ & - 0.002697\cos(3\Gamma) + 0.00148\sin(3\Gamma))(180/p). \end{aligned} \tag{2.44}$$

In this equation, Γ, in radiants, is called the day angle. It is represented by

$$\Gamma = 2p\,(d_n - 1)/365, \tag{2.45}$$

where d_n is the day number of the year, ranging from 1 on 1 January to 365 on 31 December. February is always assumed to have 28 days. Equation (44) estimates d with a maximum error of 0.0006 rad (<3') and is recommended for use in digital machines.

Another equation obtained by Perrin de Brichambaut is, in degrees (Brichambaut, as quoted by Iqbal, 1983),

$$d = \sin^{-1}\left\{0.4 \sin\left[\tfrac{360}{365}\left(d_n - 82\right)\right]\right\}. \tag{2.46}$$

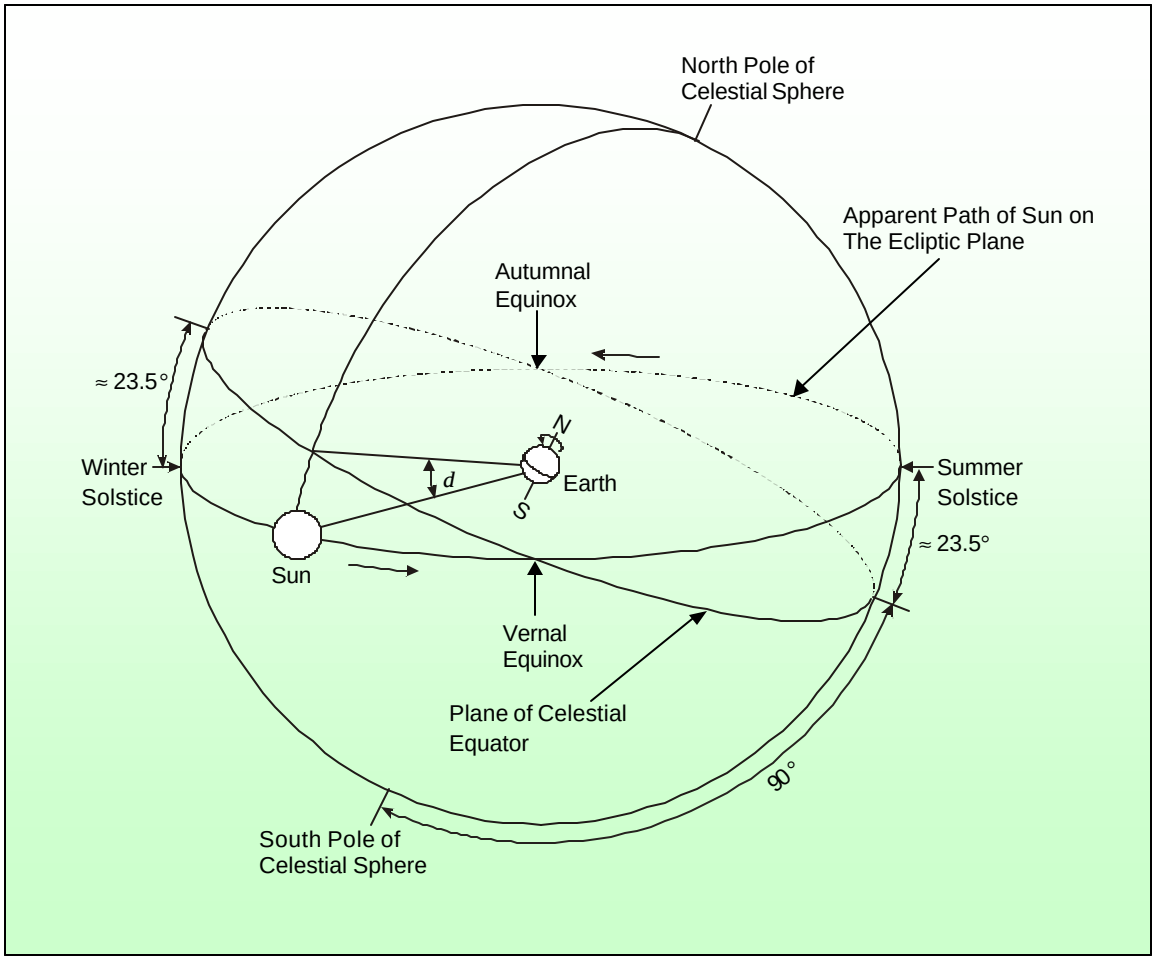

Figure 2.10: Celestial Sphere showing sun's declination angle

A further and simple equation found by Cooper is, in degrees (Cooper, as quoted by Iqbal 1983),

$$d = 23.45 \sin\left[\tfrac{360}{365}\left(d_n + 284\right)\right]. \tag{2.47}$$

A plot of the declination, d , vs. month is shown in Figure 2.11.

The hour angle, w , is the angular displacement of the sun east or west of the local meridian due to rotation of the earth on its axis at 15° per hour, morning negative, afternoon positive. The hour angle, w , is 0° at solar noon.

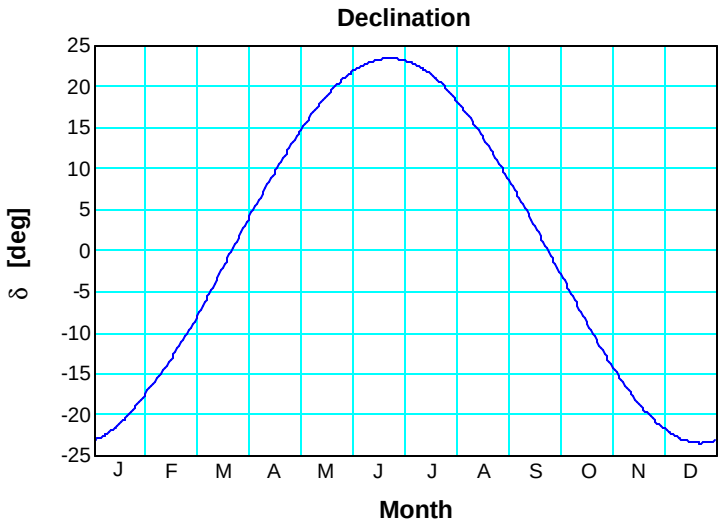

Figure 2.11: Declination vs. Month

The solar noon (i.e., the sun is on the local meridian) does not coincide with the local clock noon (Duffie & Beckman, 1991). It is necessary to convert standard time to solar time by applying two corrections. First, there is a constant correction for the difference in longitude between the observer's meridian (longitude) and the meridian on which the local standard time is based. The SEGS VI plant is located at the local longitude, L_{loc} , of 117.022°W. The

local clock time is measured with respect to the standard longitude, L_{st}, of 120°W for the Pacific Standard Time. The sun takes 4 minutes to transverse 1° of longitude. A second correction is from the equation of time, which takes into account the perturbations in the earth's rate of rotation, which affects the time the sun crosses the collector's meridian. Thus, in minutes,

$$\text{Solar Time} - \text{Standard Time} = 4 \cdot (L_{st} - L_{loc}) + E_t \tag{2.48}$$

where E_t is the equation of time, again from Spencer (Spencer, as quoted by Iqbal, 1983):

$$E_t = 229.18\,(0.000075 + 0.001868\cos\Gamma - 0.032077\sin\Gamma - 0.014615\cos(2\Gamma) - 0.04089\sin(2\Gamma)) \tag{2.49}$$

A plot of the equation of time, E_t, vs. month is shown in Figure 2.12.

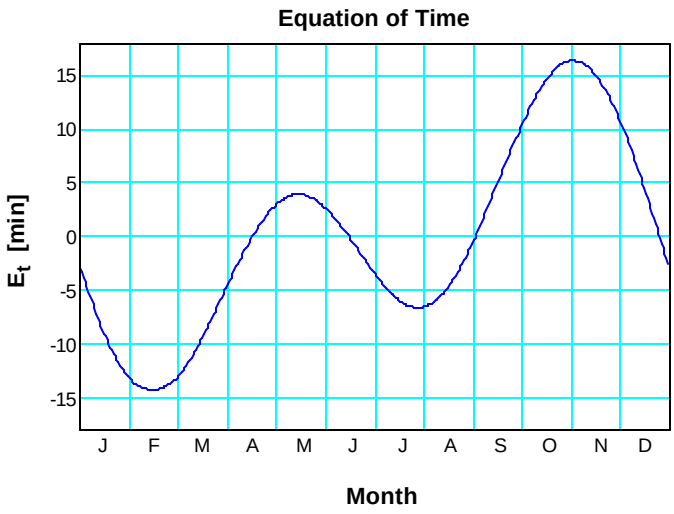

Figure 2.12: Equation of Time vs. Month

In summer, the local clock time may be the daylight saving time, which differs by 60 minutes from the standard time,

$$\text{Daylight Saving Time} - \text{Standard Time} = 60\,. \tag{2.50}$$

A fourth angle in Figure 2.9 is the latitude, f, and gives the position of the collector north or south from the earth's equator. The SEGS VI plant is located at $f = 35°\text{N}$.

There is a useful relationship among the four angles given in Figure 2.9. An equation relating the zenith angle, q_z, to the others is (Duffie & Beckman, 1991)

$$\cos q_z = \cos f \cos d \cos w + \sin f \sin d \,. \tag{2.51}$$

This equation can be used to solve for the value of the hour angle, w, at sunset. At sunset, the zenith angle, q_z, is 90° when the sun is at the horizon. Thus, the sunset hour angle, w_{sunset}, in degrees, is given by

$$\cos w_{sunset} = -\tan f \tan d \,. \tag{2.52}$$

The sunrise hour angel, $w_{sunrise}$, is consequently

$$w_{sunrise} = -w_{sunset} \,. \tag{2.53}$$

Assuming that the time for the solar noon calculated from equation (2.48) is converted from minutes into hours, the following equation gives the time at sunrise in hours from the fact that the sun rotates with 15° per hour:

$$\text{Sunrise Hour} = \text{Solar Noon} + w_{sunrise}/15 \,. \tag{2.54}$$

Finally, an expression for the hour angle, w, is given through

$$w = w_{sunrise} + (\text{Solar Time} - \text{Sunrise Hour}) \cdot 15 \,. \tag{2.55}$$

Here, the solar time is calculated from equation (2.48) after converting the result from minutes into hours.

The zenith angle, q_z, given by equation (2.51), the declination, d, given by equation (2.44) and the hour angle, w, equation (2.55), are inserted into equation (2.43) to calculate

the angle of incidence. Thus, multiplying the cosine of the angle of incidence with the magnitude of solar beam radiation gives the reduced beam radiation acting on an unshaded single-axis-tracking collector.

In reality, however, there are additional losses due to the shading by the HCE arms and bellows (Figure 2.2) and end losses. The meaning of end losses is illustrated in Figure 2.13. The sunrays that impinge on the outermost edge at the end of a trough collector are reflected and focused onto the HCE. For a nonzero angle of incidence, there is a part of the HCE at this end of the trough collector, which is not illuminated. To account for these additional optical losses, the cosine of the angle of incidence is modified through a function, the so-called incidence angle modifier. For the SEGS VI trough collectors, this function was found through measurements at a test facility at SANDIA.

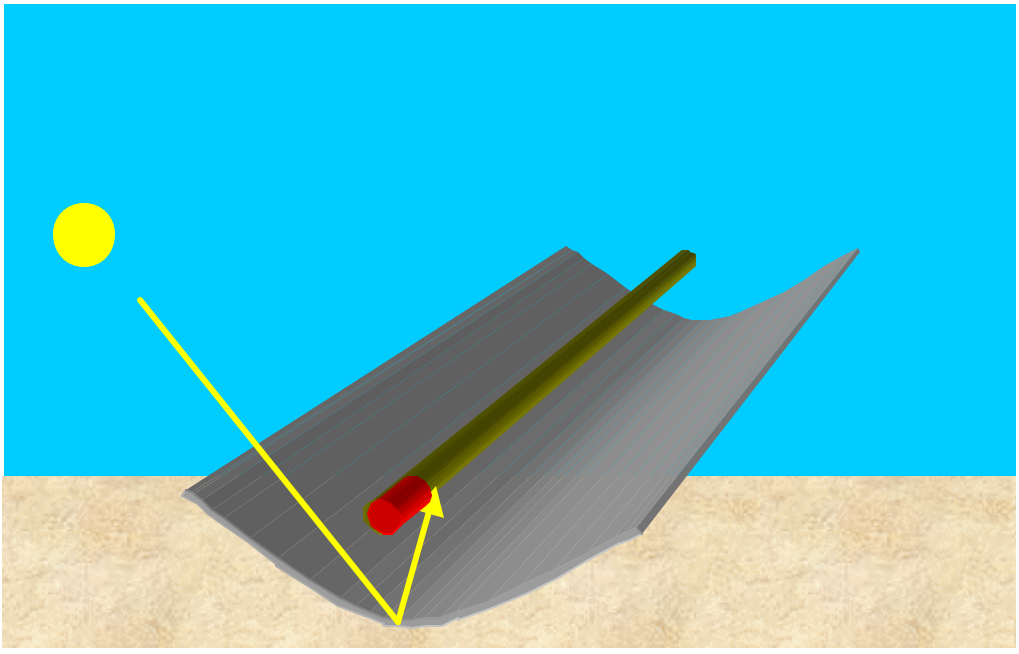

Figure 2.13: End Losses of a Trough Collector

The incidence modifier function depends on the value of the cosine of the angle of incidence; for $\cos q > 0.9$:

$$\begin{aligned} F(\cos q) = & -938564.84377331(\cos q)^6 + 5222972.5393731(\cos q)^5 \\ & - 12093484.903502(\cos q)^4 + 14912235.279499(\cos q)^3 \\ & - 10327122.89884(\cos q)^2 + 3808006.9842855\cos q - 584041.2051114 \end{aligned} \tag{2.56}$$

else:

$$\begin{aligned} F(\cos q) = & 7995.6488341455(\cos q)^8 - 45016.702352137(\cos q)^7 \\ & + 110302.75784952(\cos q)^6 - 153602.39131907(\cos q)^5 \\ & + 132938.65779691(\cos q)^4 - 73211.270566734(\cos q)^3 \\ & + 25050.730094871(\cos q)^2 - 4867.542978969\cos q + 411.23466109821 \end{aligned} \tag{2.57}$$

In Figure 2.14, the incidence angle modifier (solid line) is plotted vs. q. For a comparison, $\cos q$ (dashed line) is plotted vs. q as well.

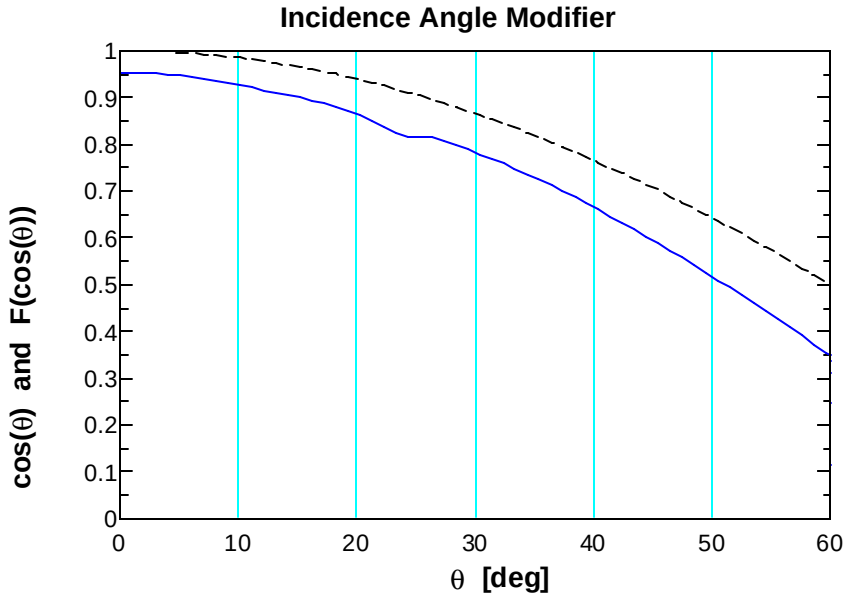

Figure 2.14: Incidence Angle Modifier vs. Angle of Incidence

From the following discussion, the absorbed solar energy per length would be the magnitude of the incoming solar beam radiation times the incidence angel modifier as a function of the cosine of the angle of incidence times the width of the collector. This, however, is only true if there would be no mutual shading of the collectors. From the trough collector field layout in Figure 2.1, it can be seen, that the collectors are arranged in rows. The distance between the collector rows is $L_{Spacing} = 13$ m. Hence, in the morning, at sunrise, when the first sunrays fall on the trough collector field, the first row may be unobstructed, but the following rows are shaded by the first. This is shown in the top figure in Figure 2.15. During the sun's path in the morning, partial shading of the collectors occurs until a particular zenith angle is reached as demonstrated in the second figure from the top in Figure 2.15. The shading reduces the effective width of the collector and thus reduces the effective aperature area of the collector on which the solar beam radiation acts. Consequently, the absorbed solar energy is reduced as well. After a certain zenith angle is reached, there is no mutual shading of the collectors anymore, as shown in the last two figures from the top in Figure 2.15. The same phenomenon occurs, of course, in the evening during sunset. For a mathematical formulation of the optical loss from mutual collector shading, it is necessary to find an equation describing the effective width of the collector. Let W be the width of the collector. The effective width of the collector, that is the non-shaded part of the collector width, may be written as (Figure 2.16)

$$W_{eff} = x \cdot W , \tag{2.58}$$

where $x \in [0;1]$. A value of 0 for x means complete shading whereas a value of 1 for x means no shading of the collector. The projection of the incoming beam radiation onto a

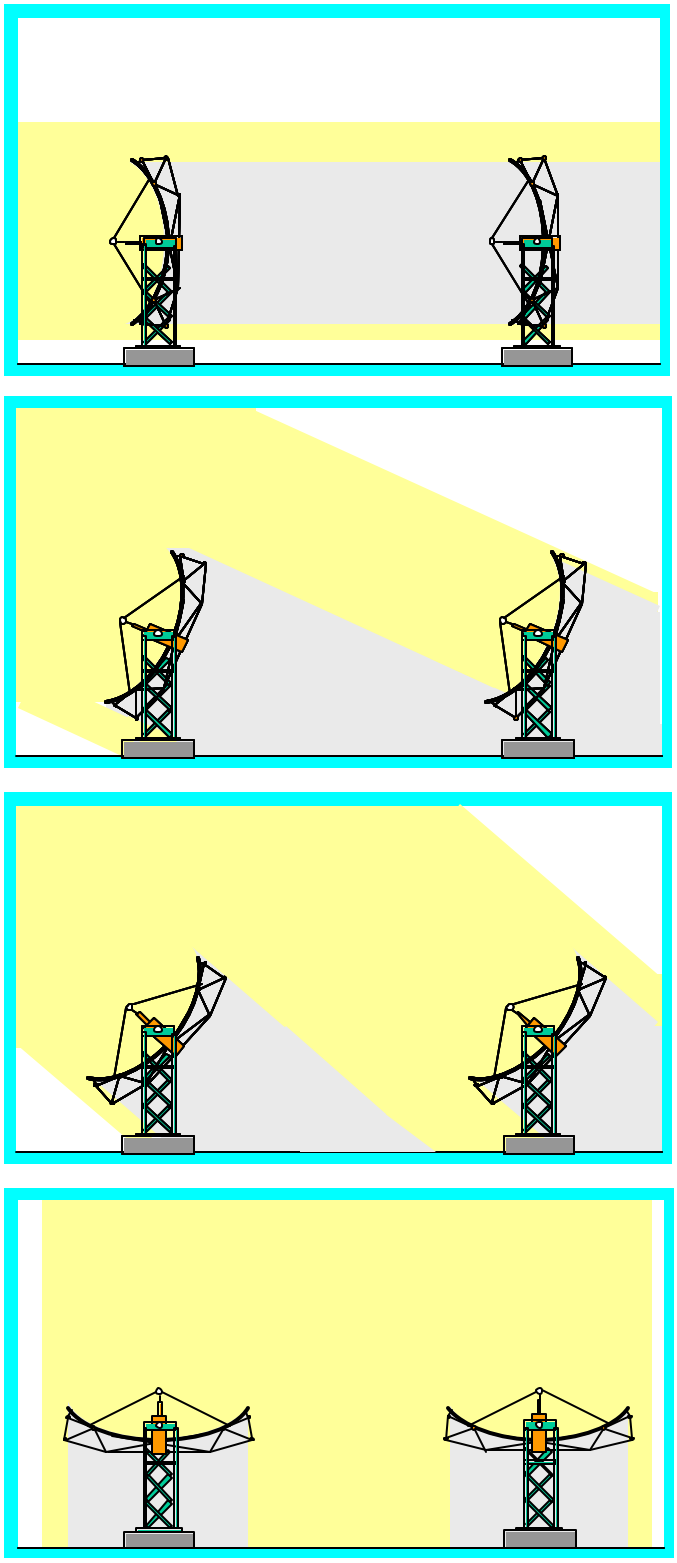

Figure 2.15: Illustration of mutual shading in a multirow collector array

plane perpendicular to the collector's rotational north-south axis yields a radiation, which direction is given by the profile angle a_p (Figure 2.16 and Figure 2.17).

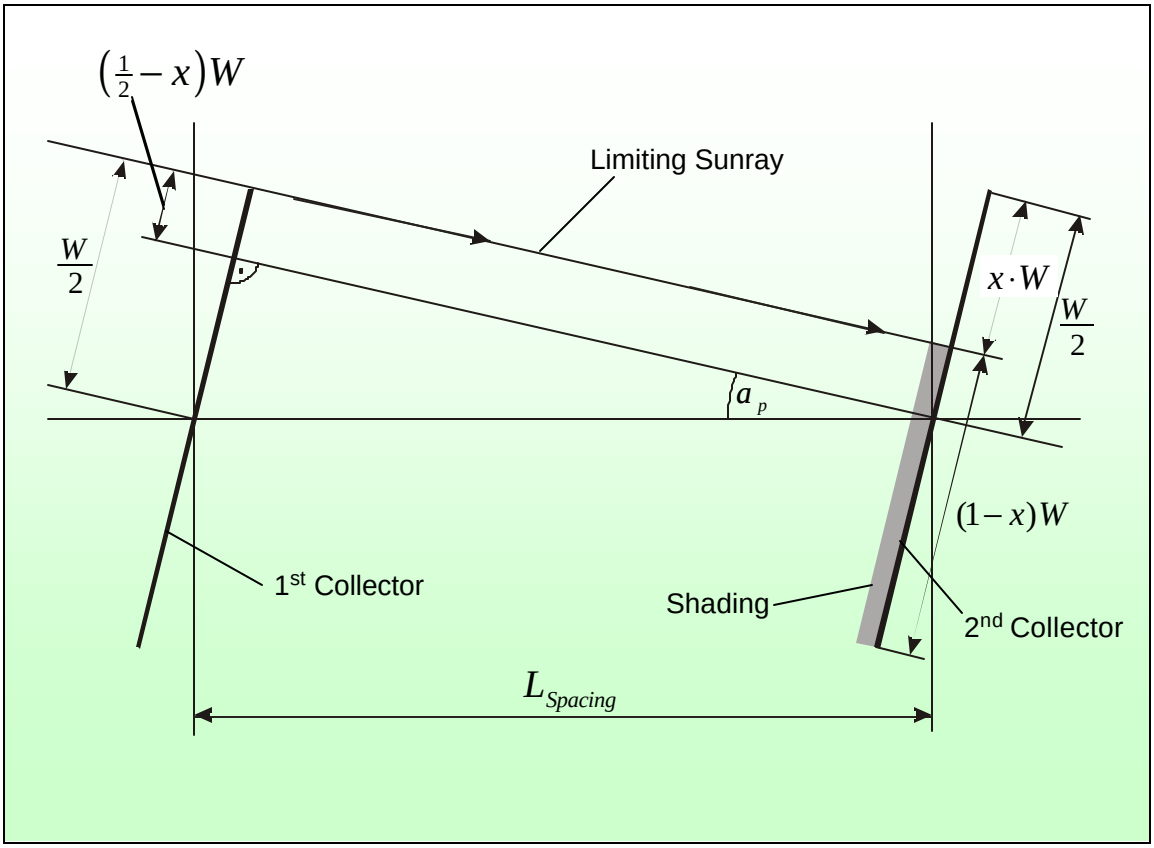

Figure 2.16: Mutual Collector Shading

Trigonometric considerations (Figure 2.16) yield

$$\begin{aligned} L_{Spacing} \sin(a_P) &= \frac{W}{2} - \left(\frac{1}{2} - x\right)W \\ &= x \cdot W \end{aligned} \tag{2.59}$$

The law of cosines for the spherical triangle O, Sun, P, Z in Figure 2.17 results in

$$\begin{aligned} \cos(q_z) &= \cos(q)\cos(90° - a_p) + \sin(q)\sin(90° - a_p)\cos(90°) \\ &= \cos(q)\sin(a_p) \end{aligned} \tag{2.60}$$

.

Thus,

$$\sin(a_p) = \frac{\cos(q_z)}{\cos(q)}. \tag{2.61}$$

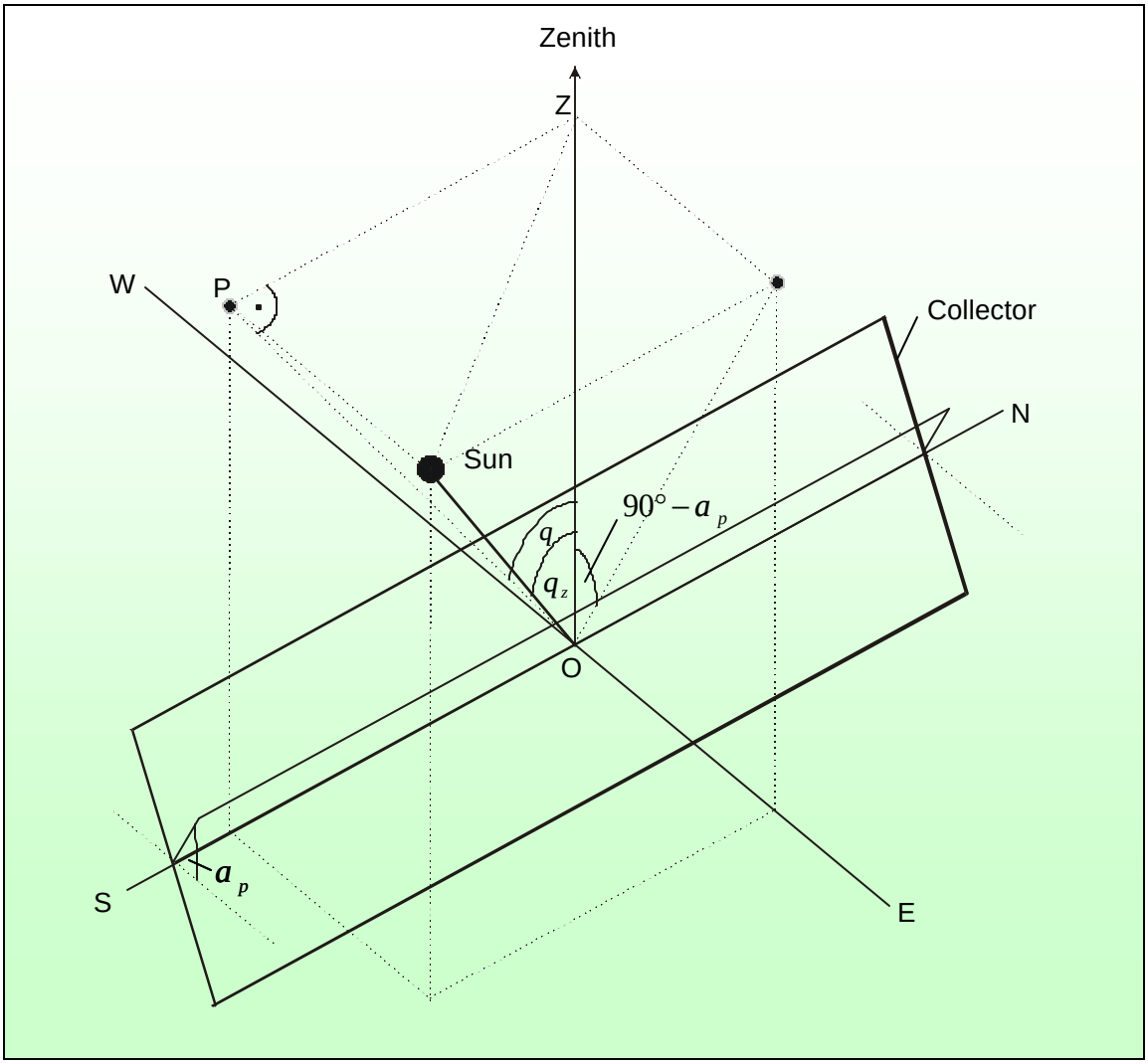

Figure 2.17: Geometric Considerations on the Collector

Inserting equation (2.61) into equation (2.59) yields an equation for x:

$$x = \frac{L_{Spacing}}{W}\frac{\cos(q_z)}{\cos(q)}, \tag{2.62}$$

where it is necessary to restrict x to be in the interval between 0 and 1:

$$x = \min\left[\max\left(0.0\,;\,\frac{L_{Spacing}}{W}\frac{\cos(q_z)}{\cos(q)}\right);1.0\right]. \tag{2.63}$$

The equation for the effective width, W_{eff}, is finally given through inserting equation (2.63) into equation (2.58),

$$W_{eff} = \min\left[\max\left(0.0\,;\,\frac{L_{Spacing}}{W}\frac{\cos(q_z)}{\cos(q)}\right);1.0\right]\cdot W\,. \tag{2.64}$$

After discussing the optical energy losses due to the tracking geometry and shading, additional optical energy losses due to radiation characteristics of the mirror, the envelope and the absorber have to be accounted.

First, the incident solar beam radiation is reflected on the trough mirror and directed onto the HCE. Two cases of reflection occur, specular reflection and diffuse reflection (Duffie & Beckman, 1991). The diffuse reflection distributes the radiation in all directions and thus the part of the incident solar beam radiation that is reflected through diffuse reflection on the trough mirrors does not contribute noticeably to the beam radiation acting on the absorber. The specular reflected part of the incident solar beam radiation is the remaining source for absorbed solar energy. The specular reflectance, r, is defined as the fraction of the specular reflected beam radiation to the incident solar beam radiation on the trough mirror. Measurements of the specular reflectance, r, accomplished at a test facility at SANDIA, yield a value of $r = 0.94$.

The remaining specular reflected solar beam radiation is transmitted through the glass envelope of the HCE before it is absorbed. When radiation passes from one medium with a

particular refractive index to a second medium with a different refractive index, there is reflection occurring at the interface between the two media (Duffie & Beckman, 1991). A part of the incoming radiation is reflected while the remaining part enters the second medium. The glass envelope of the HCE is a cover with two interfaces to cause reflection losses. A part of the incoming solar beam radiation is reflected at the first interface as discussed before. The remaining part is passed through the glass where it reaches the second interface. Of the remaining part, a portion passes through the second interface and the other portion is reflected back to the first interface, and so on. Summing up the parts of the solar beam radiation that passed through the second interface yields the amount of radiation that may be absorbed by the absorber when absorption of the glass envelope is neglected. If it is not neglected, then there is an additional absorption loss through the glass material and the remaining solar beam radiation acting on the absorber is even further reduced. The definition of the transmittance, t , accounts for the radiation losses through reflection and absorption of the glass envelope. The transmittance, t , is the fraction of the remaining solar beam radiation after transmission through the glass envelope to the incoming specular reflected solar beam radiation. The transmittance, t , was measured to $t = 0.915$.

Finally, the reflected and transmitted solar beam radiation is absorbed by the surface of the absorber tube in the HCE. The absorptance, a , is defined as the fraction of the solar beam radiation absorbed by the surface over the incoming reflected and transmitted solar beam radiation. SANDIA measured the absorptance, a , to be $a = 0.94$.

In the annulus between the absorber tube and the glass envelope, the radiation, which is not absorbed by the absorber but instead reflected back to the glass envelope, is partially reflected at the glass envelope back to the absorber again where part of it may now be

absorbed. That's why there is a slight increase of the absorbed solar beam radiation compared to the radiation from single absorption, accounted through the definition of the transmittance-absorptance product (ta) (Duffie & Beckman, 1991). For most practical solar collectors, a reasonable approximation is

$$(ta) \cong 1.01ta \ . \tag{2.65}$$

Combining the results from above, the optical efficiency from radiation characteristics is

$$e_{opt} = r\,(ta) \ . \tag{2.66}$$

Finally, an expression for the absorbed solar energy is found:

$$q_{absorbed} = G_{bn}\,F(\cos q)\,W_{eff}\,e_{opt}\,g \ . \tag{2.67}$$

In equation (2.67), g is a factor varying from one day to the other. Different amount of dirt on the mirrors and the number of broken collectors in the field influence this factor.

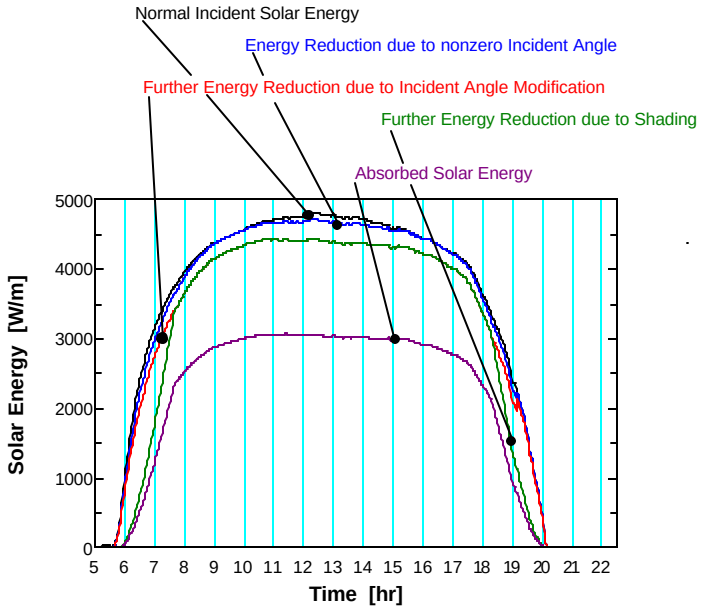

Figure 2.18: The way from Normal Incident Solar Energy to Absorbed Solar Energy considering Optical Losses for June 20, 1998

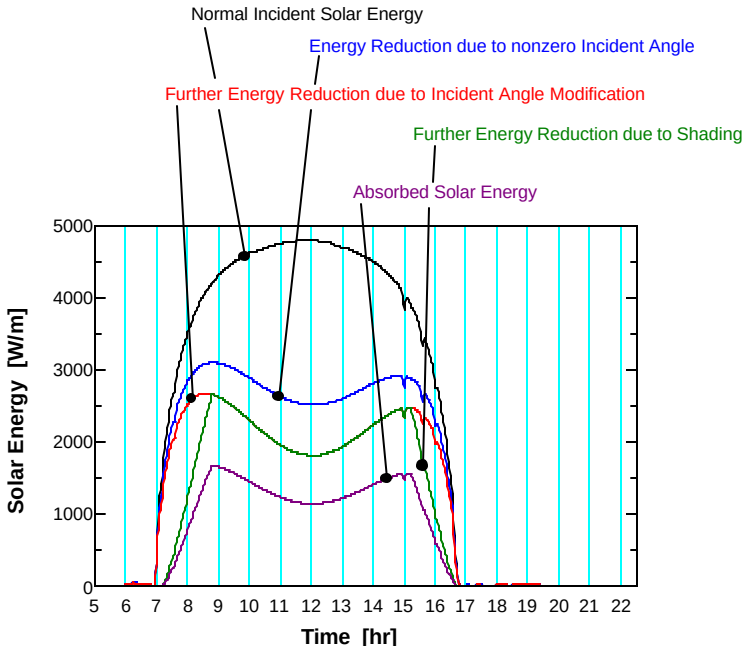

Figure 2.19: The way from Normal Incident Solar Energy to Absorbed Solar Energy considering Optical Losses for December 16, 1998

Figure 2.18 shows step by step the effect of all the optical losses discussed above for June 20, 1998. Starting with a plot for the normal incident solar energy vs. time, that is the solar energy that would be gained from the solar beam radiation without any optical losses, the reduced energy due to a nonzero incident angle from single-axis tracking is plotted in the same graph as well. Additional energy reduction, accounted by the incident angle modification leads to a third plot. The influence of shading on the energy after incident angle modification is shown in a fourth plot. Finally, the fifth curve shows the absorbed energy remaining after the additional energy loss due to radiation characteristics and broken collectors. It can be seen that the optical losses induce an energy reduction from the normal incident solar energy to the absorbed solar energy of about 36% at solar noon for June 20,

1998. The result is worse for December 16, 1998, shown in Figure 2.19, where the reduction is about 76% at solar noon.

2.3 Model Implementation and Simulation Results

The equations and expressions discussed above form a physical model for the trough collector field. This model can be used to predict the outlet temperature vs. time of the collector field when the inlet temperature of the collector field, the volume flow rate of the HTF and environmental data vs. time are known. The environmental data consist of normal incident solar radiation, ambient temperature and wind speed. Figure 2.20 shows the collector model as a block with inputs and the output. An accurate calculation of the collector field outlet temperature is necessary because the objective of the control problem is to hold this particular temperature at a constant value. Solutions of the partial differential equations (PDEs), (2.6), (2.11) and (2.13), have to be found in order to calculate the collector field outlet temperature. Analytical solutions are not possible due to the nonlinearity and complexity of the PDEs. Therefore, numerical integration was chosen for the calculation strategy. Hence, the equations from above have to be prepared for an implementation in digital machines.

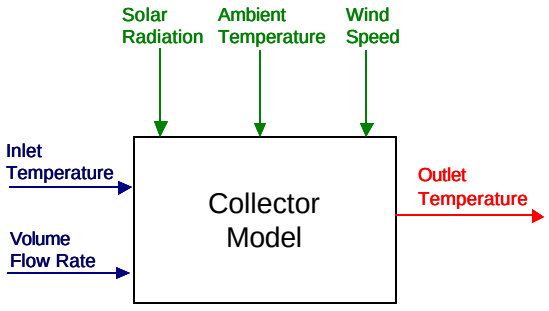

Figure 2.20: The Collector Model as a Block with Inputs and Output

2.3.1 Implementation in Digital Machines

The temperature of the HTF, T_{HTF}, the temperature of the absorber, T_{ABS}, and the temperature of the envelope, T_{ENV}, are functions of time and position on the HCE. Again, their values are determined by the PDEs (2.6), (2.11) and (2.13). Simulation software for digital machines usually provides integrators to solve nonlinear first order ordinary differential equations (ODEs). Consequently, it is useful to approximate the partial differential equations (PDEs) into a set of first order ODEs.

The set of ODEs is obtained by dividing the HCE of length $Length$ into j_0 different parts of length Δz (Figure 2.21), where

$$\Delta z = \frac{Length}{j_0}. \tag{2.68}$$

The following approximation is made:

$$\frac{\partial T_{HTF}(z,t)}{\partial z} \approx \frac{T_{HTF,j}(t) - T_{HTF,j-1}(t)}{\Delta z} \qquad , j = 1,2,..., j_0. \tag{2.69}$$

This approximation is inserted into equation (2.6). The result is a set of ODEs for the HTF temperature,

$$\begin{aligned}\frac{dT_{HTF,j}(t)}{dt} = &-\frac{\dot{V}_{HTF}(t)}{A_{ABS,i}\, n_{Collectors}\, \Delta z} T_{HTF,j}(t) \\ &+ \frac{r_{HTF}(T_{HTF,j-1})\, c_{HTF}(T_{HTF,j-1})\, \dot{V}_{HTF}(t)}{r_{HTF}(T_{HTF,j})\, c_{HTF}(T_{HTF,j})\, A_{ABS,i}\, n_{Collectors}\, \Delta z} T_{HTF,j-1}(t) \\ &+ \frac{1}{r_{HTF}(T_{HTF,j})\, c_{HTF}(T_{HTF,j})\, A_{ABS,i}} q_{gained}\left(T_{HTF,j}(t), T_{ABS,j}(t)\right)\end{aligned} \tag{2.70}$$

with the boundary condition

$$T_{HTF,0}(t) = T_{HTF,inlet}(t) \tag{2.71}$$

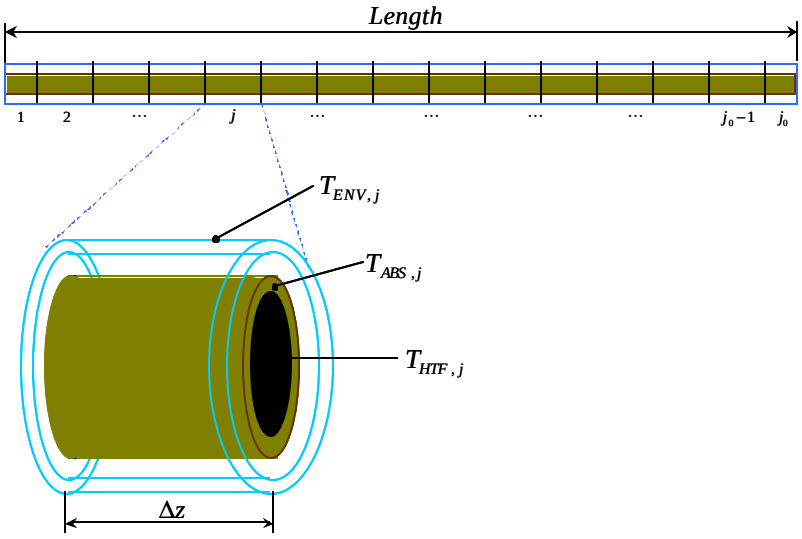

Figure 2.21: Discretization of the HCE

and the initial condition

$$T_{HTF,j}(0) = T_{HTFinit}(z_j), \qquad z_j = j \cdot \Delta z, \qquad j = 1,2,\ldots, j_0. \tag{2.72}$$

For every discrete element of the HCE with length Δz, there is an absorber temperature, $T_{ABS,j}$, determined by the ODE

$$\frac{dT_{ABS,j}(t)}{dt} = \frac{1}{r_{ABS}\, c_{ABS}\, A_{ABS}} \left[q_{absorbed}(t) - q_{internal}\left(T_{ABS,j}(t), T_{ENV,j}(t)\right) - q_{gained}\left(T_{ABS,j}(t), T_{HTF,j}(t)\right) \right], \tag{2.73}$$

with the initial condition

$$T_{ABS,j}(0) = T_{ABS,init}(z_j), \qquad z_j = j \cdot \Delta z, \qquad j = 1,2,\ldots, j_0. \tag{2.74}$$

There is also an envelope temperature, $T_{ENV,j}$, for every discrete element of the HCE, calculated from the ODE

$$\frac{dT_{ENV,j}(t)}{dt} = \frac{1}{r_{ENV}\, c_{ENV}\, A_{ENV}} \left[q_{internal}\left(T_{ABS,j}(t), T_{ENV,j}(t)\right) - q_{external}\left(T_{ENV,j}(t), T_{amb}(t)\right) \right] \tag{2.75}$$

with the initial condition

$$T_{ENV,j}(0) = T_{ENV,init}(z_j), \qquad z_j = j \cdot \Delta z, \qquad j = 1,2,..., j_0 . \tag{2.76}$$

The set of ODEs, consisting of equations (2.70), (2.73) and (2.75), and the related initial and boundary conditions were implemented in the EES (Engineering Equation Solver) simulation environment (Klein, 2001), together with the model equations for the heat transfer and the absorbed solar energy discussed above.

2.3.2 Simulation Results and Model Validation

The block diagram of the collector model in Figure 2.20 is useful to represent the model that is implemented in EES. The inputs for the implemented model, shown in Figure 2.20, are measured data from the real SEGS VI plant. Again, these inputs are the trough collector field inlet temperature (Figure 2.22), the volume flow rate (Figure 2.23), the direct normal beam radiation (Figure 2.24), the ambient temperature (Figure 2.25) and the wind speed (Figure 2.26). The following figures show the input values vs. time for September 19, 1998, which is a clear day, and for December 14, 1998, which is a partly cloudy day.

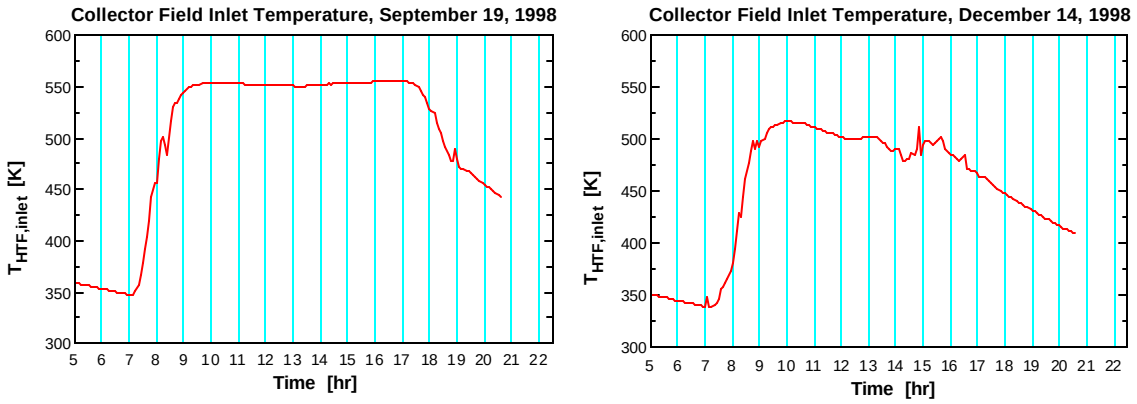

Figure 2.22: Measured Trough Collector Field Inlet Temperature for September 19, 1998 and for December 14, 1998.

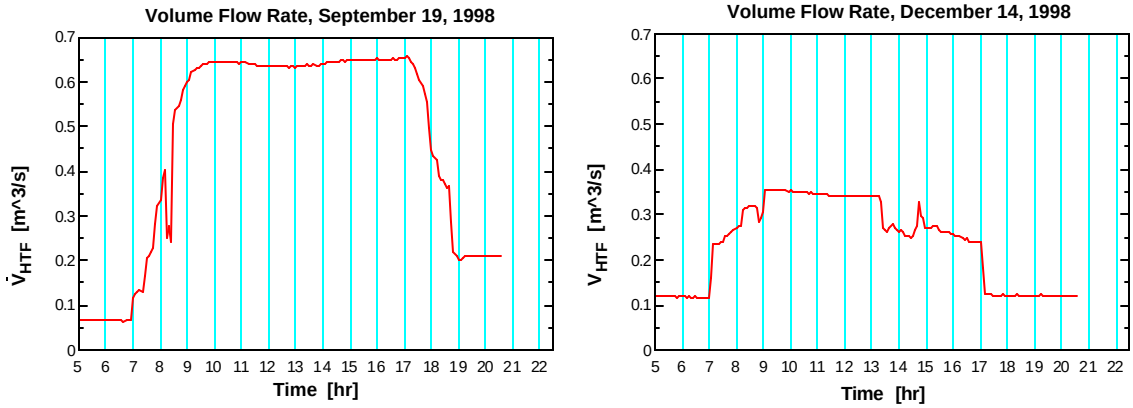

Figure 2.23: Measured Volume Flow Rate for September 19, 1998 and for December 14, 1998.

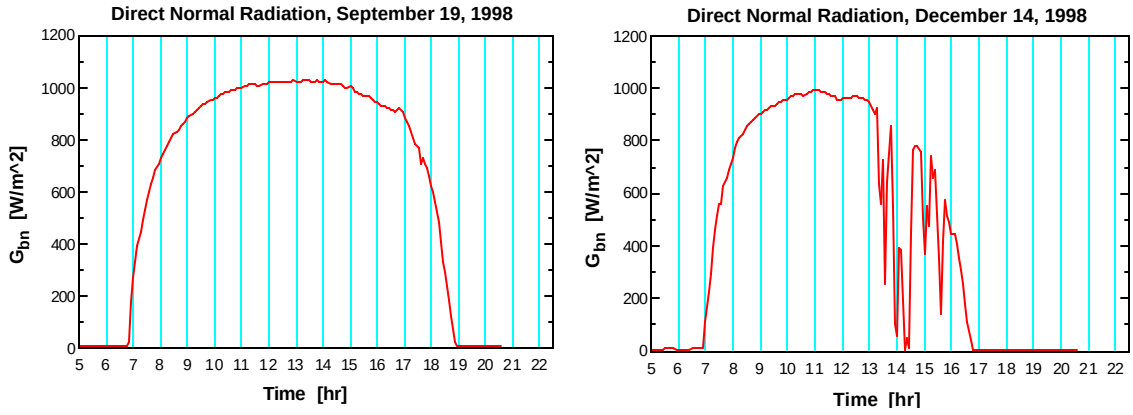

Figure 2.24: Measured Direct Normal Radiation for September 19, 1998 and for December 14, 1998.

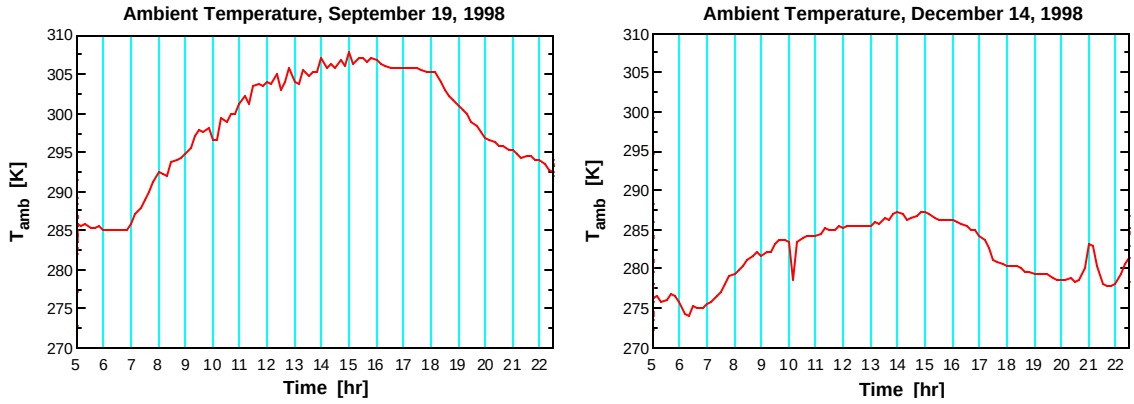

Figure 2.25: Measured Ambient Temperature for September 19, 1998 and for December 14, 1998.

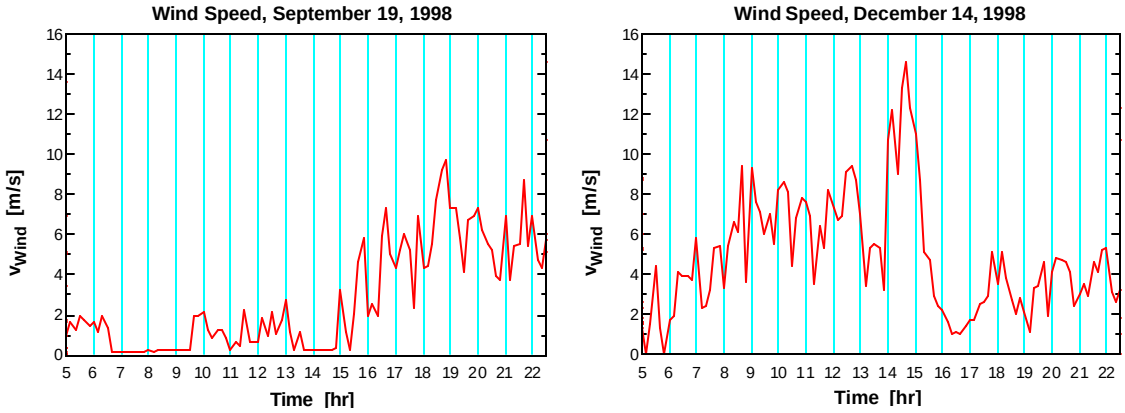

Figure 2.26: Measured Wind Speed for September 19, 1998 and for December 14, 1998.

The trough collector field outlet temperature is calculated through simulations with the model and compared with measured data of the collector outlet temperature at SEGS VI.

Figure 2.27 shows the calculated collector outlet temperature vs. the measured collector outlet temperature for June 20, 1998. The calculated values, given through the solid line, match the measured values, represented by the dashed line, very well. June 20, 1998 is a clear day with good weather conditions. For another clear day, September 19, 1998, there is also good agreement between calculated and predicted values (Figure 2.28). The same is true for December 16, 1998 (Figure 2.29).

Figure 2.30 shows the calculated collector outlet temperature vs. the measured collector outlet temperature for the partially cloudy day, December 14, 1998. Slight differences between the calculated and the measured temperatures occur at points where the slope of the temperature curve changes sign (local temperature minima and maxima). However, the overall match between the calculated outlet temperature and the measured outlet temperature is good and verifies that the implemented model is useful as a model for the real SEGS VI trough collector field.

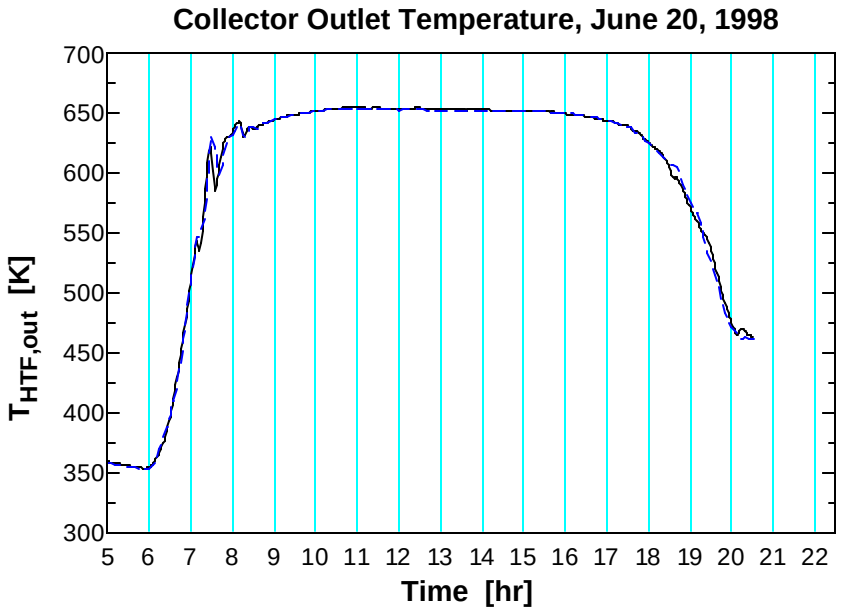

Figure 2.27: Calculated Collector Outlet Temperature vs. Time (solid line) and Measured Collector Outlet Temperature vs. Time (dashed line) on June 20, 1998

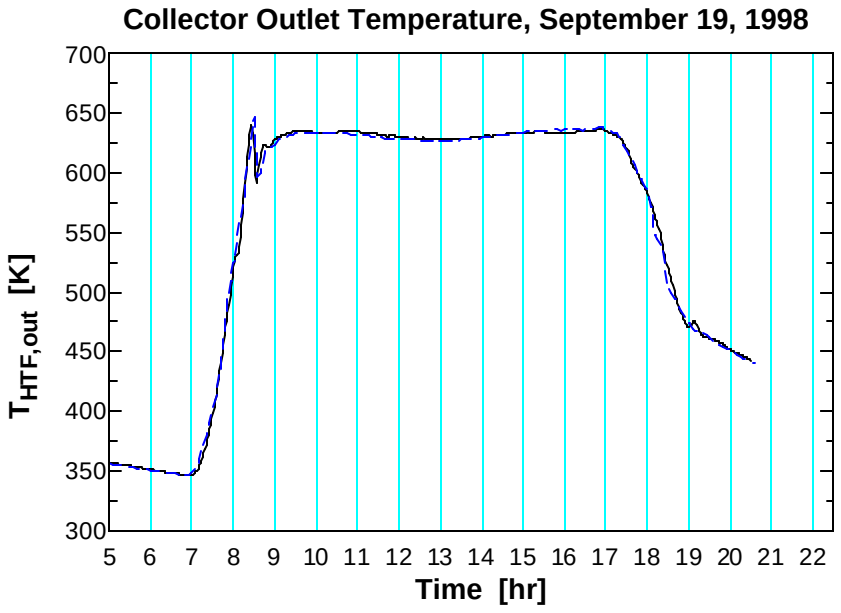

Figure 2.28: Calculated Collector Outlet Temperature vs. Time (solid line) and Measured Collector Outlet Temperature vs. Time (dashed line) on September 19, 1998

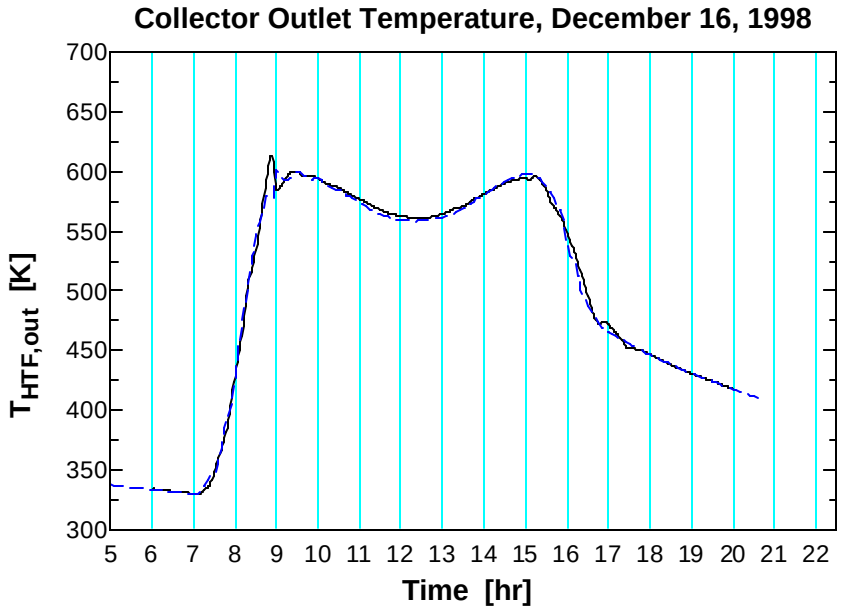

Figure 2.29: Calculated Collector Outlet Temperature vs. Time (solid line) and Measured Collector Outlet Temperature vs. Time (dashed line) on December 16, 1998

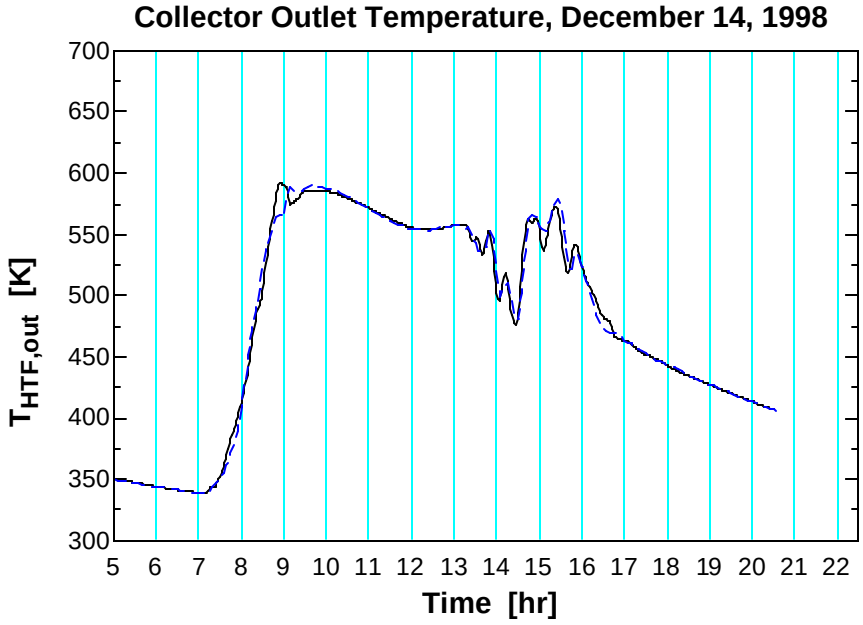

Figure 2.30: Calculated Collector Outlet Temperature vs. Time (solid line) and Measured Collector Outlet Temperature vs. Time (dashed line) on December 14, 1998

Chapter 3

Power Plant Model

3.1 Introduction

After the hot HTF leaves the trough collector field, it flows into the power plant. The part of the SEGS plant that represents the power plant is shown in Figure 3.1.

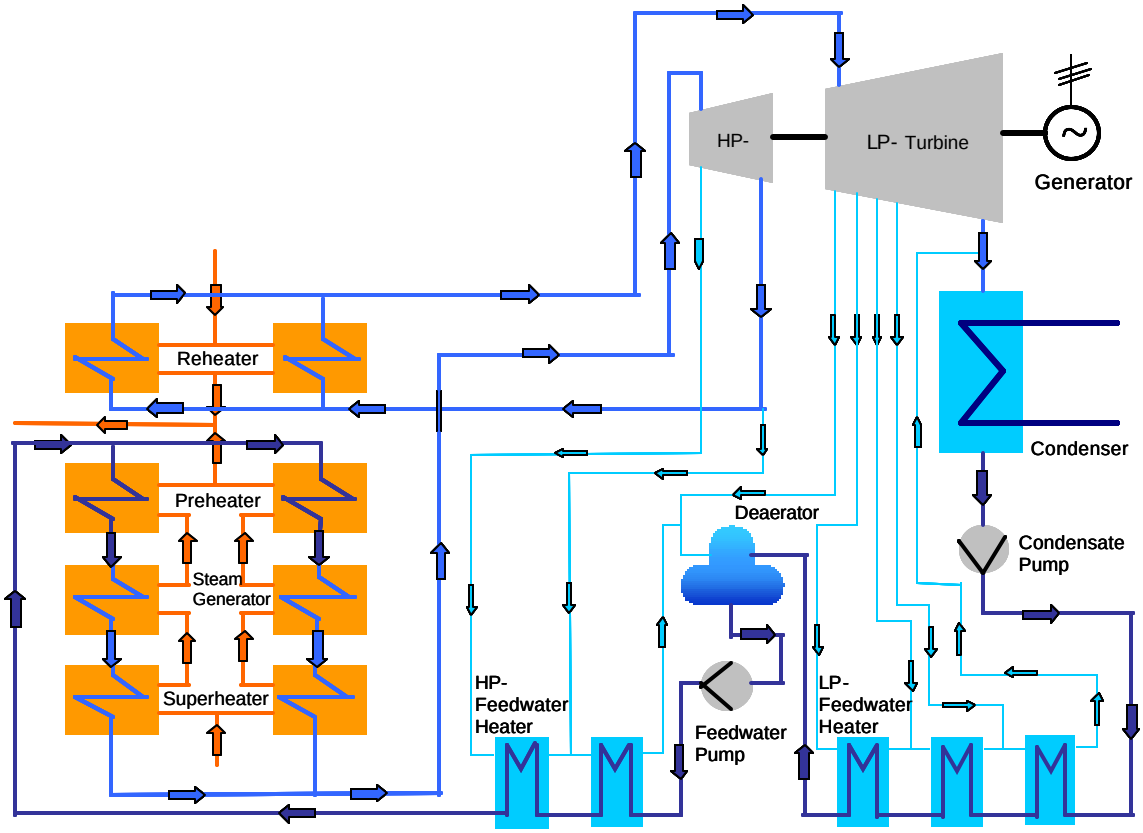

Figure 3.1: The Power Plant Part of SEGS VI

Figure 3.1 shows the power plant in pure solar mode. Pure solar mode means that nothing other than solar energy is used to heat the power plant working fluid. At SEGS VI, an additional natural-gas-fired boiler is also used to heat the working fluid when no or insufficient solar energy is available. This combined cycle mode is not considered in this work and thus the gas-fired boiler is not included in the figure.

The power plant's working fluid is water or steam. The power plant cycle is a Clausius-Rankine cycle with feedwater heating, superheating and reheating: the working fluid leaves the condenser as a condensate and is pressurized by the condensate pump to a pressure sufficient to pass through the low-pressure feedwater heaters and the deaerator. Afterwards, the water is heated up in the three low-pressure feedwater heaters through hot steam extractions withdrawn from the low-pressure turbine. The water then enters the deaerator (open or direct-contact feedwater heater) where it is mixed with hot steam from the first extraction of the low-pressure turbine. Through the mixing with steam, the efficient removal of noncondensables as well as the heating of the water occurs. Since the pressure in the deaerator cannot exceed the extraction pressure from the first extraction of the low-pressure turbine, a feedwater pump after the deaerator pumps the water to a higher pressure to allow the working fluid to pass through the following high-pressure feedwater heaters and enter the heat exchanger trains. The water is further warmed up in the two high-pressure feedwater heaters through steam extractions from the high-pressure turbine before it is split upon entering the two heat exchanger trains. A heat exchanger train consists of a preheater (economizer), a boiler (steam generator) and a superheater. The water hat was warmed up through feedwater heating enters now the preheater, which is a counterflow heat exchanger, and is heated by heat exchange with the hot HTF. The working fluid that leaves the preheater

enters the steam generator and is essentially in the saturated liquid state. In the steam generator or boiler, the working fluid changes its state from liquid to vapor through the heat energy transmitted by the hot HTF. Leaving the steam generator, the saturated steam flows into the superheater. The superheater is also a counterflow heat exchanger and the steam is superheated through heat exchange with the hot HTF that is directly coming from the collector field. The steam generated from both heat exchanger trains merges and is expanded in a high-pressure section of the turbine, after which it is split before entering two reheaters. Here, the incoming steam is reheated to a temperature near that of the superheated steam before the expansion. The reheated and merged steam now expands in the low-pressure section of the turbine to the condenser pressure. While the steam is expanding in the turbine, electricity is generated in a generator connected with the turbine. The completely expanded fluid is cooled down to saturated water by heat rejection to a cooling-water in the condenser.

A conventional Clausius-Rankine cycle does not include superheating, reheating and feedwater heating. From the Carnot cycle it is known, that heat addition at a higher temperature improves a cycle's thermal efficiency (as long as the condensate temperature remains the same). The heat addition for the Clausius-Rankine cycle in view takes place mainly in the two heat exchanger trains. Through feedwater heating, the temperature at which the water enters the heat exchanger trains is higher than it would be without feedwater heating. Thus the average temperature at which the heat is added is higher and the cycle efficiency goes up. The effect of superheating and reheating is not necessarily a higher cycle thermal efficiency because instead of using the heat for superheating, one could have used the same heat to generate saturated steam at a higher temperature. The beneficial effect of

superheating and reheating, however, is a drier steam at the turbine exhaust that leads to less erosion at the turbine blades.

The Clausius-Rankine cycle of SEGS VI as described above was modeled in order to obtain a model of the entire plant. A steady-state model is presented, developed from measured power plant data and from a report by Lippke on the power plant design conditions (Lippke, 1995). With the exception of heat exchangers, steady-state models for the power plant devices seem to be reasonable for the entire plant model since the dynamics of these systems are much faster compared to the dynamic of the HTF mass circulating in the whole solar trough collector field.

3.2 Modeling of the Power Plant

3.2.1 Simplifications

Before a steady-state model for each part of the power plant is discussed, the Clausius-Rankine cycle is simplified as shown in Figure 3.2 for easier modeling.

First, the heat exchanger train is considered to be a single heat exchanger instead of being divided into preheater, steam generator and superheater. It is not assured that the working fluid's state between preheater and steam generator and between steam generator and superheater is defined. This means that the working fluid is not necessarily leaving the preheater as saturated liquid or entering the superheater as saturated vapor. Treating the heat exchanger train as a single heat exchanger avoids dealing with this uncertainty. It is now assumed that pure water is entering the single heat exchanger and superheated steam is leaving it. But even this assumption may not be satisfied for the start-up period of the plant in

the early morning and in the late evening during the plant's shut-down period when solar energy is low.

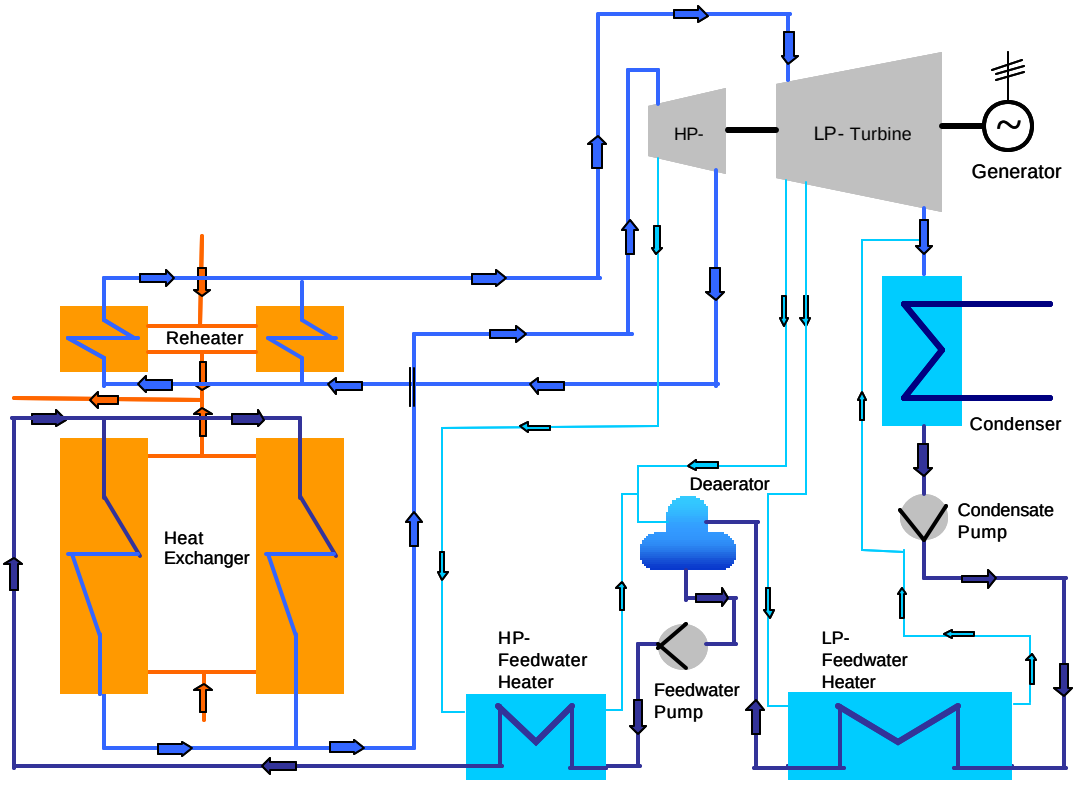

Figure 3.2: Simplification in the Power Plant Structure

Second, the three low-pressure feedwater heaters are combined to a single low-pressure feedwater heater and the two high-pressure feedwater heaters are combined to a single high-pressure feedwater heater. This approximation seems reasonable as long as the state of the water that enters the HTF heat exchangers is comparable to the state the water would have obtained if it traveled through each of the five feedwater heaters. In addition, appropriate combined average extractions from the turbine have to be found. The state of the condensate

entering the single low-pressure feedwater heater must be comparable to its state in the non-simplified system as well.

The structure of the simplified power plant is presented again in Figure 3.3, together with numbers to define the different states in the power plant.

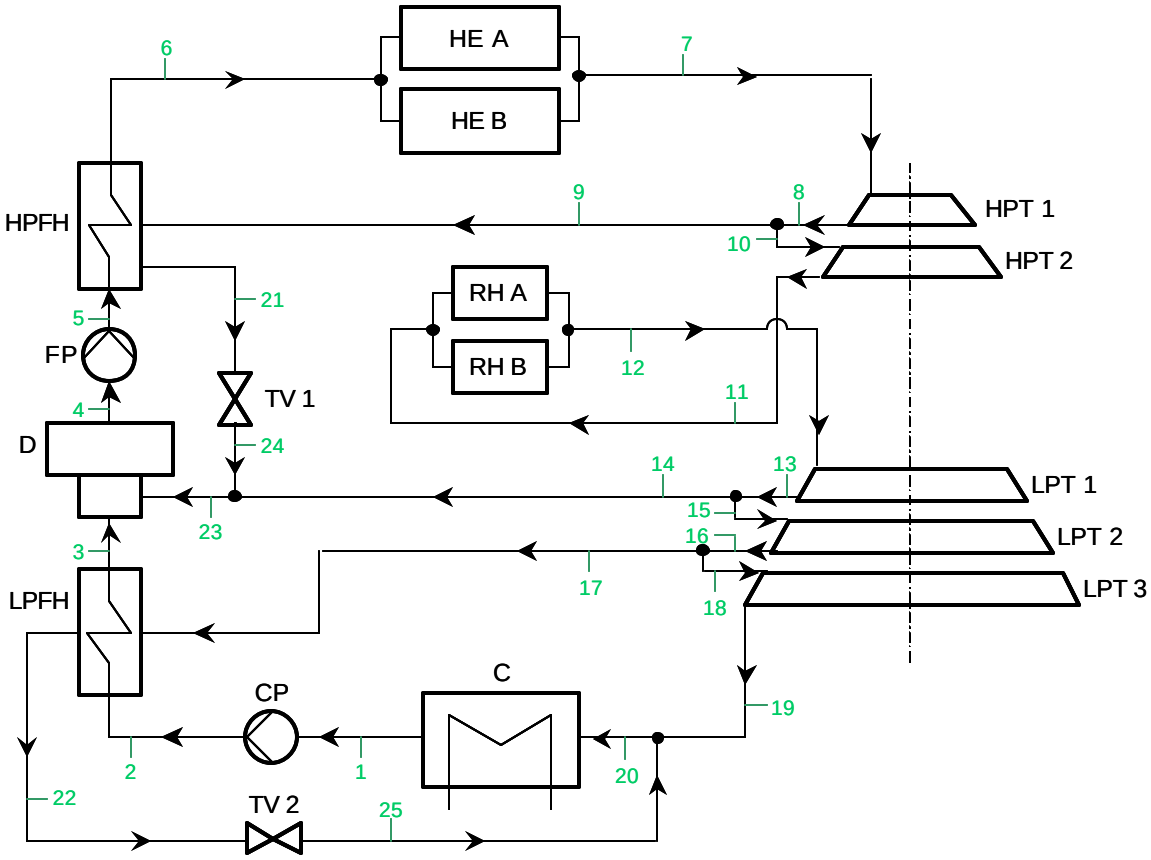

Figure 3.3: Simplified Power Plant Structure

In order to obtain a better understanding of the process, a T-s diagram is plotted for June 20, 1998 at 1.00pm. The temperatures and entropies in the diagram were calculated with the power plant model, which is presented in the next section.

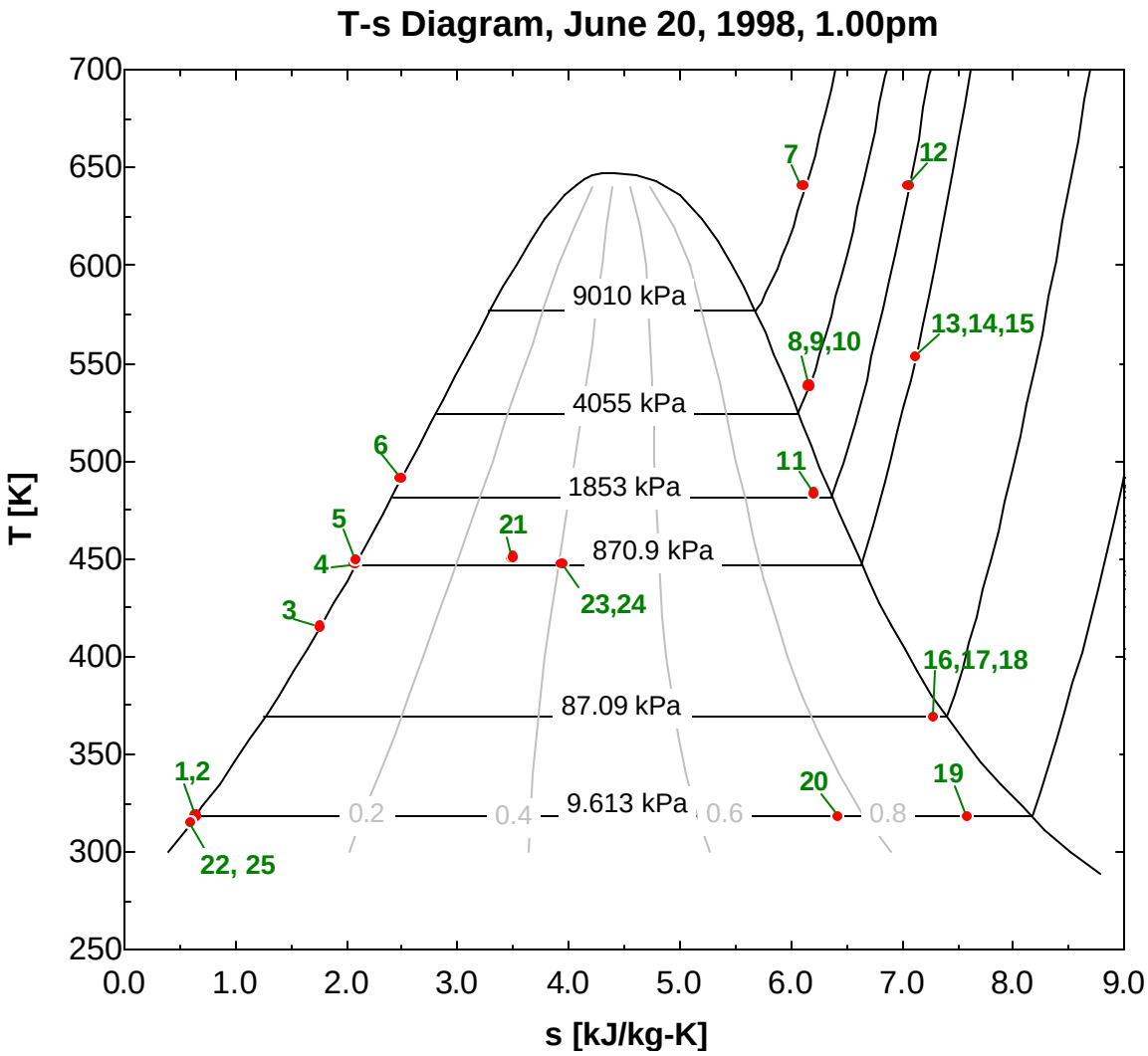

Figure 3.4: T-s diagram for the power plant Clausius-Rankine cycle

3.2.2 Modeling

3.2.2.1 Condensate Pump CP and Feedwater Pump FP

The pumps are assumed to be adiabatic, but not adiabatic reversible (El-Wakil, 1984). The internal irreversibility is primarily the result of fluid friction occurring in the pump. Thus the actual work in CP, $h_2 - h_1$, is greater than the adiabatic reversible work, $h_{2,rev} - h_1$, - the pump absorbs more work. The pump irreversibility is represented by a pump isentropic efficiency, h_{isCP}, which is given by the ratio of the ideal work to the actual work

$$h_{isCP} = \frac{h_{2,rev} - h_1}{h_2 - h_1}. \tag{3.1}$$

The enthalpy, $h_{2,rev}$, gained if the process would be adiabatic reversible, is calculated from fluid property functions as the enthalpy of water with the entropy s_1 at the pressure p_2:

$$h_{2,rev} = f_h\left(\text{Water},\ S = s_1,\ P = p_2\right). \tag{3.2}$$

The entropy s_1 is known from equation (3.112) and the pressure p_2 is calculated through equation (3.63). The EES inbuilt fluid property functions (Klein, 2001) are used for the calculation of $h_{2,rev}$. Since the isentropic efficiency, h_{isCP}, is known from Lippke's report $h_{isCP} = 0.7125$, and the enthalpy h_1 is known from equation (3.108), equation (3.1) is used to calculate the enthalpy h_2. The temperature T_2 is also calculated from EES fluid property functions as the temperature of water with the enthalpy h_2 at the pressure p_2

$$T_2 = f_T\left(\text{Water},\ H = h_2,\ P = p_2\right). \tag{3.3}$$

The entropy s_2 is calculated from EES fluid property functions as well. It is the entropy of water with the enthalpy h_2 at the pressure p_2

$$s_2 = f_s\left(\text{Water},\ H = h_2,\ p = p_2\right). \tag{3.4}$$

Equations (3.1) – (3.4) define the model for the condensate pump CP. The same calculations are made for the feedwater pump FP. From Lippke's report, the isentropic efficiency, $h_{is,FP}$, is the same as for CP, $h_{is,FP} = 0.7125$, and

$$h_{is,FP} = \frac{h_{5,rev} - h_4}{h_5 - h_4} \tag{3.5}$$

where the enthalpy h_4 is known from equation (3.76). Correspondingly to equation (3.2),

$$h_{5,rev} = f_h\left(\text{Water},\ S = s_4,\ P = p_5\right) \tag{3.6}$$

with the entropy s_4 from equation (3.80) and the pressure p_5 from equation (3.89). Thus equation (3.5) is used to calculate the enthalpy h_5. Like for CP, the temperature T_5 and the entropy s_5 are calculated from EES fluid property functions

$$T_5 = f_T\left(\text{Water},\ H = h_5,\ P = p_5\right), \tag{3.7}$$

$$s_5 = f_s\left(\text{Water},\ H = h_5,\ p = p_5\right). \tag{3.8}$$

A mass balance completes the model equations for FP

$$\dot{m}_4 - \dot{m}_5 = 0. \tag{3.9}$$

Through equation (3.9), the mass flow rate $\dot{m}_4$ is determined since $\dot{m}_5$ is known from equation (3.85). Equations (3.5) – (3.9) define a model for FP.

In this implementation, a mass balance is not part of the model equations for CP. Measurements of the mass flow rates in the heat exchanger trains HE A and HE B are

available. In order to use these measured flow rates as possible inputs to the power plant model, the mass flow rates in all the different elements of the plant are calculated from $\dot{m}_6$ through mass balances for the devices following or preceding the heat exchanger trains HE A and HE B. Thus $\dot{m}_2$ is determined from $\dot{m}_3$ through a mass balance for the low-pressure feedwater heater LPFH, equation (3.61), and $\dot{m}_1$ is calculated from $\dot{m}_{20}$ through the condenser model, equation (3.110). An additional mass balance for CP would have resulted in an over-determined equation system for the mass flow rates.

3.2.2.2 High-Pressure Turbine HPT 1, HPT 2 and Low-Pressure Turbine LPT 1, LPT 2, LPT 3

Like in pumps, internal irreversibility in turbines is very important. The expansion process is assumed to be adiabatic, but due to the irreversibility, it is not considered to be adiabatic reversible (El-Wakil, 1984). For both, the high-pressure section and the low-pressure section of the turbine, exhaust is to the two-phase region. Hence the entropy increase in the turbine does not result in a temperature increase but in an increase in enthalpy. Taking the first high-pressure section of the turbine, HPT 1, as an example, the ideal work through expansion, if the turbine section were adiabatic reversible, is $h_7 - h_{8,rev}$, but the actual work is $h_7 - h_8$. The irreversible losses in the turbine are represented by an isentropic efficiency, i.e. for the high-pressure section, $h_{is,HPT\,1}$.

It is given by the ratio of the turbine's actual work to the turbine's ideal adiabatic reversible work

$$h_{is,HPT1} = \frac{h_7 - h_8}{h_7 - h_{8,rev}}. \tag{3.10}$$

The enthalpy $h_{8,rev}$ is calculated from EES fluid property functions as the enthalpy of steam with the entropy s_7 and the pressure p_8

$$h_{8,rev} = f_h\left(\text{Steam}, S = s_7, P = p_8\right), \tag{3.11}$$

where the entropy s_7 is calculated from equation (3.176) and the pressure p_8 is determined from p_7 and a constant pressure ratio, $R_{p,HPT1}$,

$$p_8 = p_7 \cdot R_{p,HPT1}. \tag{3.12}$$

The pressure p_7 in turn is known from equation (3.174). The enthalpy h_7 is calculated from equation (3.173), hence equation (3.10) is used to determine the enthalpy h_8. The temperature T_8 and the entropy s_8 are found through EES fluid property functions as the temperature and the entropy of steam with the enthalpy h_8 at the pressure p_8,

$$T_8 = f_T\left(\text{Steam}, H = h_8, P = p_8\right), \tag{3.13}$$

$$s_8 = f_s\left(\text{Steam}, H = h_8, P = p_8\right). \tag{3.14}$$

In order to calculate the mass flow rate $\dot{m}_8$, a mass balance has to be considered

$$\dot{m}_7 - \dot{m}_8 = 0. \tag{3.15}$$

The mass flow rate $\dot{m}_7$ is known from equation (3.171).

Equations (3.10) – (3.15) form the model for the high-pressure section HPT 1 together with the assumed isentropic efficiency, $h_{is,HPT1} = 0.84$ and the assumed constant pressure ratio, $R_{p,HPT1} = 0.45$.

There is a turbine extraction withdrawn between the two high-pressure sections HPT 1 and HPT 2. This fluid splitting is primarily modeled through the following mass balance

$$\dot{m}_8 - \dot{m}_9 - \dot{m}_{10} = 0. \tag{3.16}$$

It is assumed that the mass ratio between $\dot{m}_9$ and $\dot{m}_{10}$ is known, i.e. from the position of a splitting valve, and is given as a constant value

$$\frac{\dot{m}_9}{\dot{m}_{10}} = R_{\dot{m},HPT1}. \tag{3.17}$$

For June 20, 1998, the value of $R_{\dot{m},HPT1}$ is $R_{\dot{m},HPT1} = 0.1463$. This value changes for different days. The split streams are assumed to be in the mechanical and thermodynamic equilibrium:

$$T_8 = T_9 = T_{10}, \tag{3.18}$$

$$p_8 = p_9 = p_{10}, \tag{3.19}$$

$$h_8 = h_9 = h_{10}, \tag{3.20}$$

$$s_8 = s_9 = s_{10}. \tag{3.21}$$

Equations (3.16) – (3.21) describe the model for the extraction splitter between the two high-pressure turbine sections.

The equations for the turbine sections HPT 2, LPT 1, LPT 2 and LPT 3 are equivalent to equations (3.10) – (3.15) with the exception that the outlet pressure of the high-pressure

turbine part, p_{11}, and the outlet pressure of the low-pressure turbine part, p_{19}, are not calculated from a constant pressure ratio as in equation (3.12). They are rather calculated from a mass flow rate dependent overall pressure drop, Δp_{HP}, in the high-pressure part and in the low-pressure part, Δp_{LP} of the turbine, where

$$\begin{aligned}\Delta p_{HP} = {} & 0.190594967 + 0.00141797877 \cdot \dot{m}_7 \\ & - 0.0000218417721 \cdot \dot{m}_7^2\end{aligned}, \tag{3.22}$$

and

$$\begin{aligned}\Delta p_{LP} = {} & 0.00974136866 - 0.000321840787 \cdot \dot{m}_{12} \\ & + 0.00000548092767 \cdot \dot{m}_{12}^2\end{aligned}. \tag{3.23}$$

These polynomials are found from measurements of the turbine outlet pressures at different days. The mass flow rate $\dot{m}_{12}$ is known from equation (3.177).

Thus the set of equations for the turbine section HPT 2 is

$$h_{is,HPT\,2} = \frac{h_{10} - h_{11}}{h_{10} - h_{11,rev}}, \tag{3.24}$$

$$h_{11,rev} = f\left(\text{Steam},\, S = s_{10},\, P = p_{11}\right), \tag{3.25}$$

$$p_{11} = \frac{p_{10} \cdot \Delta p_{HP}}{R_{p,HPT1}}, \tag{3.26}$$

$$T_{11} = f_T\left(\text{Steam},\, H = h_{11},\, P = p_{11}\right), \tag{3.27}$$

$$s_{11} = f_s\left(\text{Steam},\, H = h_{11},\, P = p_{11}\right), \tag{3.28}$$

$$\dot{m}_{10} - \dot{m}_{11} = 0. \tag{3.29}$$

The isentropic efficiency is assumed to be $h_{is,HPT\,2} = 0.84$.

There exists a similar set of equations for the first low-pressure turbine section LPT 1:

$$h_{isLPT1} = \frac{h_{12} - h_{13}}{h_{12} - h_{13,rev}} \ , \tag{3.30}$$

where the enthalpy h_{12} is known from equation (3.179). Similarly to equation (3.11), it is

$$h_{13,rev} = f_h\left(\text{Steam},\ S = s_{12},\ P = p_{13}\right), \tag{3.31}$$

with the entropy s_{12} from equation (3.182).

The pressure p_{13} is determined from

$$p_{13} = p_{12} \cdot R_{pLPT1}, \tag{3.32}$$

where the pressure p_{12} is known from equation (3.180). The pressure ratio $R_{p,LPT1}$ is assumed to be constant with $R_{p,LPT1} = 0.47$. The remaining equations are

$$T_{13} = f_T\left(\text{Steam},\ H = h_{13},\ P = p_{13}\right), \tag{3.33}$$

$$s_{13} = f_s\left(\text{Steam},\ H = h_{13},\ P = p_{13}\right), \tag{3.34}$$

$$\dot{m}_{12} - \dot{m}_{13} = 0 . \tag{3.35}$$

The isentropic efficiency is assumed to be $h_{isLPT1} = 0.8376$.

The turbine extraction between the first low-pressure section LPT 1 and the second low-pressure section LPT 2 can be modeled equivalently to equations (3.16) – (3.21):

$$\dot{m}_{13} - \dot{m}_{14} - \dot{m}_{15} = 0 . \tag{3.36}$$

$$\frac{\dot{m}_{14}}{\dot{m}_{15}} = R_{\dot{m}LPT1} . \tag{3.37}$$

$$T_{13} = T_{14} = T_{15}, \tag{3.38}$$

$$p_{13} = p_{14} = p_{15}, \tag{3.39}$$

$$h_{13} = h_{14} = h_{15}, \tag{3.40}$$

$$s_{13} = s_{14} = s_{15}. \tag{3.41}$$

For June 20, 1998, the value of the mass ratio is $R_{\dot{m}LPT1} = 0.02$.

The set of equations for the second low-pressure section of the turbine, LPT 2, is

$$h_{isLPT2} = \frac{h_{15} - h_{16}}{h_{15} - h_{16,rev}}\ , \tag{3.42}$$

$$h_{16,rev} = f_h\left(\text{Steam},\ S = s_{15},\ P = p_{16}\right), \tag{3.43}$$

$$p_{16} = p_{15} \cdot R_{pLPT2}, \tag{3.44}$$

$$T_{16} = f_T\left(\text{Steam},\ H = h_{16},\ P = p_{16}\right), \tag{3.45}$$

$$s_{16} = f_s\left(\text{Steam},\ H = h_{16},\ P = p_{16}\right), \tag{3.46}$$

$$\dot{m}_{15} - \dot{m}_{16} = 0. \tag{3.47}$$

The isentropic efficiency is assumed to be $h_{isLPT2} = 0.8623$ and the assumed constant pressure ratio is $R_{p,LPT2} = 0.1$.

The turbine extraction between the second low-pressure section LPT 2 and the third low-pressure section LPT 3 is similarly modeled as above:

$$\dot{m}_{16} - \dot{m}_{17} - \dot{m}_{18} = 0. \tag{3.48}$$

$$\frac{\dot{m}_{17}}{\dot{m}_{18}} = R_{\dot{m}LPT2}. \tag{3.49}$$

$$T_{16} = T_{17} = T_{18}, \tag{3.50}$$

$$p_{16} = p_{17} = p_{18}, \tag{3.51}$$

$$h_{16} = h_{17} = h_{18}, \tag{3.52}$$

$$s_{16} = s_{17} = s_{18}\,. \tag{3.53}$$

For June 20, 1998, the value of the mass ratio is $R_{\dot{m}LPT2} = 0.2$.

Finally, the model equations for the last low-pressure turbine section, LPT 3, is given through

$$h_{isLPT3} = \frac{h_{18} - h_{19}}{h_{18} - h_{19,rev}}\,, \tag{3.54}$$

$$h_{19,rev} = f_h\left(\text{Steam},\, S = s_{18},\, P = p_{19}\right), \tag{3.55}$$

$$p_{19} = \frac{p_{18} \cdot \Delta p_{LP}}{R_{pLPT1} \cdot R_{pLPT2}}, \tag{3.56}$$

$$T_{19} = f_T\left(\text{Steam},\, H = h_{19},\, P = p_{19}\right), \tag{3.57}$$

$$s_{19} = f_s\left(\text{Steam},\, H = h_{19},\, P = p_{19}\right), \tag{3.58}$$

$$\dot{m}_{18} - \dot{m}_{19} = 0\,. \tag{3.59}$$

The isentropic efficiency is assumed to be $h_{isLPT3} = 0.7$.

3.2.2.3 Low-Pressure Feedwater Heater LPFH

The low-pressure feedwater heater, LPFH, is a closed-type feedwater heater with a backward drain. Feedwater heaters are usually shell-and-tube heat exchangers (El-Wakil, 1984) and since no information on the LPFH at SEGS VI was available, it is assumed to be a shell-and-tube heat exchanger as well. The feedwater passes through the tubes and the bled steam that comes from the turbine extraction between LPT 2 and LPT 3, is on the shell side and transfers its energy to the feedwater.

Thus an energy balance between the bled steam and the feedwater is the first equation for the LPFH model

$$\dot{m}_2 h_2 - \dot{m}_3 h_3 + \dot{m}_{17} h_{17} - \dot{m}_{22} h_{22} = 0 . \tag{3.60}$$

This equation determines the drain enthalpy h_{22} since the enthalpy h_2 is known from equation (3.1), the enthalpy h_3 is calculated with equation (3.82) and the enthalpy of the bled steam, h_{17}, is known from equation (3.52). The steam mass flow rate, $\dot{m}_{17}$, is calculated from equation (3.48) and (3.49). The feedwater mass flow rate, $\dot{m}_2$, is determined from the following mass balance that is part of the LPFH model

$$\dot{m}_2 - \dot{m}_3 = 0 . \tag{3.61}$$

The mass flow rate $\dot{m}_3$ comes from equation (3.81). The drain stream leaves the LPFH with the mass flow rate $\dot{m}_{22}$ from

$$\dot{m}_{17} - \dot{m}_{22} = 0 . \tag{3.62}$$

Pressure drops of the feedwater in feedwater heaters are usually large because of the flow friction in long small-diameter tubes. For the LPFH in view, the pressure p_2 is given through

$$p_3 = p_2 \cdot \Delta p_{LPFH} \tag{3.63}$$

where $\Delta p_{LPFH} = 0.5$ is assumed to be constant. The pressure p_3 is known from equation (3.78). The temperature T_3 and the entropy s_3 are found through EES fluid property functions as the temperature and the entropy of water with the enthalpy h_3 at the pressure p_3,

$$T_3 = f_T\left(\text{Water},\ H = h_3,\ P = p_3\right), \tag{3.64}$$

$$s_3 = f_s\left(\text{Water},\ H = h_3,\ P = p_3\right). \tag{3.65}$$

Equations (3.60) – (3.65) form the model for the low-pressure feedwater heater LPFH.

3.2.2.4 Deaerator D and Throttle Valve TV 1

The deaerator D is an open- or direct-contact feedwater heater where the extraction steam is mixed directly with the incoming feedwater to produce saturated water at the extraction steam pressure (El-Wakil, 1984). Before it enters D, the extraction steam that is withdrawn between LPT 1 and LPT 2, is mixed with the drain stream of the high-pressure feedwater heater HPFH. The higher pressured drain stream passes a throttle valve to reduce its pressure to the pressure of the turbine extraction steam before the two streams merge. The pressure of the turbine extraction steam, p_{14}, is calculated from equation (3.39) and thus

$$p_{24} = p_{14} \tag{3.66}$$

defines the outlet pressure of TV 1. No heat losses are assumed for TV 1, hence

$$h_{24} = h_{21} \tag{3.67}$$

and the temperature is assumed to stay constant:

$$T_{24} = T_{21}\,. \tag{3.68}$$

The drain enthalpy h_{21} is calculated from equation (3.86) and the drain temperature T_{21} is known from equation (3.93). A mass balance on TV 1 yields

$$\dot{m}_{21} - \dot{m}_{24} = 0\,, \tag{3.69}$$

where the drain mass flow rate, $\dot{m}_{21}$, comes from equation (3.84).

The outlet entropy of TV1, s_{24}, is calculated with EES fluid property functions as the entropy of steam with the enthalpy h_{24} at the pressure p_{24}:

$$s_{24} = f_s(\text{Steam}, H = h_{24}, P = p_{24}). \tag{3.70}$$

Equations (3.66) – (3.70) are the TV 1 model equations.

The throttle's outlet stream merges with the extraction steam of the turbine. Thus the fluid that enters D at the steam side has the mass flow rate $\dot{m}_{23}$ from

$$\dot{m}_{14} + \dot{m}_{24} - \dot{m}_{23} = 0\,. \tag{3.71}$$

The extraction mass flow rate $\dot{m}_{14}$ is known from equations (3.36) and (3.37). The enthalpy of the steam entering D, h_{23}, is determined from the following energy balance

$$\dot{m}_{14}h_{14} + \dot{m}_{24}h_{24} - \dot{m}_{23}h_{23} = 0\,, \tag{3.72}$$

where the extraction steam enthalpy, h_{14}, is known from equation (3.40). The merging streams are in a mechanical equilibrium and hence

$$p_{23} = p_{14}\,. \tag{3.73}$$

The steam-side inlet temperature, T_{23}, is calculated with EES fluid property functions as the temperature of steam with enthalpy h_{23} at the pressure p_{23}:

$$T_{23} = f_T(\text{Steam},\ H = h_{23},\ P = p_{23})\,. \tag{3.74}$$

The steam-side inlet entropy, s_{23}, is also calculated with EES fluid property functions as the entropy of steam with the enthalpy h_{23} at the pressure p_{23}:

$$s_{23} = f_s(\text{Steam}, H = h_{23}, P = p_{23})\,. \tag{3.75}$$

Equations (3.71) – (3.75) form the model equations for the merging of the turbine extraction stream with the HPFH drain stream.

The deaerator is supposed to produce saturated feedwater at the extraction steam pressure. Thus the enthalpy of the saturated feedwater, h_4, is calculated from EES fluid property functions as the enthalpy of saturated water at the pressure p_{23}:

$$h_4 = f_h\left(\text{Steam},\ P = p_{23},\ X = 0\right). \tag{3.76}$$

This assumption includes that the feedwater outlet pressure of D, p_4, is the same as the steam inlet pressure p_{23},

$$p_4 = p_{23}. \tag{3.77}$$

In addition, no pressure drop in the feedwater is assumed

$$p_3 = p_4. \tag{3.78}$$

Thus the feedwater outlet temperature, T_4, can be calculated from EES property functions as the temperature of steam with the enthalpy h_4 at the pressure p_4,

$$T_4 = f_T\left(\text{Steam},\ H = h_4,\ P = p_4\right). \tag{3.79}$$

Also the feedwater outlet entropy, s_4, is calculated from fluid property functions as the entropy of steam with the enthalpy h_4 at the pressure p_4,

$$s_4 = f_s\left(\text{Steam},\ H = h_4,\ P = p_4\right). \tag{3.80}$$

A mass balance on D has to account for the fact that the feedwater inlet stream and the steam inlet stream are mixed together and form the feedwater outlet stream. The feedwater inlet stream has the mass flow rate $\dot{m}_3$ from

$$\dot{m}_3 + \dot{m}_{23} - \dot{m}_4 = 0, \tag{3.81}$$

where the mass flow rate $\dot{m}_4$ is known from equation (3.9) and the steam mass flow rate $\dot{m}_{23}$ is determined from equation (3.71). The following energy balance is used to find a value for the feedwater inlet enthalpy, h_3,

$$\dot{m}_3 h_3 + \dot{m}_{23} h_{23} - \dot{m}_4 h_4 = 0 . \tag{3.82}$$

Equations (3.76) – (3.82) form the model equations for the deaerator D.

3.2.2.5 High-Pressure Feedwater Heater HPFH

The high-pressure feedwater heater HPFH is like the LPFH a closed-type feedwater heater with a backward drain. Assuming again a shell-and-tube heat exchanger (El-Wakil, 1984), an energy balance is established between the bled steam and the feedwater

$$\dot{m}_5 h_5 - \dot{m}_6 h_6 + \dot{m}_9 h_9 - \dot{m}_{21} h_{21} = 0 . \tag{3.83}$$

Through this equation, the feedwater outlet enthalpy, h_6, is calculated since the extraction enthalpy, h_9, is determined from equation (3.20) and the feedwater inlet enthalpy, h_5, is given through equation (3.5). The extraction mass flow rate, $\dot{m}_9$, is calculated from equations (3.16) and (3.17). The drain mass flow rate, $\dot{m}_{21}$, follows from

$$\dot{m}_9 - \dot{m}_{21} = 0 . \tag{3.84}$$

The feedwater mass flow rate, $\dot{m}_5$, is determined from the following mass balance for the feedwater

$$\dot{m}_5 - \dot{m}_6 = 0 \tag{3.85}$$

where the mass flow rate $\dot{m}_6$ is an input of the power plant model.

The drain enthalpy, h_{21}, is calculated from an effectiveness equation for HPFH

$$e_{HPFH} = \frac{h_9 - h_{21}}{h_9 - h_5}, \tag{3.86}$$

From measurements of the water inlet conditions and steam outlet conditions of the heat exchanger trains A and B (HE A and HE B), it seems that the effectiveness, e_{HPFH}, is a function of the fraction of the two inlet mass flow rates, $\frac{\dot{m}_9}{\dot{m}_5}$, and of the feedwater mass flow rate, $\dot{m}_5$, itself. From Lippke's report, design values of the two mass flow rates are given. They are $\dot{m}_{50} = 38.969$ kg/s and $\dot{m}_{90} = 5.7319$ kg/s. These design values are used to define the following variable

$$B = \frac{1}{2}\left(\frac{\dot{m}_9 / \dot{m}_5}{\dot{m}_{90} / \dot{m}_{50}} + \frac{\dot{m}_5}{\dot{m}_{50}} \right), \tag{3.87}$$

that is used to estimate the effectiveness, e_{HPFH}, from the following polynomial

$$\begin{aligned} e_{HPFH} = {} & 0.433509942 - 1.72903764 \cdot B \\ & + 3.21718006 \cdot B^2 - 1.29319762 \cdot B^3. \end{aligned} \tag{3.88}$$

This polynomial was found through fitting measured heat exchanger train inlet water data when measured heat exchanger train outlet steam data were used as model inputs.

A constant pressure drop is considered in the feedwater and also at the steam side of the HPFH

$$p_6 = p_5 \cdot \Delta p_{HPFH,c}, \tag{3.89}$$

$$p_{21} = p_9 \cdot \Delta p_{HPFH,h}. \tag{3.90}$$

Estimated from Lippke's report, the values for the pressure ratios are $\Delta p_{HPFH,c} = 0.8286$ and $\Delta p_{HPFH,h} = 0.236$. Equation (3.89) gives a value for the feedwater inlet pressure p_5, since the

feedwater outlet pressure, p_6, is known from equation (3.126). Correspondingly, equation (3.90) yields a value for the drain pressure p_{21}, since the extraction pressure, p_9, is known from equation (3.19). The feedwater outlet temperature, T_6, and the feedwater outlet entropy, s_6, are calculated from fluid property functions as the temperature and entropy of water with the enthalpy h_6 at the pressure p_6:

$$T_6 = f_T\left(\text{Water},\ H = h_6,\ P = p_6\right), \tag{3.91}$$

$$s_6 = f_s\left(\text{Water},\ H = h_6,\ P = p_6\right). \tag{3.92}$$

Likewise, the drain temperature, T_{21}, and the drain entropy, s_{21}, are calculated from fluid property functions as the temperature and entropy of steam with the enthalpy h_{21} at the pressure p_{21}:

$$T_{21} = f_T\left(\text{Steam},\ H = h_{21},\ P = p_{21}\right), \tag{3.93}$$

$$s_{21} = f_s\left(\text{Steam},\ H = h_{21},\ P = p_{21}\right). \tag{3.94}$$

Equations (3.83) – (3.94) define the model for the high-pressure feedwater heater HPFH.

3.2.2.6 Condenser C and Throttle Valve TV 2

The condenser C is primarily a heat-transfer equipment with the purpose to condense the exhaust steam from the low-pressure part of the turbine and thus recover the high-quality feedwater for reuse in the cycle (El-Wakil, 1984). Before the turbine exhaust enters the condenser, it is mixed with the drain stream of the low-pressure feedwater heater LPFH. This drain stream passes a throttle valve TV 2 before it is mixed with the exhaust stream. Since

the mixing streams are in a mechanical equilibrium, the throttle valve's outlet pressure, p_{25}, is the same as the exhaust pressure

$$p_{25} = p_{19}. \tag{3.95}$$

The turbine exhaust pressure, p_{19}, is determined by equation (3.56). The pressure drop induced by TV 2 is given through

$$p_{25} = p_{22} \cdot \Delta p_{TV2}, \tag{3.96}$$

where the pressure ratio is estimated to $\Delta p_{TV2} = 0.57$. This equation is used to calculate the LPFH drain pressure, p_{22}. This pressure is used to calculate the LPFH drain temperature, T_{22}, and the drain entropy, s_{22}, from fluid property functions as the temperature and entropy of steam with the enthalpy h_{22} at the pressure p_{22}:

$$T_{22} = f_T\left(\text{Steam}, H = h_{22}, P = p_{22}\right), \tag{3.97}$$

$$s_{22} = f_s\left(\text{Steam}, H = h_{22}, P = p_{22}\right). \tag{3.98}$$

The drain enthalpy, h_{22}, is known from equation (3.60). The enthalpy stays constant in the adiabatic throttle valve TV 2

$$h_{25} = h_{22}. \tag{3.99}$$

In addition, a constant temperature is assumed

$$T_{25} = T_{22}. \tag{3.100}$$

There is no loss of mass in TV 2, hence

$$\dot{m}_{22} - \dot{m}_{25} = 0. \tag{3.101}$$

The mass flow rate $\dot{m}_{22}$ is calculated from equation (3.62). The entropy of the throttle valve's outlet stream is calculated from fluid property functions as the entropy of steam with the enthalpy h_{25} at the pressure p_{25}:

$$s_{25} = f\left(\text{Steam}, H = h_{25}, P = p_{25}\right). \tag{3.102}$$

Equations (3.95) – (3.102) form the model equations for the throttle valve TV 2.

Before entering the condenser, the throttled drain stream is mixed with the low-pressure turbine exhaust. This fact is described through the following mass balance

$$\dot{m}_{19} + \dot{m}_{25} - \dot{m}_{20} = 0. \tag{3.103}$$

This equation is used to calculate the mass flow rate $\dot{m}_{20}$ since the exhaust mass flow rate $\dot{m}_{19}$ is known from equation (3.59). The fluid entering C is in a mechanical equilibrium with the merging streams and thus

$$p_{20} = p_{19}. \tag{3.104}$$

The enthalpy of the fluid that enters the condenser C, h_{20}, is determined from the following energy balance

$$\dot{m}_{19}h_{19} + \dot{m}_{25}h_{25} - \dot{m}_{20}h_{20} = 0. \tag{3.105}$$

The enthalpy of the exhaust, h_{19}, is known from equation (3.54). The temperature T_{20} is calculated from fluid property functions as the temperature of steam with the enthalpy h_{20} at the pressure p_{20}

$$T_{20} = f_T\left(\text{Steam}, H = h_{20}, P = p_{20}\right). \tag{3.106}$$

The entropy s_{20} is also calculated from fluid property functions as the entropy of steam with the enthalpy h_{20} at the pressure p_{20}:

$$s_{20} = f_s\left(\text{Steam},\ H = h_{20},\ P = p_{20}\right). \tag{3.107}$$

Equations (3.103) – (3.107) define the model for the mixing of the turbine exhaust with the LPFH drain stream.

The mixed fluid enters the condenser and looses its energy to the circulating cooling water until it leaves the condenser as saturated liquid. Thus the enthalpy of the outlet flow, h_1, is assumed to be the enthalpy of saturated water at the pressure p_{20} and is calculated from fluid property functions:

$$h_1 = f_h\left(\text{Steam},\ P = p_{20},\ X = 0\right). \tag{3.108}$$

Hence the pressure is assumed to remain constant

$$p_1 = p_{20}, \tag{3.109}$$

and the mass flow rate stays constant as well

$$\dot{m}_{20} - \dot{m}_1 = 0. \tag{3.110}$$

The outlet temperature T_1 and the entropy s_1 are calculated from EES fluid property functions as the temperature and the entropy of steam with the enthalpy h_1 at the pressure p_1:

$$T_1 = f_T\left(\text{Steam},\ H = h_1,\ P = p_1\right), \tag{3.111}$$

$$s_1 = f_s\left(\text{Steam}, H = h_1, P = p_1\right). \tag{3.112}$$

The incoming cooling water temperature, T_{Cooli}, is one of the inputs to the power plant model but does not affect the enthalpy h_1 in this implementation due to the assumption of saturated

liquid outlet conditions in equation (3.108). The pressure of the incoming cooling water, $p_{Cool,i}$, is assumed to be the ambient pressure

$$p_{Cool,i} = p_{atm}\,. \tag{3.113}$$

From fluid property functions, the cooling water inlet enthalpy, $h_{Cool,i}$, is calculated as the enthalpy of water with the temperature $T_{Cool,i}$ at the pressure $p_{Cool,i}$

$$h_{Cool,i} = f\left(\text{Water}, T = T_{Cool,i}, P = p_{Cool,i}\right). \tag{3.114}$$

There is no pressure drop assumed in the cooling water and the cooling water outlet pressure, $p_{Cool,o}$, is

$$p_{Cool,o} = p_{Cool,i}, \tag{3.115}$$

Also the mass flow rate of the cooling water remains constant

$$\dot{m}_{Cool,i} - \dot{m}_{Cool,o} = 0\,, \tag{3.116}$$

where $\dot{m}_{Cool,o}$ is the cooling water outlet mass flow rate and $\dot{m}_{Cool,i}$ is the mass flow rate of the incoming cooling water and is estimated to be proportional to the heat exchanger train inlet mass flow rate, $\dot{m}_6$:

$$\dot{m}_{Cool,i} = 39.38 \cdot \dot{m}_6\,. \tag{3.117}$$

The factor 39.38 was determined from measurements of the cooling water outlet temperature to satisfy the following energy balance

$$\dot{m}_{Cool,i}\left(h_{Cool,o} - h_{Cool,i}\right) = \dot{m}_{20}\left(h_{20} - h_1\right). \tag{3.118}$$

From this equation, the cooling water outlet enthalpy $h_{Cool,o}$ is calculated. From this enthalpy, the temperature of the outlet cooling water, $T_{Cool,o}$, is determined from fluid property functions as the temperature of water with the enthalpy $h_{Cool,o}$ at the pressure $p_{Cool,o}$:

$$T_{Cool,o} = f_T\left(\text{Water}, H = h_{Cool,o}, P = p_{Cool,o}\right). \tag{3.119}$$

Equations (3.108) – (3.119) define model for the condenser C.

3.2.2.7 Heat Exchanger Train HE A and HE B and Reheater RH A and RH B

The heat exchanger trains HE A and HE B and the reheaters RH A and RH B are very important parts of the power plant since they represent the interface between the HTF cycle and the power plant cycle. The heat transfer between the HTF and the working fluid of the power plant occurs in these heat exchangers.

From the HTF side, the HTF is split into two streams where one stream flows into the heat exchanger trains and the other stream flows into the reheaters. From the pipe geometry, the amount of HTF that flows into the reheaters cannot exceed 25% of the entire HTF that leaves the expansion vessel. However, the splitting fraction that is not measured in the plant differs from operator to operator. As an approximate value for the splitting fraction, the design values from Lippke's report are used in this approach (Lippke, 1995). The HTF splits evenly between the two heat exchanger trains HE A and HE B. The same is true for the two reheaters RH A and RH B. The HTF that leaves the expansion vessel is split into a stream of fraction a_A that flows into HE A, into a stream of fraction a_B that flows into HE B, into a stream of fraction b_A that flows into RH A and finally into a stream of fraction b_B that flows

into RH B. From Lippke's report, the design values of these fractions are $a_A = a_B = 0.4375$ and $b_A = b_B = 0.0625$.

There is also splitting at the water or steam side. The feedwater of fraction F_{HEA} enters HE A. The remaining part of the feedwater with fraction F_{HEB} enters HE B and

$$F_{HEB} = 1 - F_{HEA}. \tag{3.120}$$

These fractions may differ from day to day. At June 20, 1998, the feedwater fraction for HE A is $F_{HEA} = 0.49$. There is also splitting occurring in front of the reheaters. The expanded steam flows into RH A with fraction F_{RHA} and F_{RHB} is the fraction determining the steam that enters RH B.

Correspondingly,

$$F_{RHB} = 1 - F_{RHA}. \tag{3.121}$$

At June 20, 1998, the fraction for RH A is $F_{RHA} = 0.53$.

From the definition of the flow fractions, it follows the mass flow rates

$$\dot{m}_{HEA} = F_{HEA} \cdot \dot{m}_6, \tag{3.122}$$

$$\dot{m}_{HEB} = F_{HEB} \cdot \dot{m}_6. \tag{3.123}$$

Here, $\dot{m}_{HEA}$ is the mass flow rate of the fluid that passes through HE A and $\dot{m}_{HEB}$ is the mass flow rate of the fluid that passes through HE B. The mass flow rate of the feedwater that enters the heat exchanger trains, $\dot{m}_6$, is an input to the power plant model. Measurements from the real SEGS VI plant of that value are available. These measurements can be used as possible inputs for simulations with the power plant model. The pressures p_{HEA} and p_{HEB}

that develop in the two heat exchanger trains HE A and HE B respectively, are functions of the mass flow rates $\dot{m}_{HEA}$ and $\dot{m}_{HEB}$. The polynomials were found from measurements of the mass flow rate and the pressure at SEGS VI:

$$\begin{aligned} p_{HEA} = {} & 1373.83964 - 374.607738 \cdot \dot{m}_{HEA} + 128.736553 \cdot \dot{m}_{HEA}^2 \\ & - 8.0075749 \cdot \dot{m}_{HEA}^3 + 0.177361045 \cdot \dot{m}_{HEA}^4 + p_{atm} \end{aligned}, \tag{3.124}$$

$$\begin{aligned} p_{HEB} = {} & 683.996786 + 343.994696 \cdot \dot{m}_{HEB} \\ & + 4.56017193 \cdot \dot{m}_{HEB}^2 + p_{atm} \end{aligned}. \tag{3.125}$$

From these two pressures, the pressure of the feedwater that enters the two heat exchanger trains, p_6, is calculated as

$$p_6 = F_{HEA} \cdot p_{HEA} + F_{HEB} \cdot p_{HEB}. \tag{3.126}$$

The feedwater temperature T_6 is determined from equation (3.91). The temperatures of the two feedwater streams into HE A and HE B, $T_{Water,HEA}$ and $T_{Water,HEB}$, are assumed to be the same as T_6

$$T_{WaterHEA} = T_6, \tag{3.127}$$

$$T_{WaterHEB} = T_6. \tag{3.128}$$

Equations (3.122) – (3.128) model the splitting of the feedwater into the two heat exchanger train's inlet flows.

The exhaust steam from the high-pressure part of the turbine is also split two enter the two reheaters RH A and RH B. Thus similar equations can be found. The mass flow rates are

$$\dot{m}_{RHA} = F_{RHA} \cdot \dot{m}_{11}, \tag{3.129}$$

$$\dot{m}_{RHB} = F_{RHB} \cdot \dot{m}_{11}, \tag{3.130}$$

where the exhaust mass flow rate, $\dot{m}_{11}$, is found from equation (3.29). From measurements on the real power plant, it can be seen that a pressure drop occurs in the steam on its way from the high-pressure turbine outlet to the two reheaters RH A and RH B. Thus the two pressures p_{RHA} and p_{RHB} that develop in RH A and RH B respectively, are determined from the exhaust pressure p_{11} as

$$p_{RHA} = p_{11} \cdot \Delta p_{RHA}, \tag{3.131}$$

$$p_{RHB} = p_{11} \cdot \Delta p_{RHB}. \tag{3.132}$$

The pressure p_{11} is known from equation (3.26). The two pressure ratios Δp_{RHA} and Δp_{RHB} are functions of the two mass flow rates $\dot{m}_{RHA}$ and $\dot{m}_{RHB}$. These functions are polynomials found through a curve fit on the measured data from SEGS VI

$$\begin{aligned}\Delta p_{RHA} = 1.03315016 - 0.00615276988 \cdot \dot{m}_{RHA} \\ + 0.000167339399 \cdot \dot{m}_{RHA}^2\end{aligned}, \tag{3.133}$$

$$\begin{aligned}\Delta p_{RHB} = 1.01609492 - 0.00408501006 \cdot \dot{m}_{RHB} \\ + 0.0000767853121 \cdot \dot{m}_{RHB}^2\end{aligned}. \tag{3.134}$$

The temperature of the fluid that enters RH A, $T_{Steam,RHA,i}$, and the temperature of the fluid that enters RH B, $T_{Steam,RHB,i}$, is assumed to match the temperature of the high-pressure turbine exhaust T_{11} and thus

$$T_{Steam,RHA,i} = T_{11}, \tag{3.135}$$

$$T_{Steam,RHB,i} = T_{11}. \tag{3.136}$$

Equations (3.129) – (3.136) model the splitting of the high-pressure turbine exhaust into the two streams entering RH A and RH B.

The HTF that leaves the expansion vessel is split into the parts that enter HE A, HE B, RH A and RH B as explained above. The temperature of the four split HTF streams that enter the heat exchangers and reheaters are assumed to have the expansion vessel temperature, T_{Exp}. The four streams leave the heat exchangers and reheaters, each with its own HTF outlet temperature, and merge to form the inlet flow of the solar trough collector field. The HTF outlet temperature for HE A is $T_{HTF,HEA}$, the HTF outlet temperature for HE B is $T_{HTF,HEB}$, the HTF outlet temperature for RH A is $T_{HTF,RHA}$ and the HTF outlet temperature for RH B is $T_{HTF,RHB}$. Since no HTF mass is lost on its way through HE A, HE B, RH A and RH B, the HTF inlet temperature of the solar trough collector field, $T_{HTF,inlet}$, is calculated from the flow fractions defined above:

$$T_{HTF,inlet} = a_A T_{HTF,HEA} + a_B T_{HTF,HEB} + b_A T_{HTF,RHA} + b_B T_{HTF,RHB}. \tag{3.137}$$

Since the overall HTF volume flow rate, $\dot{V}_{HTF}$, is available as measurement data from the real SEGS VI plant, it is used together with the flow fractions to calculated the heat that is transferred to the working fluid in the different heat exchangers and reheaters:

$$\dot{Q}_{HEA} = a_A \rho_{HTF} c_{HTF} \dot{V}_{HTF} \left(T_{Exp} - T_{HTF,HEA} \right), \tag{3.138}$$

$$\dot{Q}_{HEB} = a_B \rho_{HTF} c_{HTF} \dot{V}_{HTF} \left(T_{Exp} - T_{HTF,HEB} \right), \tag{3.139}$$

$$\dot{Q}_{RHA} = b_A \rho_{HTF} c_{HTF} \dot{V}_{HTF} \left(T_{Exp} - T_{HTF,RHA} \right), \tag{3.140}$$

$$\dot{Q}_{RHB} = b_B \rho_{HTF} c_{HTF} \dot{V}_{HTF} \left(T_{Exp} - T_{HTF,RHB} \right). \tag{3.141}$$

To predict the outlet temperatures of the HTF, the log mean temperature difference for counterflow with an overall heat transfer coefficient is applied as a common calculation

method for heat exchangers. From Incropera & DeWitt (2001), the heat in equations (3.138) – (3.141) is balanced with

$$\dot{Q}_{HEA} = UA_{HEA} \frac{\Delta T_{HEA,1} - \Delta T_{HEA,2}}{\ln\left(\Delta T_{HEA,1} / \Delta T_{HEA,2}\right)}, \tag{3.142}$$

$$\dot{Q}_{HEB} = UA_{HEB} \frac{\Delta T_{HEB,1} - \Delta T_{HEB,2}}{\ln\left(\Delta T_{HEB,1} / \Delta T_{HEB,2}\right)}, \tag{3.143}$$

$$\dot{Q}_{RHA} = UA_{RHA} \frac{\Delta T_{RHA,1} - \Delta T_{RHA,2}}{\ln\left(\Delta T_{RHA,1} / \Delta T_{RHA,2}\right)}, \tag{3.144}$$

$$\dot{Q}_{RHB} = UA_{RHB} \frac{\Delta T_{RHB,1} - \Delta T_{RHB,2}}{\ln\left(\Delta T_{RHB,1} / \Delta T_{RHB,2}\right)}. \tag{3.145}$$

In these equations, the temperature differences are

$$\Delta T_{HEA,1} = T_{Exp} - T_{Steam,HEA}, \tag{3.146}$$

$$\Delta T_{HEA,2} = T_{HTF,HEA} - T_{Water,HEA}, \tag{3.147}$$

$$\Delta T_{HEB,1} = T_{Exp} - T_{Steam,HEB}, \tag{3.148}$$

$$\Delta T_{HEB,2} = T_{HTF,HEB} - T_{Water,HEB}, \tag{3.149}$$

$$\Delta T_{RHA,1} = T_{Exp} - T_{Steam,RHA,o}, \tag{3.150}$$

$$\Delta T_{RHA,2} = T_{HTF,RHA} - T_{Steam,RHA,i}, \tag{3.151}$$

$$\Delta T_{RHB,1} = T_{Exp} - T_{Steam,RHB,o}, \tag{3.152}$$

$$\Delta T_{RHB,2} = T_{HTF,RHB} - T_{Steam,RHB,i}, \tag{3.153}$$

where $T_{Steam,HEA}$ is the working fluid outlet temperature of HE A, and $T_{Steam,HEB}$, $T_{Steam,RHA,o}$ and $T_{Steam,RHB,o}$ are the working fluid outlet temperatures of HE B, RH A and RH B

respectively. The overall heat transfer coefficients are different from heat exchanger to heat exchanger. They depend on the mass flow rate of the HTF and the mass flow rate of the working fluid. Since the overall HTF volume flow rate, $\dot{V}_{HTF}$, and the mass flow rate $\dot{m}_6$ of the working fluid are available as measured data, the following variable is defined that is equally dependent on the HTF volume flow rate and the mass flow rate:

$$M = \frac{1}{2}\left(\frac{\dot{V}_{HTF}}{\dot{V}_{HTF,0}} + \frac{\dot{m}_6}{\dot{m}_{6,0}} \right). \tag{3.154}$$

Here, $\dot{V}_0 = 0.624$ m^3/s and $\dot{m}_{6,0} = 39.9$ kg/s are the values of the HTF volume flow rate and the mass flow rate at solar noon on June 20, 1998. The variable M is used to find expressions for the different overall heat transfer coefficient-area products:

$$\begin{aligned} UA_{HEA} = &-792.404548 + 5631.66157 \cdot M \\ &- 5732.19845 \cdot M^2 + 2201.04063 \cdot M^3, \end{aligned} \tag{3.155}$$

$$\begin{aligned} UA_{HEB} = &-1460.34016 + 8693.5446 \cdot M \\ &- 10858.5127 \cdot M^2 + 4905.3059 \cdot M^3, \end{aligned} \tag{3.156}$$

$$UA_{RHA} = -8217.68129 + 92925.7393 \cdot M + 168323.253 \cdot M^2, \tag{3.157}$$

$$UA_{RHB} = 13356.4707 - 68312.7678 \cdot M + 348273.243 \cdot M^2. \tag{3.158}$$

These polynomials were found through a curve fit on overall heat transfer coefficients that were calculated from measurement data and plotted vs. M. From equations (3.138) – (3.158), the HTF outlet temperatures $T_{HTF,HEA}$, $T_{HTF,HEB}$, $T_{HTF,RHA}$ and $T_{HTF,RHB}$ could be determined if the working fluid outlet temperatures, $T_{Steam,HEA}$, $T_{Steam,HEB}$, $T_{Steam,RHA,o}$ and $T_{Steam,RHB,o}$ were known. In order to calculate the working fluid outlet temperatures, an energy balance would be preferable, but since the flow fractions a_A, a_B, b_A and b_B are uncertain, a heat exchanger

effectiveness relation was chosen instead. From Incropera & De Witt (2001) it follows for each heat exchanger and reheater

$$e_{HEA} = \frac{T_{Steam,HEA} - T_{Water,HEA}}{T_{Exp} - T_{Water,HEA}}, \tag{3.159}$$

$$e_{HEB} = \frac{T_{Steam,HEB} - T_{Water,HEB}}{T_{Exp} - T_{Water,HEB}}, \tag{3.160}$$

$$e_{RHA} = \frac{T_{Steam,RHA,o} - T_{Steam,RHA,i}}{T_{Exp} - T_{Steam,RHA,i}}, \tag{3.161}$$

$$e_{RHB} = \frac{T_{Steam,RHB,o} - T_{Steam,RHB,i}}{T_{Exp} - T_{Steam,RHB,i}}. \tag{3.162}$$

Each effectiveness, e_{HEA}, e_{HEB}, e_{RHA} and e_{RHB}, is assumed to be dependent on both the HTF volume flow rate and the mass flow rate of the working fluid. Through a curve fit on effectiveness values that were calculated from measured data and plotted vs. *M*, the following equations for the effectiveness were found

$$\begin{aligned} e_{HEA} = {} & 0.276005152 + 4.8581535 \cdot M - 12.1350267 \cdot M^2 \\ & + 12.7277158 \cdot M^3 - 4.81249776 \cdot M^4 \end{aligned}, \tag{3.163}$$

$$\begin{aligned} e_{HEB} = {} & 0.960949494 - 0.0622394235 \cdot M \\ & + 0.00829799829 \cdot M^2 \end{aligned}, \tag{3.164}$$

$$\begin{aligned} e_{RHA} = {} & -1.55221859 + 15.7766242 \cdot M - 35.5777164 \cdot M^2 \\ & + 34.4175845 \cdot M^3 - 12.1448263 \cdot M^4 \end{aligned}, \tag{3.165}$$

$$\begin{aligned} e_{RHB} = {} & -1.28023253 + 13.429928 \cdot M - 29.1850288 \cdot M^2 \\ & + 27.6156082 \cdot M^3 - 9.66507556 \cdot M^4 \end{aligned}. \tag{3.166}$$

The working fluid outlet enthalpies, $h_{Steam,HEA}$, $h_{Steam,HEB}$, $h_{Steam,RHA,o}$ and $h_{Steam,RHB,o}$ are calculated from fluid property functions as the enthalpies of steam at the related outlet temperatures and pressures

$$h_{Steam,HEA} = f_h\left(\text{Steam}, T = T_{Steam,HEA}, P = p_{HEA}\right), \tag{3.167}$$

$$h_{Steam,HEB} = f_h\left(\text{Steam}, T = T_{Steam,HEB}, P = p_{HEB}\right), \tag{3.168}$$

$$h_{Steam,RHA,o} = f_h\left(\text{Steam}, T = T_{Steam,RHA,o}, P = p_{RHA}\right), \tag{3.169}$$

$$h_{Steam,RHB,o} = f_h\left(\text{Steam}, T = T_{Steam,RHB,o}, P = p_{RHB}\right). \tag{3.170}$$

Note that this calculation might be inaccurate if the fluid that leaves the heat exchangers or reheaters is still in the two-phase region after it was heated up by the HTF energy. This may occur in the morning during the start-up of the plant or in the evening during the plant shutdown period when solar energy is low.

The two streams that leave HE A and HE B merge to a single stream with mass flow rate $\dot{m}_7$ and thus

$$\dot{m}_{HEA} + \dot{m}_{HEB} - \dot{m}_7 = 0\,. \tag{3.171}$$

The temperature T_7 and the enthalpy h_7 of the single stream that flows into the high-pressure part of the turbine are determined from the working fluid flow fractions

$$T_7 = F_{HEA} \cdot T_{Steam,HEA} + F_{HEB} \cdot T_{Steam,HEB}, \tag{3.172}$$

$$h_7 = F_{HEA} \cdot h_{Steam,HEA} + F_{HEB} \cdot h_{Steam,HEB}. \tag{3.173}$$

The pressure p_7 is also calculated from the flow fractions

$$p_7 = F_{HEA} \cdot p_{HEA} + F_{HEB} \cdot p_{HEB`} - \Delta p_{HE}, \tag{3.174}$$

but from measurements on the real SEGS VI plant, it follows that a pressure drop occurs in the working fluid on its way from the heat exchanger trains to the high-pressure part of the turbine. This pressure drop is estimated as a function of the mass flow rate $\dot{m}_7$. The following polynomial was found from measured data

$$\Delta p_{HE} = -9.81020595 + 2.7603402 \cdot \dot{m}_7 + 0.278971331 \cdot \dot{m}_7^2 . \tag{3.175}$$

The entropy s_7 is calculated from fluid property functions as the entropy of steam with the enthalpy h_7 at the pressure p_7

$$s_7 = f_s\left(\text{Steam},\ H = h_7,\ P = p_7\right). \tag{3.176}$$

Equations (3.171) – (3.176) form a model for the mixing of the two streams that leave HE A and HE B. In a similar manner, the mixing of the two streams that leave RH A and RH B can be described. Thus the following equations are used to calculate the mass flow rate $\dot{m}_{12}$, the temperature T_{12}, the enthalpy h_{12}, the pressure p_{12} and the entropy s_{12} of the fluid that enters the low-pressure part of the turbine:

$$\dot{m}_{RHA} + \dot{m}_{RHB} - \dot{m}_{12} = 0 , \tag{3.177}$$

$$T_{12} = F_{RHA} \cdot T_{Steam,RHA,o} + F_{RHB} \cdot T_{Steam,RHB,o}, \tag{3.178}$$

$$h_{12} = F_{RHA} \cdot h_{Steam,RHA,o} + F_{RHB} \cdot h_{Steam,RHB,o}, \tag{3.179}$$

$$p_{12} = F_{RHA} \cdot p_{RHA} + F_{RHB} \cdot p_{RHB} - \Delta p_{RH} , \tag{3.180}$$

$$\Delta p_{RH} = -124.845039 + 5.63854205 \cdot \dot{m}_{12} - 0.0510125894 \cdot \dot{m}_{12}^2 , \tag{3.181}$$

$$s_{12} = f_s\left(\text{Steam}, H = h_{12}, P = p_{12}\right). \tag{3.182}$$

These equations complete the model for HE A, HE B, RH A and RH B that is given through equations (3.120) – (3.182).

3.2.2.8 Calculation of the Gross Output

In order to estimate the produced power of the plant, the gross output P_{Gross} is calculated as the summation of the turbine work

$$\begin{aligned} P_{Gross} = & \dot{m}_7 h_7 - \dot{m}_8 h_8 \\ & + \dot{m}_{10} h_{10} - \dot{m}_{11} h_{11} \\ & + \dot{m}_{12} h_{12} - \dot{m}_{13} h_{13} \\ & + \dot{m}_{15} h_{15} - \dot{m}_{16} h_{16} \\ & + \dot{m}_{18} h_{18} - \dot{m}_{19} h_{19} \end{aligned} \quad . \tag{3.183}$$

With this last equation, the entire power plant model is eventually defined.

3.3 Model Implementation and Simulation Results

The model discussed in the previous section can be used to predict the HTF inlet temperature, $T_{HTF,inlet}$, of the collector field vs. time and the gross output, P_{Gross}, vs. time.

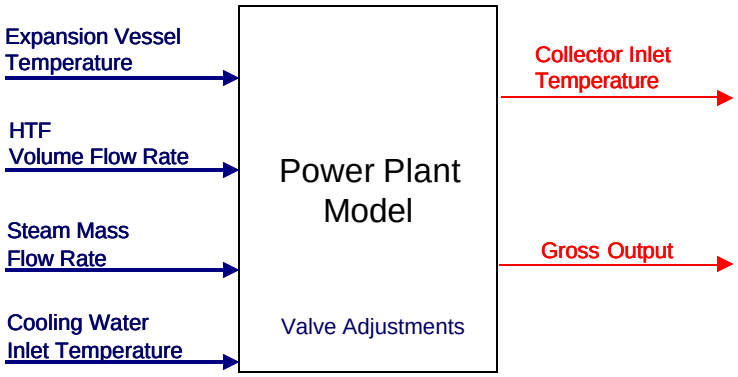

Figure 3.5: The Power Plant Model as a Block with Inputs and Outputs

The input values of the power plant model are the expansion vessel HTF temperature, T_{Exp}, the HTF volume flow rate, $\dot{V}_{HTF}$, the steam mass flow rate, $\dot{m}_6$, and the cooling water inlet temperature, T_{Cooli}, vs. time. In addition, valve adjustments have to be known that define the mass flow rates of the turbine extractions. Figure 3.5 shows the power plant model as a block with inputs and outputs.

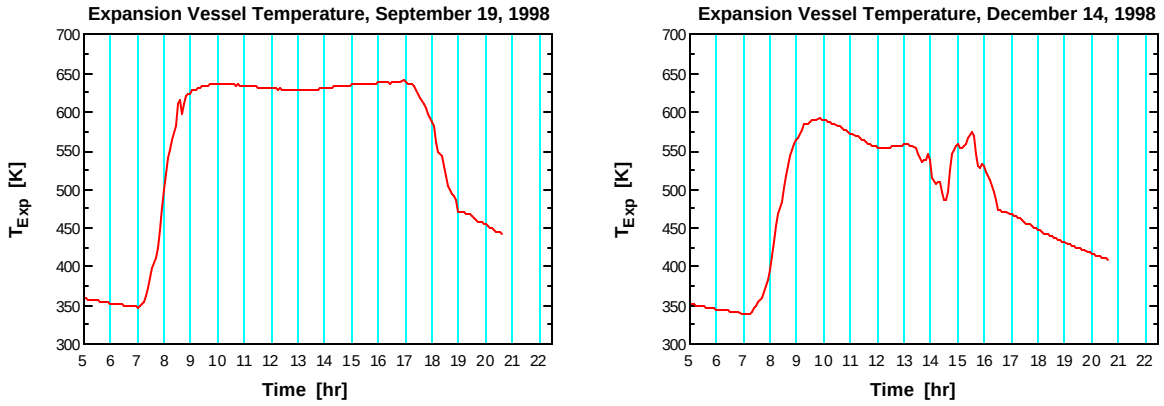

Figure 3.6: Measured Expansion Vessel Temperature for September 19, 1998 and for December 14, 1998

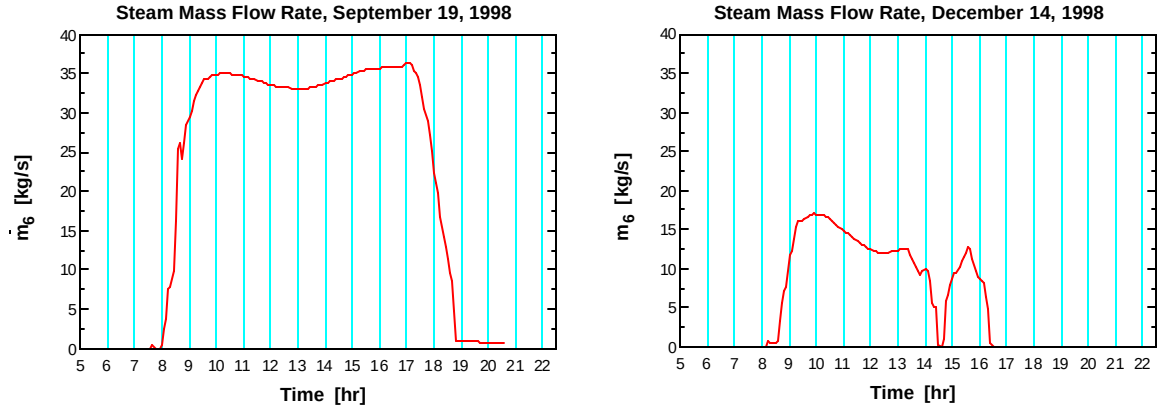

Figure 3.7: Measured Steam Mass Flow Rate for September 19, 1998 and for December 14, 1998

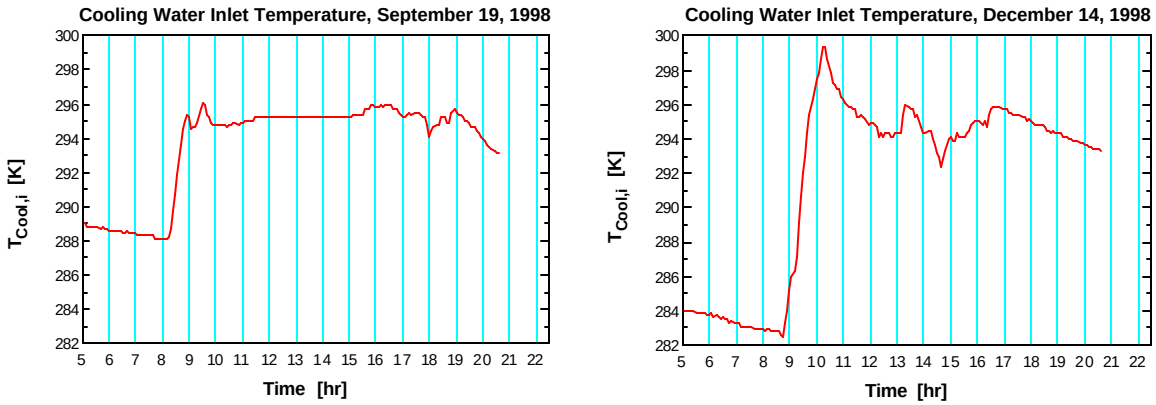

Figure 3.8: Measured Cooling Water Inlet Temperature for September 19, 1998 and for December 14, 1998

The measured input values vs. time for September 19, 1998, which is a clear day, and for December 14, 1998, which is a partly cloudy day, are shown in Figure 3.6 to Figure 3.8. The measured HTF volume flow rate for these days is shown in Figure 2.23 in the previous chapter.

The HTF trough collector field inlet temperature and the gross output are calculated through simulations with the power plant model and compared with the corresponding measured data from SEGS VI (Figures 3.9 – 3.12).

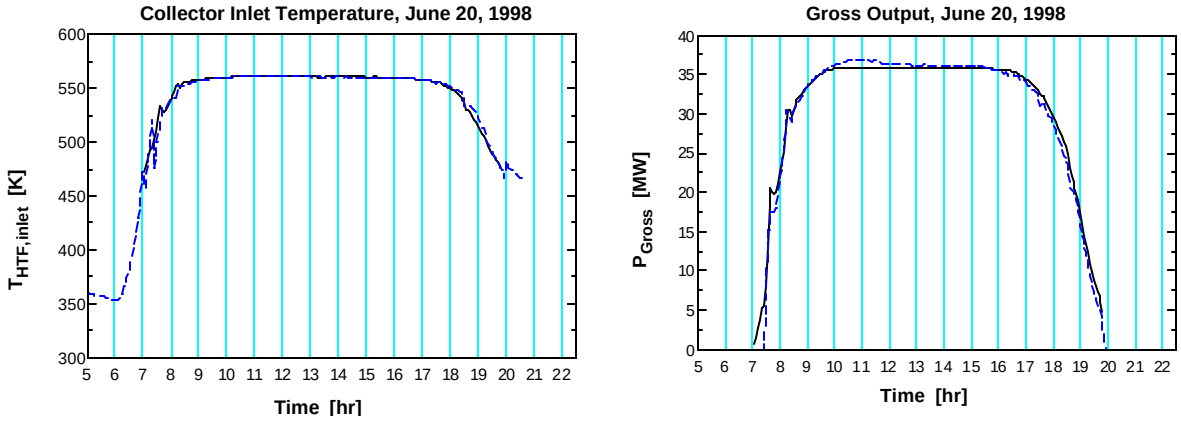

Figure 3.9: Calculated Collector Inlet Temperature vs. Time and Calculated Gross Output vs. Time (solid lines) and corresponding measurements (dashed lines) for June 20, 1998

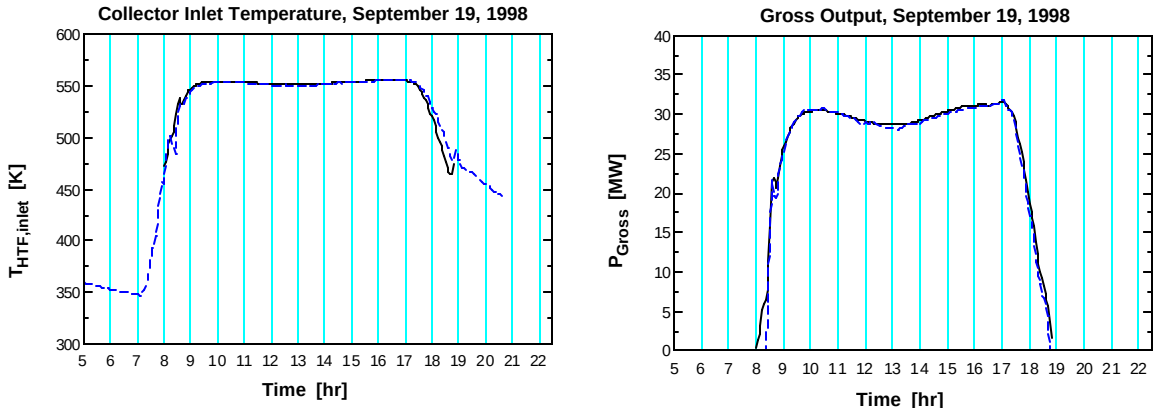

Figure 3.10: Calculated Collector Inlet Temperature vs. Time and Calculated Gross Output vs. Time (solid lines) and corresponding measurements (dashed lines) for September 19, 1998

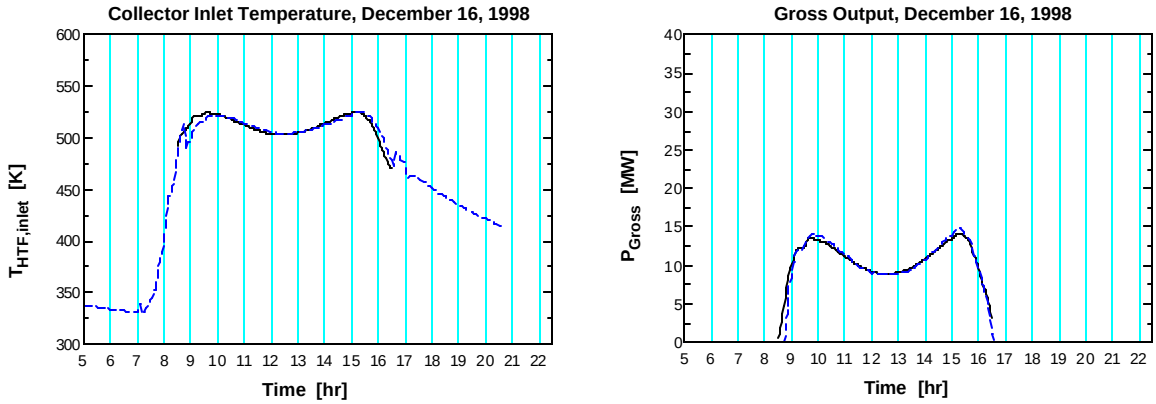

Figure 3.11: Calculated Collector Inlet Temperature vs. Time and Calculated Gross Output vs. Time (solid lines) and corresponding measurements (dashed lines) for December 16, 1998

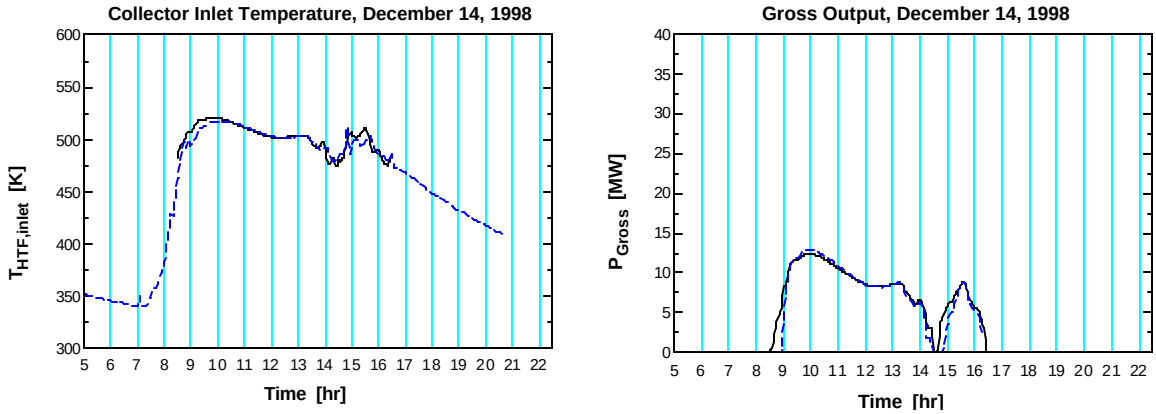

Figure 3.12: Calculated Collector Inlet Temperature vs. Time and Calculated Gross Output vs. Time (solid lines) and corresponding measurements (dashed lines) for December 14, 1998

Figure 3.9 shows the calculated collector inlet temperature and the calculated gross output vs. measured data for June 20, 1998. The calculated values, given through the solid line, match the measured values, represented by the dashed line, sufficiently. The considered day, June 20, 1998, is a day with good weather conditions. For other clear days, September 19, 1998 in Figure 3.10 and December 16, 1998 in Figure 3.11, the predicted values match the measured values similarly well.

For a partially cloudy day as December 14, 1998, depicted in Figure 3.12, the calculated collector inlet temperature and the measured one do not agree as well as for the clear days. However, the predicted values are still an adequate estimate of the measured values. The same is true for the calculated gross output.

These results verify that the power plant model as explained above and implemented in EES is useful as a model for the real SEGS VI power plant. In order to obtain a model for the entire plant, that is, the trough collector field with the power plant, the trough collector field model and the power plant model are linked together as explained next.

Chapter 4

Combined Plant Model

The trough collector field model presented in Chapter 2 and the power plant model discussed in Chapter 3 are combined to form the entire plant model as shown in Figure 4.1.

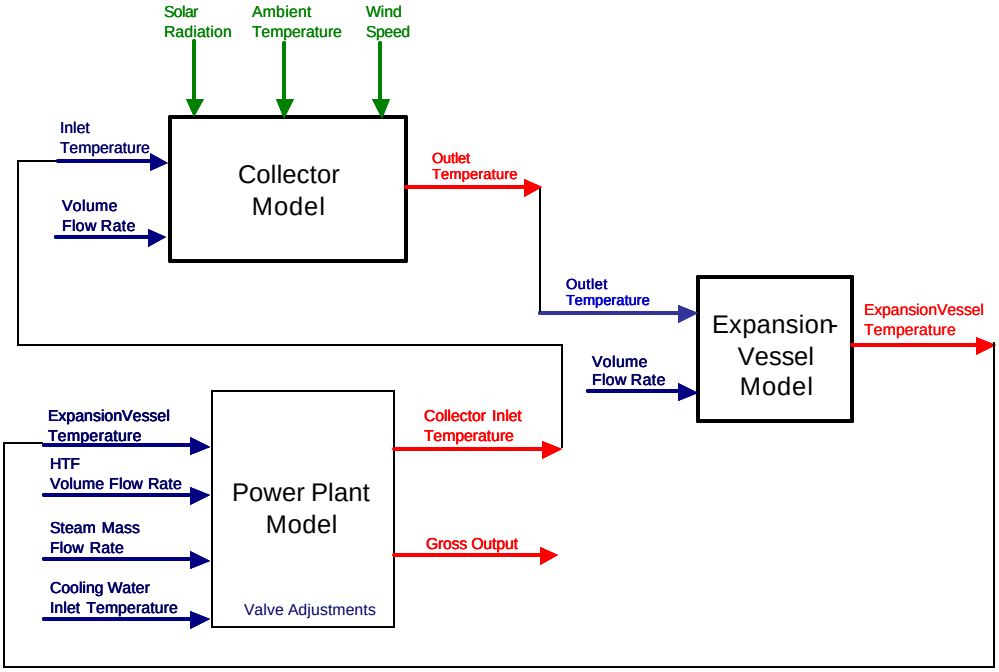

Figure 4.1: Combination of Collector Model and Power Plant Model

As can be seen from Figure 4.1, the expansion vessel model is the link between collector and power plant model.

The expansion vessel is assumed to be a fully mixed tank and thus can be described by a single differential equation for temperature obtained from an energy balance on the expansion vessel

$$\frac{dT_{Exp}}{dt} = -\frac{\dot{V}_{HTF}}{V_{Exp}} T_{Exp} + \frac{\dot{V}_{HTF}}{V_{Exp}} T_{HTF,j_0} . \tag{4.1}$$

Here, T_{Exp} is the expansion vessel temperature and V_{Exp} is the expansion vessel volume with $V_{Exp} = 287.7\ \mathrm{m}^3$.

The combined plant model can be considered as a single block with inputs and outputs as depicted in Figure 4.2.

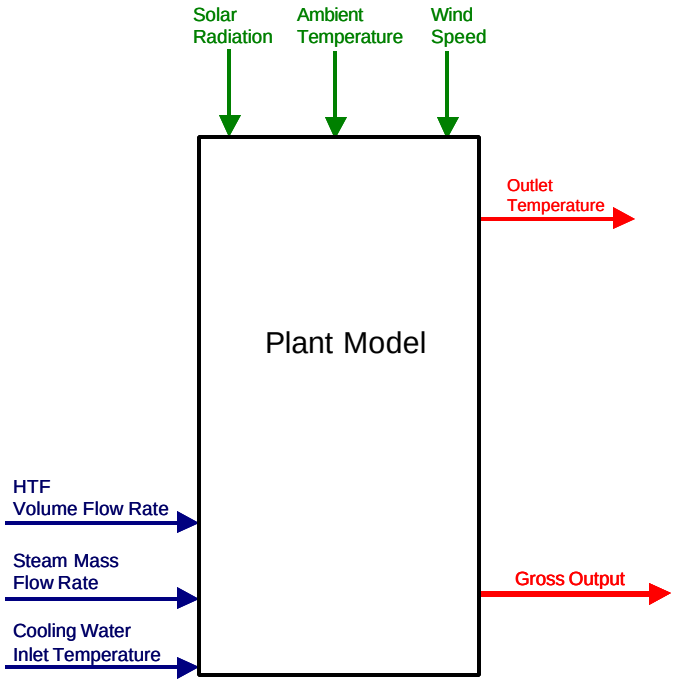

Figure 4.2: The Plant Model as a Block with Inputs and Outputs

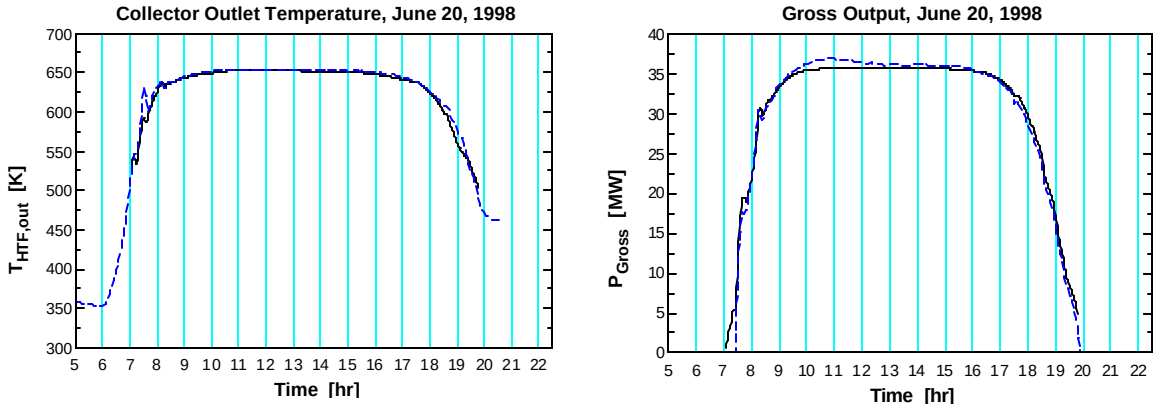

Figure 4.3: With Plant Model calculated Collector Outlet Temperature vs. Time and Gross Output vs. Time (solid lines) and Measured Values (dashed lines) for June 20, 1998

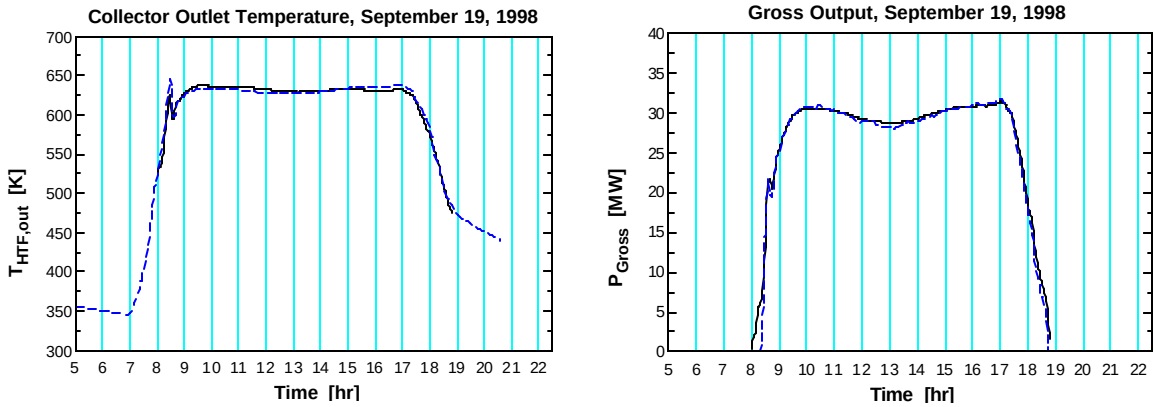

Figure 4.4: With Plant Model calculated Collector Outlet Temperature vs. Time and Gross Output vs. Time (solid lines) and Measured Values (dashed lines) for September 19, 1998

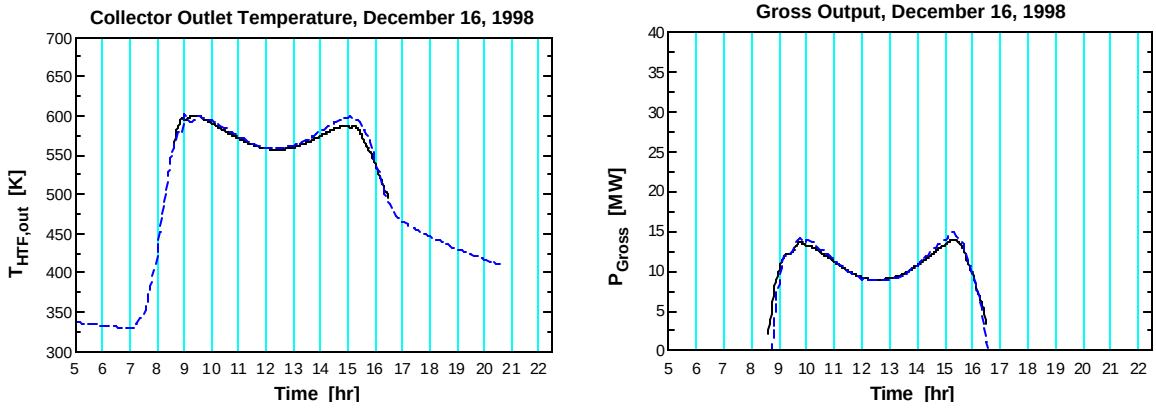

Figure 4.5: With Plant Model calculated Collector Outlet Temperature vs. Time and Gross Output vs. Time (solid lines) and Measured Values (dashed lines) for December 16, 1998

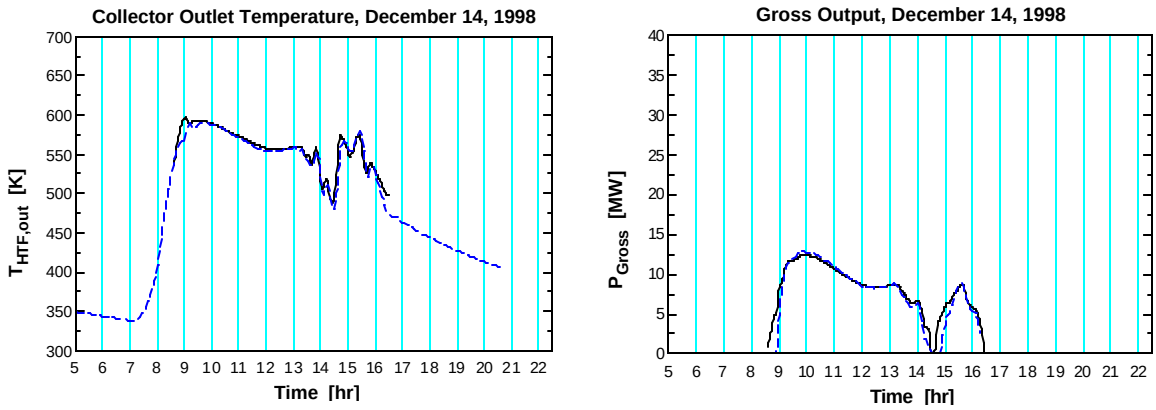

Figure 4.6: With Plant Model calculated Collector Outlet Temperature vs. Time and Gross Output vs. Time (solid lines) and Measured Values (dashed lines) for December 14, 1998

The combined plant model was implemented in EES and measured data from the real SEGS VI plant were chosen as inputs. The measured inputs are the HTF volume flow rate (Figure 2.23), the steam mass flow rate (Figure 3.7), the cooling water inlet temperature (Figure 3.8) and environmental data as the direct normal solar radiation (Figure 2.24), the ambient temperature (Figure 2.25) and the wind speed (Figure 2.26). The collector outlet temperature and the gross output as the two considered outputs of the plant, are calculated through simulations with the plant model and compared with measured data from SEGS VI.

Figure 4.3 shows in the left-hand side figure the plant model calculated collector outlet temperature vs. the measured collector outlet temperature for June 20, 1998. The calculated values, given through the solid line, match the measured values, represented by the dashed line, well. There is also good agreement between the calculated gross output and the measured gross output. The slight difference between calculated and measured values that can be seen at around 11 hr is probably due to an inaccurate measurement of the steam mass

flow rate at SEGS VI that was used as an input to the plant model for the simulation. June 20, 1998 was a clear day and for the other clear days that are considered, September 19, 1998 in Figure 4.4 and December 16, 1998 in Figure 4.5, similar good results can be stated.

Even for the partially cloudy day, December 14, 1998, the calculated collector outlet temperature and the calculated gross output match the measured values well as shown in Figure 4.6.

These results show that the plant model, as it was described in this and the previous chapters, is very useful to predict the collector outlet temperature and the produced power of the real SEGS VI plant. For this model, a control algorithm has to be found that obtains the ability to hold the collector outlet temperature at a constant set point through the adjustment of the HTF volume flow rate. The control algorithm that was chosen for this study is taken from the model predictive control framework as explained in Rawlings and Muske (1993). Its implementation and performance for the plant model is described in the next chapter.

Chapter 5

Linear Model Predictive Control

5.1 Introduction

In Chapter 1, it was explained that a human controller in the SEGS VI plant tries to maintain a constant set point collector outlet temperature of the HTF by adjusting the volume flow rate of the HTF. The objective of this work is to simulate the human controller's behavior through automatic controls. A linear model predictive controller is developed for the SEGS VI plant model as shown in Figure 5.1.

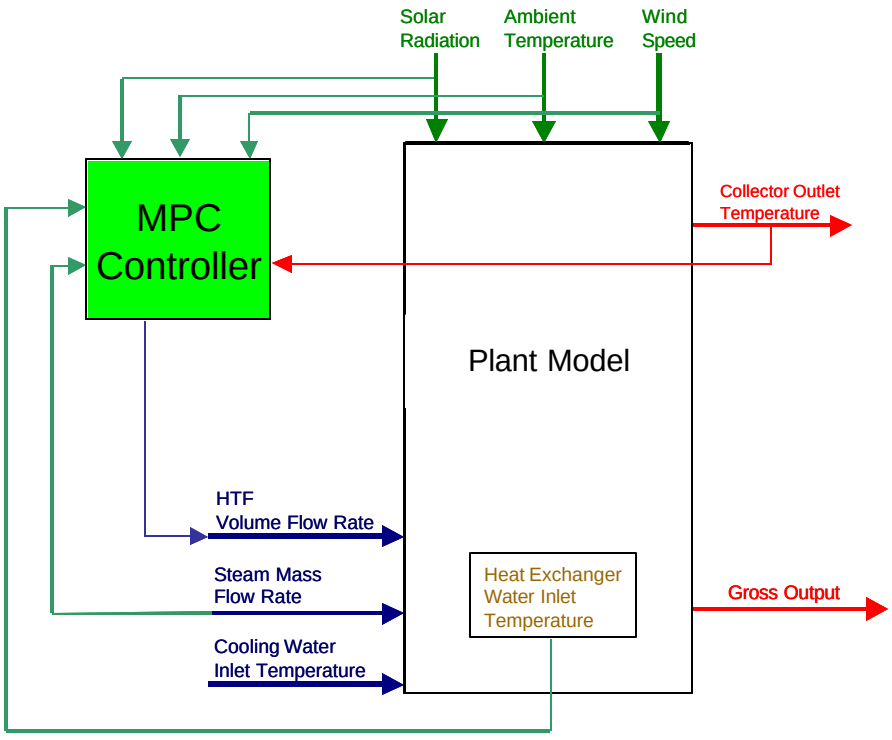

Figure 5.1: The MPC controller for the plant model

The MPC controller measures the collector outlet temperature, the solar radiation, the ambient temperature, the wind speed, the steam mass flow rate in the power plant and the heat exchanger train water inlet temperature to calculate the HTF volume flow rate that drives the collector outlet temperature into the set point.

Linear model predictive control (MPC) is a linear optimal control strategy: the essence of MPC is to optimize, over the manipulable inputs, forecasts of process behavior (Rawlings, 2000). A feature of MPC is the incorporation of constraints on the manipulated and controlled variables into the optimization procedure.

In the case of SEGS VI, forecasts of process behavior mean the prediction of how the collector field outlet temperature of the HTF will behave for a possible variation of the HTF volume flow rates from now to a point of time in the future. The difference between now and a future point in time is called the time horizon. If a forecast is made at successive points in time, there is at each of these points in time a prediction made along a time horizon of the same length. Thus it is thought of a horizon that moves with time from one prediction point of time to the next. This is why MPC belongs to a class of control algorithms also referred to as receding horizon control or moving horizon control.

The optimization of forecasts of process behavior implies that there is a performance objective. What is the optimal forecasted process behavior? Since an optimization is usually formulated as a minimization, the performance objective is formulated as a minimization of a cost functional that is minimal for the optimal forecasted process behavior. The goal of the human controller at SEGS VI is to maintain the HTF collector field outlet temperature at a specified set point. Thus, the optimal forecasted process behavior is that the future HTF collector field outlet temperatures are at the set point and that no change in the HTF volume

flow rate occure from one point in time to the next point in time. The second criterion reflects the desire of not having rapid changes in the flow rate. This criterion may be useful for damping potential oscillations in the HTF collector field outlet temperature while approaching the set point. Consequently, the value of a cost function that is to be minimized must increase with an increasing difference between the forecasted HTF collector field outlet temperatures and the set point temperature. It also must increase with an increasing change in the HTF volume flow rate from one point in time to the next point in time. The aim is to find the optimal sequence of HTF volume flow rates among all possible flow rates, that minimizes the cost function, while keeping the HTF volume flow rates and also the dependent HTF collector field outlet temperatures between specified upper and lower bounds. A solution to this problem through MATLAB optimization procedures will be shown later.

The MPC algorithms presented here are based on a theoretical framework taken from Rawlings and Muske (1993). In order to obtain a better understanding of the subject, a simplified model rather than the SEGS VI plant model is chosen to explain the control strategy. The simplified model is presented next.

5.2 The Simplified Model

The simplified model, shown in Figure 5.2, consists of four elements: a solar collector, an expansion vessel, a heat exchanger and a HTF pump. Differential equations for temperature are used to model the system. The simplified system can be described by a system of four nonlinear differential equations as explained in the following.

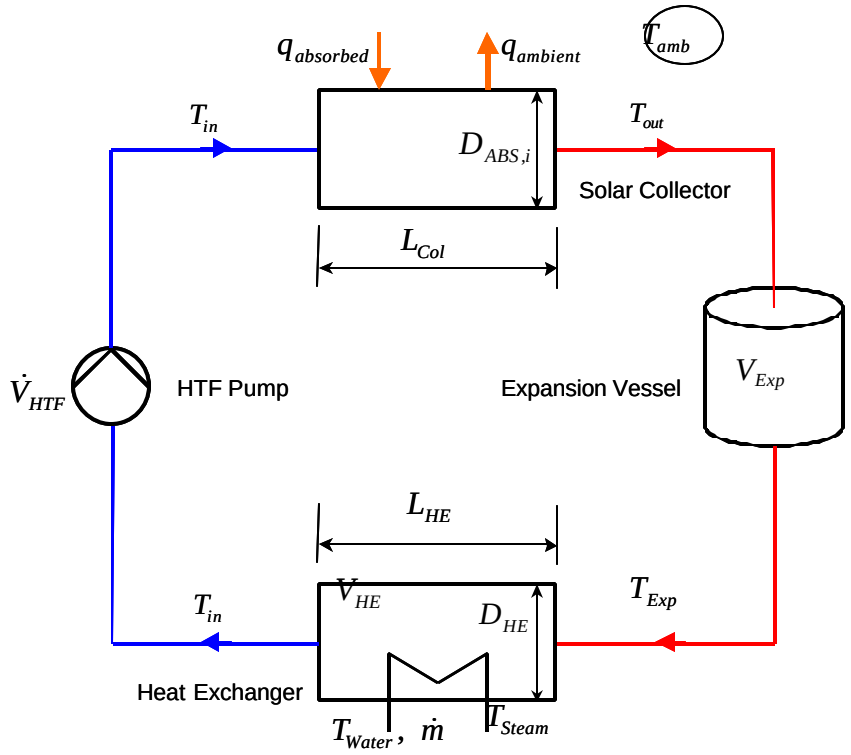

Figure 5.2: The Structure of the Simpl ified Model

An energy balance on the collector leads to the following differential equation for the HTF collector outlet temperature

$$\frac{dT_{out}(t)}{dt} = -\frac{\dot{V}_{HTF}(t)}{V_{Col}} T_{out}(t) + \frac{\dot{V}_{HTF}(t)}{V_{Col}} T_{in}(t) + \frac{L_{Col}}{r_{HTF} \quad c_{HTF} \quad V_{Col}} \left(q_{absorbed}(t) - q_{ambient}(t) \right) \qquad (5.1)$$

where V_{Col} is the overall volume of the collector, given by

$$V_{Col} = \tfrac{p}{4} D_{ABS,i}^2 \cdot L_{Col} \,, \qquad (5.2)$$

with the length of the collector

$$L_{Col} = Length \cdot n_{Collectors} \,. \qquad (5.3)$$

The heat transfer to the environment, $q_{ambient}$, is described by

$$q_{ambient}(t) = h_{ambient} \quad A_{ABS,surf,i} \quad \left(T_{out}(t) - T_{amb}(t)\right) \tag{5.4}$$

with a heat transfer coefficient of $h_{ambient} = 2.5\ \mathrm{Wm^{-2}K^{-1}}$ and the surface area $A_{ABS,surf,i}$ from equation (2.22). The initial condition for equation (5.1) is

$$T_{out}(0) = T_{out,init} \quad . \tag{5.5}$$

The expansion vessel temperature is determined through

$$\frac{dT_{Exp}(t)}{dt} = -\frac{\dot{V}_{HTF}(t)}{V_{Exp}} T_{Exp}(t) + \frac{\dot{V}_{HTF}(t)}{V_{Exp}} T_{out}(t) \tag{5.6}$$

with the expansion vessel volume, $V_{Exp} = 287.7\ \mathrm{m^3}$. The initial condition for equation (5.6) is

$$T_{Exp}(0) = T_{Exp,init} \, . \tag{5.7}$$

Finally, the loop is closed through an energy balance on the heat exchanger trains

$$\frac{dT_{in}(t)}{dt} = -\frac{(a_A + a_B)\cdot \dot{V}_{HTF}(t)}{V_{HE}} T_{in}(t) + \frac{(a_A + a_B)\cdot \dot{V}_{HTF}(t)}{V_{HE}} T_{Exp}(t) - \frac{L_{HE}}{r_{HTF} \quad c_{HTF} \quad V_{HE}} q_{transferred}(t) \tag{5.8}$$

where a_A and a_B are the flow fractions from Chapter 3.2.3.7. The heat transfer in the heat exchanger is given by

$$q_{transferred}(t) = h_{HE}(t) A_{HE,surf} \left(T_h(t) - T_c(t)\right) \, , \tag{5.9}$$

where the temperature of the hot fluid, T_h, is the mean temperature of the HTF in the heat exchanger

$$T_h(t) = \tfrac{1}{2}\left(T_{Exp}(t) + T_{in}(t)\right) \tag{5.10}$$

and the temperature of the cold working fluid, T_c, is the mean temperature

$$T_c(t) = \tfrac{1}{2}\left(T_{Steam}(t) + T_{Water}(t)\right). \tag{5.11}$$

The heat transfer coefficient, h_{HE}, is dependent on the two flow rates that are available as measurements from SEGS VI

$$h_{HE}(t) = 74000 \cdot \left(\frac{\dot{V}_{HTF}(t)/\dot{V}_{HTF,0} + \dot{m}(t)/\dot{m}_0}{2} \right) \mathrm{Wm^{-2}K^{-1}} \tag{5.12}$$

where $\dot{m}$ is the mass flow rate of the working fluid (water or steam). The reference flow rates are $\dot{V}_{HTF,0} = 0.624\ \mathrm{m^3 s^{-1}}$ for the HTF volume flow rate and $\dot{m}_0 = 39.9\ \mathrm{kg\,s^{-1}}$ for the mass flow rate of the working fluid. They are flow rates at solar noon measured at June 20, 1998. The surface area is determined from

$$A_{HE,surf} = p \quad D_{HE} \tag{5.13}$$

with an assumed diameter of $D_{HE} = 1\ \mathrm{m}$. The volume of the heat exchanger, V_{HE}, is calculated from

$$V_{HE} = \tfrac{p}{4} D_{HE}^2\ L_{HE} \tag{5.14}$$

with an assumed length of $L_{HE} = 10\ \mathrm{m}$. The initial condition for equation (5.8) is

$$T_{in}(0) = T_{in,init}. \tag{5.15}$$

The temperature of the Steam, T_{Steam}, is calculated from a heat exchanger effectiveness equation

$$e_{HE}(t) = \frac{T_{Steam}(t) - T_{Water}(t)}{T_{Exp}(t) - T_{Water}(t)}, \tag{5.16}$$

formulated as the following differential equation

$$\frac{dT_{Steam}(t)}{dt} = 0.01 \cdot \left(\left(-T_{Steam}(t) \right) + e_{HE}(t) \left(T_{Exp}(t) - T_{Water}(t) \right) + T_{Water}(t) \right) . \tag{5.17}$$

The algebraic equation (5.16) is formulated as a differential equation (5.17) because the model predictive control framework as used in this work considers only differential equations as system equations. The factor 0.01 s^{-1} was introduced to adjust the time constant of this differential equation to the time constant range of the entire system in order to avoid a stiff differential equation system. The heat exchanger effectiveness is assumed to be flow rate dependent

$$e_{HE}(t) = (-0.1) \cdot \left(\frac{\dot{V}_{HTF}(t) / \dot{V}_{HTF,0} + \dot{m}(t) / \dot{m}_0}{2} \right) + 1.025 . \tag{5.18}$$

The initial condition for equation (5.17) is

$$T_{Steam}(0) = T_{Steam,init} . \tag{5.19}$$

The validation of the simplified model is shown in Figure 5.3 for June 20, 1998, a clear day, and in Figure 5.4 for December 14, 1998, a partially cloudy day, where the measured input values for the simplified model are the direct normal solar radiation to calculate $q_{absorbed}$, the ambient temperature, $T_{ambient}$, the HTF volume flow rate, $\dot{V}_{HTF}$, the working fluid mass flow rate, $\dot{m}$, and the water inlet temperature of the heat exchanger, T_{Water}. Calculated are the collector outlet temperature, T_{out}, and the steam outlet temperature of the heat exchanger, T_{Steam}.

As seen from Figure 5.3 and Figure 5.4, the simplified model can be used to calculate acceptable HTF temperatures compared to the ones measured at SEGS VI.

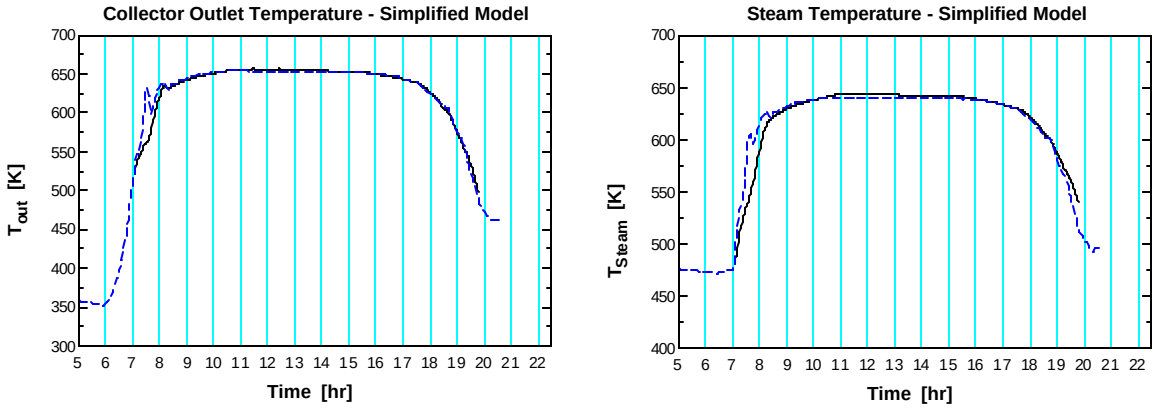

Figure 5.3: The simplified model calculated collector outlet temperature (solid line) and measured collector outlet temperature (dashed line) are shown in the left hand figure and the calculated steam temperature (solid line) and measured steam temperature (dashed line) are shown in the right hand figure for June 20, 1998

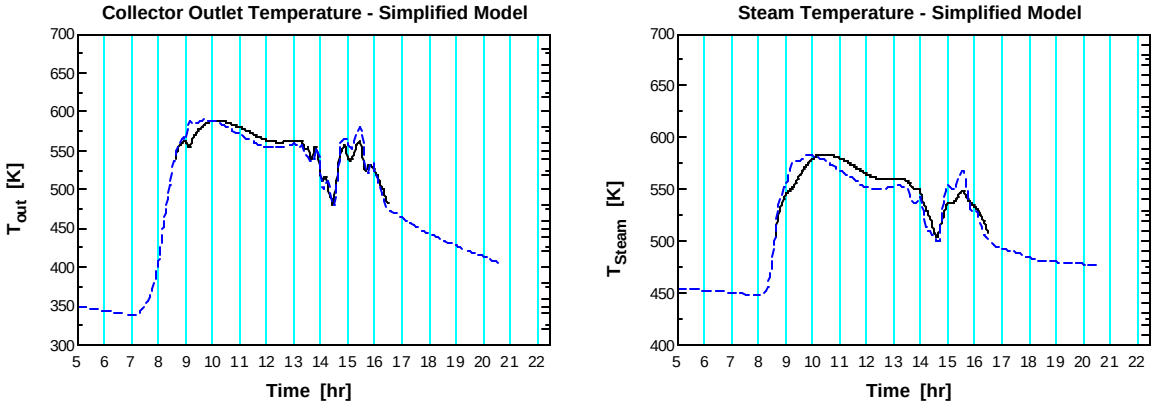

Figure 5.4: The simplified model calculated collector outlet temperature (solid line) and measured collector outlet temperature (dashed line) are shown in the left hand figure and the calculated steam temperature (solid line) and measured steam temperature (dashed line) are shown in the right hand figure for December 14, 1998

In what follows, the simplified model is used to explain the model predictive control scheme. The name of the control method indicates: a model of the controlled system plays the major role. It is used to predict values over the time horizon. For the control algorithm presented by

Rawlings and Muske (1993), linear equations are needed. In the next section, it is explained how the simplified model has to be transformed to obtain linear equations.

5.3 Models for Linear MPC

The models in linear MPC are discrete-time linear models in state-space form. First, the linear model in state-space form is explained, later the time discretization of this model.

The state-space form of a linear model or better linear differential system is

$$\dot{x}(t) = A(t)x(t) + B(t)u(t). \tag{5.20}$$

Here t is the time variable, $x(t)$ is a real n-dimensional time-varying column vector which denotes the state of the system, and $u(t)$ is a real m-dimensional column vector which indicates the input variable (Kwakernaak & Sivan, 1972). The time-varying matrix $A(t)$ is of dimension $(n \times n)$ and the time-varying matrix $B(t)$ is of dimension $(n \times m)$. Let $y(t)$ be a real p-dimensional system variable that can be observed or measured or through which the system influences its environment.

Such a variable is called an output variable of the system and is expressed through the output equation of the system

$$y(t) = C(t)x(t) + D(t)u(t) \tag{5.21}$$

with the time-varying matrix $C(t)$ of dimension$(p \times n)$ and the time-varying matrix $D(t)$ of dimension $(p \times m)$. There exists an initial condition for the system described by equation (5.20)

$$x(0) = x_{init}. \tag{5.22}$$

If the matrices *A*, *B*, *C*, and *D* are constant, the system is time-invariant:

$$\dot{x}(t) = A\,x(t) + B\,u(t) \ , \tag{5.23}$$

$$y(t) = C\,x(t) + D\,u(t) \ . \tag{5.24}$$

For linear MPC as it is considered in this work, it is necessary to obtain model equations in the form of equation (5.23) and (5.24) with an initial condition (5.22). Does the simplified model already obtain this form? If not, what has to be done to gain a system model of that form?

To answer the first question, the simplified model equations (5.1), (5.6), (5.8) and (5.17) are written down again with the introduction of some abbreviations. The time constant t_{Col} for the collector is defined as

$$\frac{1}{t_{Col}(t)} = \frac{\dot{V}_{HTF}(t)}{V_{Col}} \ . \tag{5.25}$$

The crosssectional area of the collector is A_{Col}. An overall heat transfer coefficient-area product, UA_{Col}, is introduced as

$$UA_{Col} = h_{ambient}\, A_{ABS,surf,i} \ . \tag{5.26}$$

With these definitions, the differential equation for the collector outlet temperature (5.1) may now be written as

$$\frac{dT_{out}(t)}{dt} = \frac{1}{t_{Col}(t)}\left(T_{in}(t) - T_{out}(t)\right) + \frac{q_{absorbed}(t) - UA_{Col}\left(T_{out}(t) - T_{amb}(t)\right)}{A_{Col}\, r_{HTF}\left(T_{out}(t)\right) c_{HTF}\left(T_{out}(t)\right)} . \tag{5.27}$$

There is a time constant for the expansion vessel, t_{Exp}, given through

$$\frac{1}{t_{Exp}(t)} = \frac{\dot{V}_{HTF}(t)}{V_{Exp}} \ . \tag{5.28}$$

Thus the differential equation for the expansion vessel temperature (5.6) becomes

$$\frac{dT_{Exp}(t)}{dt} = \frac{1}{t_{Exp}(t)}\left(T_{out}(t) - T_{Exp}(t)\right). \tag{5.29}$$

The heat exchanger time constant, t_{HE}, is calculated as

$$\frac{1}{t_{HE}(t)} = \frac{(a_A + a_B)\cdot \dot{V}_{HTF}(t)}{V_{HE}}. \tag{5.30}$$

The cross-sectional area of the heat exchanger is A_{HE} and the time dependent overall heat transfer coefficient – area product, UA_{HE}, is given by

$$UA_{HE}(t) = h_{HE}(t)\, A_{HE,surf}. \tag{5.31}$$

With these definitions, the differential equation for the collector inlet temperature (5.8) results in

$$\frac{dT_{in}(t)}{dt} = \frac{1}{t_{HE}(t)}\left(T_{Exp}(t) - T_{in}(t)\right) - \frac{UA_{HE}(t)\left(T_{Exp}(t) + T_{in}(t) - T_{Steam}(t) - T_{Water}(t)\right)}{2\cdot A_{HE}\; r_{HTF}\left(T_{in}(t)\right) c_{HTF}\left(T_{in}(t)\right)}. \tag{5.32}$$

Remember, the differential equation for the steam outlet temperature of the heat exchanger (5.17) is

$$\frac{dT_{Steam}(t)}{dt} = 0.01\cdot\left(\left(-T_{Steam}(t)\right) + e_{HE}(t)\left(T_{Exp}(t) - T_{Water}(t)\right) + T_{Water}(t)\right). \tag{5.33}$$

The following considerations are based on the set of the four differential equations (5.27), (5.29), (5.32) and (5.33). For a comparison with the time-invariant linear state-space model (5.23), the following state vector is introduced

$$x(t) = \begin{bmatrix} T_{out}(t) \\ T_{Exp}(t) \\ T_{in}(t) \\ T_{Steam}(t) \end{bmatrix}. \tag{5.34}$$

The input vector is defined as

$$u(t) = \begin{bmatrix} q_{absorbed}(t) \\ T_{ambient}(t) \\ \dot{V}_{HTF}(t) \\ \dot{m}(t) \\ T_{Water}(t) \end{bmatrix}, \tag{5.35}$$

and the initial condition is given through

$$x(0) = \begin{bmatrix} T_{out,init} \\ T_{Exp,init} \\ T_{in,init} \\ T_{Steam,init} \end{bmatrix}. \tag{5.36}$$

Considering the definition of these vectors, it can be seen that the set of differential equations (5.27), (5.29), (5.32) and (5.33) does not form a model of the type given by equation (5.23). Time-dependent factors like the inverse time constant $1/t_{Col}(t)$ in equation (5.27) form a product with the temperatures of the incoming and outgoing HTF ($T_{in}(t)$ and $T_{out}(t)$ in equation (5.27)). Thus, a time-invariant matrix A cannot exist. But not even a time-varying linear state-space model (equation (5.20)) is given since the temperature dependent HTF density and HTF specific heat are in the denominator of a fraction where the related HTF temperature is in the numerator as it is the case in equation (5.27) and (5.32). Therefore the model defined by the four differential equations (5.27), (5.29), (5.32) and (5.33) is not of the linear state-space form as defined above. Considering again the vector definitions made in (5.34), (5.35) and (5.36), the simplified model is of the very general form

$$\dot{x}(t) = f\left[x(t), u(t), t\right]. \tag{5.37}$$

Equation (5.37) stands for:

$$\begin{bmatrix} \frac{dT_{out}(t)}{dt} \\ \frac{dT_{Exp}(t)}{dt} \\ \frac{dT_{in}(t)}{dt} \\ \frac{dT_{Steam}(t)}{dt} \end{bmatrix} = \begin{bmatrix} \frac{1}{t_{Col}(t)}\left(T_{in}(t)-T_{out}(t)\right)+\frac{q_{absorbed}(t)-UA_{Col}\left(T_{out}(t)-T_{amb}(t)\right)}{A_{Col}\, r_{HTF}\left(T_{out}(t)\right)c_{HTF}\left(T_{out}(t)\right)} \\ \frac{1}{t_{Exp}(t)}\left(T_{out}(t)-T_{Exp}(t)\right) \\ \frac{1}{t_{HE}(t)}\left(T_{Exp}(t)-T_{in}(t)\right)-\frac{UA_{HE}(t)\left(T_{Exp}(t)+T_{in}(t)-T_{Steam}(t)-T_{Water}(t)\right)}{2\cdot A_{HE}\, r_{HTF}\left(T_{in}(t)\right)c_{HTF}\left(T_{in}(t)\right)} \\ 0.01\cdot\left(\left(-T_{Steam}(t)\right)+e_{HE}(t)\left(T_{Exp}(t)-T_{Water}(t)\right)+T_{Water}(t)\right) \end{bmatrix} \quad (5.38)$$

Since the simplified model is not in the required form for implementation in the linear MPC algorithm, it is necessary to make approximations of the simplified model to convert the equations to the required form (5.23).

5.3.1 Model Linearization

The linearization procedure, taken from Kwakernaak and Sivan (1972), is first presented theoretically by starting with the general form of the system (5.37). Suppose that $u_{nom}(t)$ is a given input to system (5.37) and $x_{nom}(t)$ is a known solution of the state differential equation (5.37). Then, $x_{nom}(t)$ satisfies

$$\dot{x}_{nom}(t) = f\left[x_{nom}(t), u_{nom}(t), t\right], \qquad 0 \le t \le t_{END}. \quad (5.39)$$

Note the time interval is finite with the upper bound t_{END} and the lower bound at zero (without losing generality). The goal is to find approximations to neighboring solutions, for small deviations from x_{nom} and for small deviations from u_{nom}. It is referred to u_{nom} as a nominal input and to x_{nom} as a nominal trajectory. A common assumption is that the system is operated close to nominal conditions, which means that u and x deviate only slightly from u_{nom} and x_{nom}.

Thus it can be written

$$u(t) = u_{nom}(t) + \tilde{u}(t), \qquad 0 \le t \le t_{END}, \tag{5.40}$$

$$x(0) = x_{nom}(0) + \tilde{x}(0), \tag{5.41}$$

where $\tilde{u}(t)$ and $\tilde{x}(0)$ are small perturbations. Correspondingly, it is

$$x(t) = x_{nom}(t) + \tilde{x}(t), \qquad 0 \le t \le t_{END}. \tag{5.42}$$

After substituting equation (5.40) and equation (5.42) into the state differential equation (5.37), a Taylor expansion is made, yielding

$$\begin{aligned} \dot{x}_{nom}(t) + \dot{\tilde{x}}(t) = {} & f\left[x_{nom}(t), u_{nom}(t), t\right] + J_x\left[x_{nom}(t), u_{nom}(t), t\right]\tilde{x}(t) \\ & + J_u\left[x_{nom}(t), u_{nom}(t), t\right]\tilde{u}(t) + hot, \qquad 0 \le t \le t_{END} \end{aligned}. \tag{5.43}$$

Here J_x and J_u are the Jacobian matrices of f with respect to x and u. That is, J_x is a matrix the (i,j)-th element of which is

$$\left(J_x\right)_{i,j} = \frac{\partial f_i}{\partial x_j}, \tag{5.44}$$

where f_i is the i-th component of f and x_j is the j-th component of x. J_u is similarly defined. The higher order term, *hot*, is supposed to be "small" with respect to $\tilde{x}$ and $\tilde{u}$ and thus is neglected. Equation (5.43) can then be expressed as

$$\dot{\tilde{x}}(t) = J_x\left[x_{nom}(t), u_{nom}(t), t\right]\tilde{x}(t) + J_u\left[x_{nom}(t), u_{nom}(t), t\right]\tilde{u}(t), \qquad 0 \le t \le t_{END,} \tag{5.45}$$

meaning that $\tilde{x}$ and $\tilde{u}$ approximately satisfy a linear equation of the form given in equation (5.20) if $A(t) = J_x\left[x_{nom}(t), u_{nom}(t), t\right]$ and $B(t) = J_u\left[x_{nom}(t), u_{nom}(t), t\right]$. Equation (5.45) is called linearized state differential equation, its initial condition is $\tilde{x}(0)$ from equation (5.41).

This method is used to linearize equation (5.38). Thus it is necessary to determine the Jacobian matrices J_x and J_u for system (5.38). For a better understanding, equation (5.38) is now written as

$$\begin{bmatrix} \dfrac{dT_{out}(t)}{dt} \\ \dfrac{dT_{Exp}(t)}{dt} \\ \dfrac{dT_{in}(t)}{dt} \\ \dfrac{dT_{Steam}(t)}{dt} \end{bmatrix} = \begin{bmatrix} f_1[x(t),u(t),t] \\ f_2[x(t),u(t),t] \\ f_3[x(t),u(t),t] \\ f_4[x(t),u(t),t] \end{bmatrix} . \tag{5.46}$$

Thus, the components of the vector on the right-hand side are

$$f_1[x(t),u(t),t] = \frac{1}{t_{Col}(t)}\left(T_{in}(t) - T_{out}(t)\right) + \frac{q_{absorbed}(t) - UA_{Col}\left(T_{out}(t) - T_{amb}(t)\right)}{A_{Col}\, r_{HTF}\left(T_{out}(t)\right) c_{HTF}\left(T_{out}(t)\right)}, \tag{5.47}$$

$$f_2[x(t),u(t),t] = \frac{1}{t_{Exp}(t)}\left(T_{out}(t) - T_{Exp}(t)\right), \tag{5.48}$$

$$f_3[x(t),u(t),t] = \frac{1}{t_{HE}(t)}\left(T_{Exp}(t) - T_{in}(t)\right) - \frac{UA_{HE}(t)\left(T_{Exp}(t) + T_{in}(t) - T_{Steam}(t) - T_{Water}(t)\right)}{2 \cdot A_{HE}\, r_{HTF}\left(T_{in}(t)\right) c_{HTF}\left(T_{in}(t)\right)}, \tag{5.49}$$

$$f_4[x(t),u(t),t] = 0.01 \cdot \left(\left(-T_{Steam}(t)\right) + e_{HE}(t)\left(T_{Exp}(t) - T_{Water}(t)\right) + T_{Water}(t)\right). \tag{5.50}$$

From the definition of the Jacobian matrix in equation (5.44) and the state vector in (5.34), the Jacobian matrix J_x for system (5.38) is

$$J_x[x(t),u(t),t]=\begin{bmatrix} \frac{\partial f_1}{\partial T_{out}} & \frac{\partial f_1}{\partial T_{Exp}} & \frac{\partial f_1}{\partial T_{in}} & \frac{\partial f_1}{\partial T_{Steam}} \\ \frac{\partial f_2}{\partial T_{out}} & \frac{\partial f_2}{\partial T_{Exp}} & \frac{\partial f_2}{\partial T_{in}} & \frac{\partial f_2}{\partial T_{Steam}} \\ \frac{\partial f_3}{\partial T_{out}} & \frac{\partial f_3}{\partial T_{Exp}} & \frac{\partial f_3}{\partial T_{in}} & \frac{\partial f_3}{\partial T_{Steam}} \\ \frac{\partial f_4}{\partial T_{out}} & \frac{\partial f_4}{\partial T_{Exp}} & \frac{\partial f_4}{\partial T_{in}} & \frac{\partial f_4}{\partial T_{Steam}} \end{bmatrix}, \tag{5.51}$$

and regarding the input vector in (5.35), the Jacobian matrix J_u is

$$J_u[x(t),u(t),t]=\begin{bmatrix} \frac{\partial f_1}{\partial q_{absorbed}} & \frac{\partial f_1}{\partial T_{amb}} & \frac{\partial f_1}{\partial \dot{V}_{HTF}} & \frac{\partial f_1}{\partial \dot{m}} & \frac{\partial f_1}{\partial T_{Water}} \\ \frac{\partial f_2}{\partial q_{absorbed}} & \frac{\partial f_2}{\partial T_{amb}} & \frac{\partial f_2}{\partial \dot{V}_{HTF}} & \frac{\partial f_2}{\partial \dot{m}} & \frac{\partial f_2}{\partial T_{Water}} \\ \frac{\partial f_3}{\partial q_{absorbed}} & \frac{\partial f_3}{\partial T_{amb}} & \frac{\partial f_3}{\partial \dot{V}_{HTF}} & \frac{\partial f_3}{\partial \dot{m}} & \frac{\partial f_3}{\partial T_{Water}} \\ \frac{\partial f_4}{\partial q_{absorbed}} & \frac{\partial f_4}{\partial T_{amb}} & \frac{\partial f_4}{\partial \dot{V}_{HTF}} & \frac{\partial f_4}{\partial \dot{m}} & \frac{\partial f_4}{\partial T_{Water}} \end{bmatrix}. \tag{5.52}$$

In the following, each derivative in the matrices J_x and J_u is listed and new variables for some of these derivatives are introduced for clarity:

$$\frac{\partial f_1}{\partial T_{out}} = -\frac{1}{t_{Col}(t)} - \frac{UA_{Col}}{A_{Col}\ \ r_{HTF}\left(T_{out}(t)\right)\ \ c_{HTF}\left(T_{out}(t)\right)} - \frac{\left(\frac{\partial r_{HTF}}{\partial T_{out}} c_{HTF} + r_{HTF}\frac{\partial c_{HTF}}{\partial T_{out}}\right)}{A_{Col}\left(r_{HTF}\left(T_{out}(t)\right)\ \ c_{HTF}\left(T_{out}(t)\right)\right)^2}\left[q_{absorbed}(t) - UA_{Col}\left(T_{out}(t) - T_{amb}(t)\right)\right], \quad (5.53)$$

$$= -\frac{1}{t_{Col}(t)} - \frac{UA_{Col}}{A_{Col}\ \ r_{HTF}\left(T_{out}(t)\right)\ \ c_{HTF}\left(T_{out}(t)\right)} - N(t)$$

$$\frac{\partial f_1}{\partial T_{Exp}} = 0, \quad (5.54)$$

$$\frac{\partial f_1}{\partial T_{in}} = \frac{1}{t_{Col}(t)}, \quad (5.55)$$

$$\frac{\partial f_1}{\partial T_{Steam}} = 0. \quad (5.56)$$

……..

$$\frac{\partial f_2}{\partial T_{out}} = \frac{1}{t_{Exp}(t)}, \quad (5.57)$$

$$\frac{\partial f_2}{\partial T_{Exp}} = -\frac{1}{t_{Exp}(t)}, \quad (5.58)$$

$$\frac{\partial f_2}{\partial T_{in}} = 0, \quad (5.59)$$

$$\frac{\partial f_2}{\partial T_{Steam}} = 0. \quad (5.60)$$

$$\frac{\partial f_3}{\partial T_{out}} = 0, \tag{5.61}$$

$$\frac{\partial f_3}{\partial T_{Exp}} = \frac{1}{t_{HE}(t)} - \frac{UA_{HE}(t)}{2 \cdot A_{HE}\ r_{HTF}\left(T_{in}(t)\right) c_{HTF}\left(T_{in}(t)\right)}, \tag{5.62}$$

$$\begin{aligned}\frac{\partial f_3}{\partial T_{in}} &= -\frac{1}{t_{HE}(t)} - \frac{UA_{HE}(t)}{2 \cdot A_{HE}\ r_{HTF}\left(T_{in}(t)\right) c_{HTF}\left(T_{in}(t)\right)} \\ &\quad + \frac{UA_{HE}(t)\left[\frac{\partial r_{HTF}}{\partial T_{in}} c_{HTF} + r_{HTF}\frac{\partial c_{HTF}}{\partial T_{in}}\right]}{2 \cdot A_{HE}\left(r_{HTF}\left(T_{in}(t)\right) c_{HTF}\left(T_{in}(t)\right)\right)^2}\left(T_{in}(t) + T_{Exp}(t) - T_{Steam}(t) - T_{Water}(t)\right), \\ &= -\frac{1}{t_{HE}(t)} - \frac{UA_{HE}(t)}{2 \cdot A_{HE}\ r_{HTF}\left(T_{in}(t)\right) c_{HTF}\left(T_{in}(t)\right)} + N_{HE}(t)\end{aligned} \tag{5.63}$$

$$\frac{\partial f_3}{\partial T_{Steam}} = \frac{UA_{HE}(t)}{2 \cdot A_{HE}\ r_{HTF}\left(T_{in}(t)\right) c_{HTF}\left(T_{in}(t)\right)}. \tag{5.64}$$

……..

$$\frac{\partial f_4}{\partial T_{out}} = 0, \tag{5.65}$$

$$\frac{\partial f_4}{\partial T_{Exp}} = 0.01 \cdot e_{HE}(t), \tag{5.66}$$

$$\frac{\partial f_4}{\partial T_{in}} = 0, \tag{5.67}$$

$$\frac{\partial f_4}{\partial T_{Steam}} = -0.01. \tag{5.68}$$

……..

$$\frac{\partial f_1}{\partial q_{absorbed}} = \frac{1}{A_{Col}\ r_{HTF}\left(T_{out}(t)\right) c_{HTF}\left(T_{out}(t)\right)}, \tag{5.69}$$

$$\frac{\partial f_1}{\partial T_{amb}} = \frac{UA_{Col}}{A_{Col}\ r_{HTF}\left(T_{out}(t)\right) c_{HTF}\left(T_{out}(t)\right)}, \tag{5.70}$$

$$\frac{\partial f_1}{\partial \dot{V}_{HTF}} = \frac{1}{V_{Col}}\left(T_{in}(t) - T_{out}(t)\right), \tag{5.71}$$

$$\frac{\partial f_1}{\partial \dot{m}} = 0, \tag{5.72}$$

$$\frac{\partial f_1}{\partial T_{Water}} = 0. \tag{5.73}$$

……..

$$\frac{\partial f_2}{\partial q_{absorbed}} = 0, \tag{5.74}$$

$$\frac{\partial f_2}{\partial T_{amb}} = 0, \tag{5.75}$$

$$\frac{\partial f_2}{\partial \dot{V}_{HTF}} = \frac{1}{V_{Exp}}\left(T_{out}(t) - T_{Exp}(t)\right), \tag{5.76}$$

$$\frac{\partial f_2}{\partial \dot{m}} = 0, \tag{5.77}$$

$$\frac{\partial f_2}{\partial T_{Water}} = 0. \tag{5.78}$$

……..

$$\frac{\partial f_3}{\partial q_{absorbed}} = 0, \tag{5.79}$$

$$\frac{\partial f_3}{\partial T_{amb}} = 0, \tag{5.80}$$

$$\frac{\partial f_3}{\partial \dot{V}_{HTF}} = \frac{(a_A + a_B)}{V_{HE}}\left(T_{Exp}(t) - T_{in}(t)\right) - \frac{74000 \cdot A_{surf,HE}}{4 \cdot \dot{V}_{HTF,0}\, A_{HE}\; r_{HTF}\left(T_{in}(t)\right) c_{HTF}\left(T_{in}(t)\right)}\left(T_{Exp}(t) + T_{in}(t) - T_{Steam}(t) - T_{Water}(t)\right),$$
$$= \frac{(a_A + a_B)}{V_{HE}}\left(T_{Exp}(t) - T_{in}(t)\right) - \frac{K(t)}{2 \cdot A_{HE}\; r_{HTF}\left(T_{in}(t)\right) c_{HTF}\left(T_{in}(t)\right) \dot{V}_{HTF,0}} \tag{5.81}$$

$$\frac{\partial f_3}{\partial \dot{m}} = -\frac{74000 \cdot A_{surf,HE}}{4 \cdot \dot{m}_0\, A_{HE}\; r_{HTF}\left(T_{in}(t)\right) c_{HTF}\left(T_{in}(t)\right)}\left(T_{Exp}(t) + T_{in}(t) - T_{Steam}(t) - T_{Water}(t)\right), \tag{5.82}$$
$$= -\frac{K(t)}{2 \cdot A_{HE}\; r_{HTF}\left(T_{in}(t)\right) c_{HTF}\left(T_{in}(t)\right) \dot{m}_0}$$

$$\frac{\partial f_3}{\partial T_{Water}} = \frac{UA_{HE}(t)}{2 \cdot A_{HE}\; r_{HTF}\left(T_{in}(t)\right) c_{HTF}\left(T_{in}(t)\right)}. \tag{5.83}$$

……

$$\frac{\partial f_4}{\partial q_{absorbed}} = 0, \tag{5.84}$$

$$\frac{\partial f_4}{\partial T_{amb}} = 0, \tag{5.85}$$

$$\frac{\partial f_4}{\partial \dot{V}_{HTF}} = -\frac{0.0005}{\dot{V}_{HTF,0}}\left(T_{Exp}(t) - T_{Water}(t)\right), \tag{5.86}$$

$$\frac{\partial f_4}{\partial \dot{m}} = -\frac{0.0005}{\dot{m}_0}\left(T_{Exp}(t) - T_{Water}(t)\right), \tag{5.87}$$

$$\frac{\partial f_4}{\partial T_{Water}} = 0.01 \cdot \left(1 - e_{HE}(t)\right). \tag{5.88}$$

If the Jacobian matrices J_x from equation (5.51) and J_u from equation (5.52) with their elements given through equations (5.53) – (5.88) are evaluated for a nominal input, $u_{nom}(t)$, and a nominal trajectory, $x_{nom}(t)$, then a time-varying linearized state differential equation of the form given in equation (5.45) is found. Next, the four linear differential equations are presented that are found after multiplying and simplifying the right-hand side of equation (5.45). For a small perturbation of the collector outlet temperature, $\tilde{T}_{out}(t)$, around a nominal solution, the approximate linear differential equation is

$$\begin{aligned}\frac{d\tilde{T}_{out}(t)}{dt} = &\frac{\tilde{q}_{absorbed}(t)}{A_{Col}\ \ r_{HTF}\left(T_{out,nom}(t)\right)\ \ c_{HTF}\left(T_{out,nom}(t)\right)} - \frac{UA_{Col}\left[\tilde{T}_{out}(t) - \tilde{T}_{amb}(t)\right]}{A_{Col}\ \ r_{HTF}\left(T_{out,nom}(t)\right)\ \ c_{HTF}\left(T_{out,nom}(t)\right)} \\ &+ \frac{1}{t_{Col,nom}(t)}\left[\tilde{T}_{in}(t) - \tilde{T}_{out}(t)\right] + N_{nom}(t)\ \ \tilde{T}_{out}(t) \\ &+ \frac{1}{V_{Col}}\left(T_{in,nom}(t) - T_{out,nom}(t)\right)\ \ \dot{\tilde{V}}_{HTF}(t)\end{aligned}, \tag{5.89}$$

with the initial condition

$$\tilde{T}_{out}(0) = \tilde{T}_{out,init}. \tag{5.90}$$

The linear differential equation for a small perturbation of the expansion vessel temperature, $\tilde{T}_{Exp}$, around a nominal solution is

$$\frac{d\tilde{T}_{Exp}(t)}{dt} = \frac{1}{t_{Exp,nom}(t)}\left[\tilde{T}_{out}(t) - \tilde{T}_{Exp}(t)\right] + \frac{1}{V_{Exp}}\left(T_{out,nom}(t) - T_{Exp,nom}(t)\right)\dot{\tilde{V}}_{HTF}(t), \tag{5.91}$$

with the initial condition

$$\tilde{T}_{Exp}(0) = \tilde{T}_{Exp,init}. \tag{5.92}$$

For the collector inlet temperature, the linearized differential equation is

$$\begin{aligned}\frac{d\tilde{T}_{in}(t)}{dt} = {} & \frac{1}{t_{HE,nom}(t)}\left[\tilde{\dot{T}}_{Exp}(t) - \tilde{\dot{T}}_{in}(t)\right] \\ & - \frac{UA_{HE,nom}(t)\left(\tilde{T}_{Exp}(t) + \tilde{T}_{in}(t) - \tilde{T}_{Steam}(t) - \tilde{T}_{Water}(t)\right)}{2 \cdot A_{HE}\ r_{HTF}\left(T_{in,nom}(t)\right)c_{HTF}\left(T_{in,nom}(t)\right)} + N_{HE,nom}(t)\,\tilde{T}_{in}(t) \\ & + \frac{(a_A + a_B)}{V_{HE}}\left(T_{Exp,nom}(t) - T_{in,nom}(t)\right)\tilde{\dot{V}}_{HTF}(t) \\ & - \frac{K_{nom}(t)}{2 \cdot A_{HE}\ r_{HTF}\left(T_{in,nom}(t)\right)c_{HTF}\left(T_{in,nom}(t)\right)}\left[\frac{\tilde{\dot{V}}_{HTF}(t)}{\dot{V}_{HTF,0}} + \frac{\tilde{\dot{m}}}{\dot{m}_0}\right]\end{aligned}, \quad (5.93)$$

with the initial condition

$$\tilde{T}_{in}(0) = \tilde{T}_{in,init}. \quad (5.94)$$

Finally, the linear differential equation for a small perturbation of the steam outlet temperature of the heat exchanger, $\tilde{T}_{Steam}$, around a nominal solution is

$$\begin{aligned}\frac{d\tilde{T}_{Steam}}{dt} = {} & 0.01 \cdot \left[\left(-\tilde{T}_{Steam}(t)\right) + e_{HE,nom}(t)\left(\tilde{T}_{Exp}(t) - \tilde{T}_{Water}(t)\right) + \tilde{T}_{Water}(t)\right] \\ & - 0.0005 \cdot \left(T_{Exp,nom}(t) - T_{Water,nom}(t)\right)\left[\frac{\tilde{\dot{V}}_{HTF}(t)}{\dot{V}_{HTF,0}} + \frac{\tilde{\dot{m}}(t)}{\dot{m}_0}\right]\end{aligned}, \quad (5.95)$$

with the initial condition

$$\tilde{T}_{Steam}(0) = \tilde{T}_{Steam,init}. \quad (5.96)$$

To obtain a time-invariant linearized state differential equation from (5.45), a steady-state situation as nominal solution is considered, where all quantities are constant. A constant input to the system means that the absorbed solar energy, the ambient temperature, the HTF volume flow rate, the mass flow rate and the water temperature are held constant. For such a constant input, temperatures will evolve throughout the plant that stay constant with ongoing

time if no further change in the input variables occurs. The constant input together with the constant temperatures is called a steady-state situation. If the constant input is taken as nominal input, u_{nom}, and the evolved constant temperatures as nominal trajectory, x_{nom}, then the Jacobian matrices J_x and J_u have constant elements if evaluated for this nominal solution. In this case, the linearized state differential equation (5.45) is time-invariant and a model of the form (5.23) is found that can be applied to the MPC algorithm

$$\dot{\tilde{x}}(t) = A\tilde{x}(t) + B\tilde{u}(t). \tag{5.97}$$

However, a slight variation of equation (5.97) is used here since a distinction is made between manipulable inputs and inputs that cannot be manipulated or that are not considered to be manipulated for the purpose of the collector outlet temperature control (as the steam mass flow rate $\dot{m}(t)$ in this study). In order to control the collector outlet temperature, only the HTF volume flow rate $\dot{V}_{HTF}(t)$ is adjusted and the following scalar is defined

$$u_m(t) = \dot{V}_{HTF}(t). \tag{5.98}$$

The input variable $u_m(t)$ stands for manipulable input.

In addition, the vector of non-manipulated inputs is defined as

$$u_d(t) = \begin{bmatrix} q_{absorbed}(t) \\ T_{ambient}(t) \\ \dot{m}(t) \\ T_{Water}(t) \end{bmatrix}. \tag{5.99}$$

Instead of using the input vector $u(t)$ from equation (5.35), the two input variables $u_m(t)$ and $u_d(t)$ are taken.

Thus, the time-invariant matrix B is divided into the vector B_m and into the matrix B_d to express equation (5.97) as

$$\dot{\tilde{x}}(t) = A\tilde{x}(t) + B_m \tilde{u}_m(t) + B_d \tilde{u}_d(t). \tag{5.100}$$

The measured output variable $y(t)$ of the system is the collector outlet temperature $T_{out}(t)$, the variable that has to be controlled. From equation (5.24) it follows then

$$\tilde{y}(t) = C\tilde{x}(t), \tag{5.101}$$

with

$$C = \begin{bmatrix} 1 & 0 & 0 & 0 \end{bmatrix} \tag{5.102}$$

from the definition of $x(t)$ in equation (5.34).

The linear model given through equations (5.100) and (5.101) with the initial condition in equation (5.41) is compared to the nonlinear model from equation (5.38). Both models were implemented in EES to predict the collector outlet temperature $T_{out}(t)$ and the steam temperature $T_{Steam}(t)$ for a clear day, June 20, 1998 and a partially cloudy day, December 14, 1998.

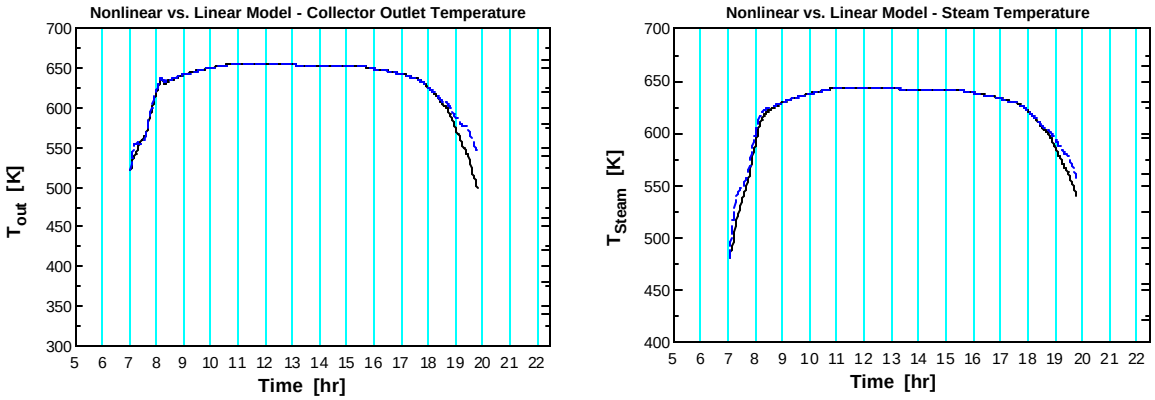

Figure 5.5: A comparison between the simplified nonlinear model (solid line) and its linearized model (dashed line) through the prediction of the collector outlet temperature and the steam temperature for June 20, 1998

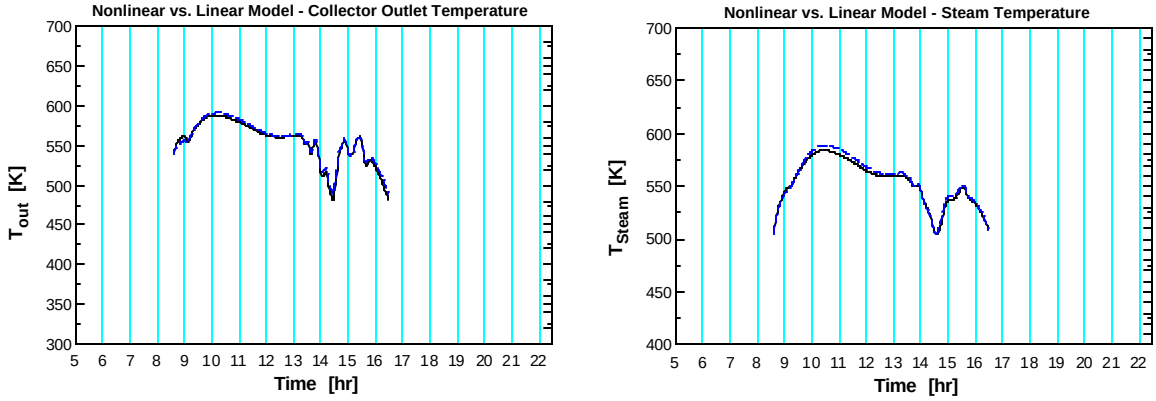

Figure 5.6: A comparison between the simplified nonlinear model (solid line) and its linearized model (dashed line) through a prediction of the collector outlet temperature and the steam temperature for December 14, 1998

In Figure 5.5 the prediction of the nonlinear model indicated by the solid line and the prediction of the linear model indicated by the dashed line are plotted together in the same graph for June 20, 1998. A comparison yields that the calculation with the linear model matches the prediciton of the nonlinear model well for most of the daytime. Only at the end of the plant operation when solar energy decreases, the linear model predictions differ remarkably from the ones made with the nonlinear model. A nearly perfect match is achieved for the partially cloudy day, shown in Figure 5.6.

Since the objective of this work is to develop a controller for the complex plant model from Chapter 4, a linearized model for the complex plant model was obtained by applying the same linearization method as discussed for the simplified model above. The linearization of the complex model is not shown here since the resulting terms are large and it is tedious to obtain them. But a comparison between the complex nonlinear model predicted collector outlet temperature and the collector outlet temperature that was calculated with the linearized model is presented for four days in 1998, shown in Figure 5.7.

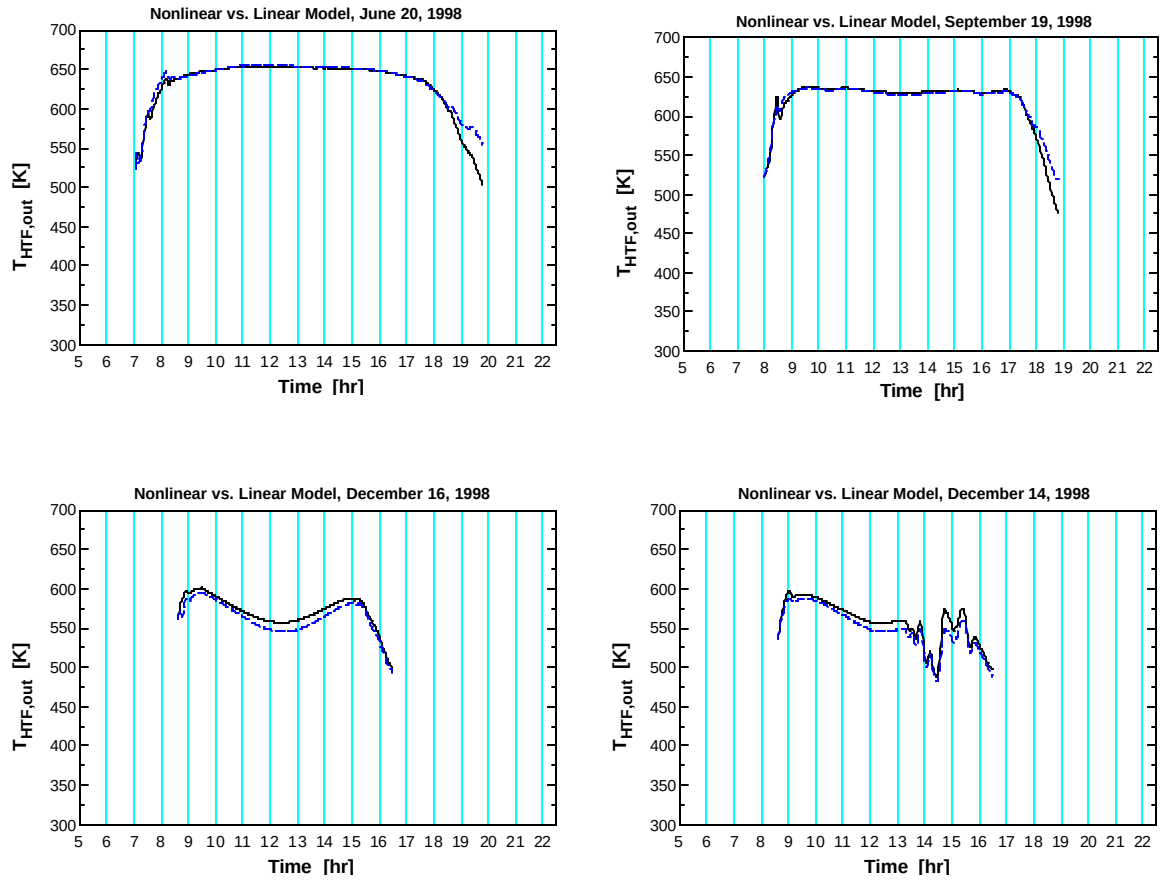

Figure 5.7: Predictions of the collector outlet temperature, calculated from the complex nonlinear model (solid line) and its linearized linear models (dashed line) for a comparison at four different days in 1998

The predictions made with the linearized model for June 20, 1998 and September 19, 1998 match the nonlinear model predictions well until the transient is reached. Then, the predictions differ strongly from each other. The linear model calculated collector outlet temperatures for the two days in December 1998 differ from the nonlinear model temperatures especially during solar noon. However, as will be seen later, the linear models are sufficiently accurate to achieve reasonable MPC control performance on the nonlinear plant model.

5.3.2 Discrete-Time Models

The linear differential equation system (5.100), the output equation (5.101) and the initial condition in equation (5.41) form a continuous-time system. However, MPC deals with discrete-time systems. Consequently, the linear time-invariant continuous-time system has to be transformed into an equivalent discrete-time system of the form

$$\tilde{x}_{k+1} = A_d\,\tilde{x}_k + B_{m,d}\,\tilde{u}_{m,k} + B_{d,d}\,\tilde{u}_{d,k}, \tag{5.103}$$

$$\tilde{y}_k = C_d\,\tilde{x}_k \tag{5.104}$$

where $\tilde{x}_k$ is the state and $\tilde{u}_{m,k}$, $\tilde{u}_{d,k}$ the inputs at time instants t_k, $k = 0,1,2,...$ The initial condition is $\tilde{x}_0$. The sampling period, Δ, is the constant difference between two time instants

$$\Delta = t_{i+1} - t_i \ . \tag{5.105}$$

A derivation of the following transformation for the discrete-time system can be found in Kwakernaak and Sivan (1972) and yields

$$A_d = \mathrm{e}^{A\Delta}, \tag{5.106}$$

$$B_{m,d} = (A_d - I)A^{-1}B_m, \tag{5.107}$$

$$B_{d,d} = (A_d - I)A^{-1}B_d, \tag{5.108}$$

$$C_d = C. \tag{5.109}$$

Through these equations, the discrete-time equations that represent the continuous-time system are obtained. In the following only the discrete-time system is considered and the *d*-index at the matrices is omitted, bearing in mind that the system matrices are the matrices of a discrete-time system.

Before the linear discrete-time model is used in the MPC algorithms, equation (5.103) is augmented by the input step disturbance d_k. This results in

$$\tilde{x}_{k+1} = A\,\tilde{x}_k + B_m\left(\tilde{u}_{m,k} + d_k\right) + B_d\,\tilde{u}_{d,k}\,. \tag{5.110}$$

The affine term d_k serves the purpose of adding integral control, what is explained later.

Constraints on the collector outlet temperature as the output and on the HTF volume flow rate as the manipulable input are considered

$$\tilde{T}_{out,min} \le \tilde{T}_{out,k} \le \tilde{T}_{out,max}\,, \tag{5.111}$$

$$\dot{\tilde{V}}_{HTF,min} \le \dot{\tilde{V}}_{HTF,k} \le \dot{\tilde{V}}_{HTF,max}\,, \tag{5.112}$$

or equivalently

$$\tilde{y}_{min} \le \tilde{y}_k \le \tilde{y}_{max}\,, \tag{5.113}$$

$$\tilde{u}_{m,min} \le \tilde{u}_{m,k} \le \tilde{u}_{m,max}\,. \tag{5.114}$$

The time-invariant linear discrete-time model given through (5.110) and (5.104) together with the constraints (5.113) and (5.114) is now ready for use in the MPC framework from Rawlings and Muske (1993) that is explained next.

5.4 The Model Predictive Control Framework

5.4.1 Receding Horizon Regulator Formulation

As explained in the introduction Chapter 5.1, a cost function that is to be minimized for optimal control must increase with an increasing difference between the forecasted HTF collector field outlet temperatures and the set point temperature. In addition, it must increase with an increasing rate of change in the HTF volume flow rate. Thus the receding horizon

regulator is based on the minimization of the following infinite horizon open-loop quadratic objective function at time k (Rawlings & Muske, 1993):

$$\Phi_k = \frac{1}{2}\sum_{j=0}^{\infty}\left[Q\left(\tilde{T}_{out,k+j} - \tilde{T}_{out,set}\right)^2 + S\Delta\dot{\tilde{V}}^2_{HTF,k+j} \right], \tag{5.115}$$

where Q is a penalty parameter on the difference between the collector outlet temperature and the set point temperature with $Q > 0$. The parameter S with $S > 0$ is a penalty parameter on the rate of change of the HTF volume flow rate as the input in which

$$\Delta\dot{\tilde{V}}_{HTF,k+j} = \dot{\tilde{V}}_{HTF,k+j} - \dot{\tilde{V}}_{HTF,k+j-1}. \tag{5.116}$$

For this input velocity, the following constraints are considered

$$\Delta\dot{\tilde{V}}_{HTF,\min} \le \Delta\dot{\tilde{V}}_{HTF,k} \le \dot{\tilde{V}}_{HTF,\max}. \tag{5.117}$$

The parameters Q and S are the tuning parameters of the receding horizon regulator. A large value of Q in comparison to S may drive the collector outlet temperature quickly to its set point at the expense of large changes in the HTF volume flow rate. If S is chosen large relatively to Q the control action is reduced but the rate at which the collector outlet temperature approaches its set point is slowed down. Tuning the parameters is a non-trivial problem in MPC. The cost function in equation (5.115) is now written as

$$\Phi_k = \frac{1}{2}\sum_{j=0}^{\infty}\left[Q\left(\tilde{y}_{k+j} - \tilde{y}_{set}\right)^2 + S\Delta\tilde{u}^2_{m,k+j} \right]. \tag{5.118}$$

This follows from equation (5.98) and equation (5.101).

The set point of the outlet temperature, $\tilde{y}_{set}$, is the collector outlet temperature of the plant in a steady state satisfying (for discrete-time systems)

$$\tilde{x}_{set} = A\,\tilde{x}_{set} + B_m\left(\tilde{u}_{m,set} + d_k\right) + B_d\,\tilde{u}_{d,k}\,, \tag{5.119}$$

$$\tilde{y}_{set} = C\,\tilde{x}_{set}\,. \tag{5.120}$$

The following substitutions are made to simplify the formulation

$$z_{k+j} \leftarrow \tilde{y}_{k+j} - C\tilde{x}_{set}\,, \tag{5.121}$$

$$w_{k+j} \leftarrow \tilde{x}_{k+j} - \tilde{x}_{set}\,, \tag{5.122}$$

$$v_{m,k+j} \leftarrow \tilde{u}_{m,k+j} - \tilde{u}_{m,set}\,, \tag{5.123}$$

$$v_{d,k+j} \leftarrow \tilde{u}_{d,k+j}\,, \tag{5.124}$$

and the infinite horizon quadratic criterion, equation (5.118), yields

$$\Phi_k = \frac{1}{2}\sum_{j=0}^{\infty}\left[Q\,z_{k+j}^2 + S\,\Delta v_{m,k+j}^2\right]. \tag{5.125}$$

The constraints, formulated in equation (5.113), (5.114) and (5.117), are in their substituted form

$$z_{min} \le z_k \le z_{max}\,, \tag{5.126}$$

$$v_{m,min} \le v_{m,k} \le v_{m,max}\,, \tag{5.127}$$

$$\Delta v_{m,min} \le \Delta v_{m,k} \le \Delta v_{m,max}\,. \tag{5.128}$$

The vector v^N contains the N future open-loop control moves

$$v^N = \begin{bmatrix} v_{m,k} \\ v_{m,k+1} \\ \vdots \\ v_{m,k+N-1} \end{bmatrix}. \tag{5.129}$$

For all times $k + j \ge k + N$, the input $v_{m,k+j}$ is set to zero.

The receding horizon regulator is the optimal control problem

$$\min_{v^N} \Phi_k \tag{5.130}$$

subject to the constraints in equation (5.126), (5.127) and (5.128). From the first input value in v^N, $v_{m,k}$, the HTF volume flow rate $\dot{V}_{HTF,k}$ is recovered and then injected into the plant. This procedure is repeated at each successive control interval, following the feedback law

$$\tilde{u}_{m,k} = r\left(\tilde{x}_k\right) \tag{5.131}$$

by using the plant measurement of the collector outlet temperature to update the state vector at time k.

For an implementation of the optimal control problem (5.130) in digital machines, it is formulated as a quadratic program for v^N. In this work, the quadratic program is solved with MATLAB using the command `quadprog` (MathWorks, 2001). The derivation of the quadratic program from equation (5.130) is not shown here. It follows from tedious straightforward algebraic manipulations. The result is given in Rawlings and Muske (1993) and is presented below. The quadratic program that represents the optimization of the optimal control problem denoted in (5.130) is

$$\min_{v^N} \Phi_k = \frac{1}{2}(v^N)^T H v^N + \left(G w_k - F v_{k-1}\right)^T v^N \tag{5.132}$$

such that

$$\begin{bmatrix} I \\ -I \\ D \\ -D \\ W \\ -W \end{bmatrix} v^N \le \begin{bmatrix} i_1 \\ i_2 \\ d_1 \\ d_2 \\ w_1 \\ w_2 \end{bmatrix}. \tag{5.133}$$

The matrix H and the vectors G and F are computed as

$$H = \begin{bmatrix} B_m^T \bar{Q} B_m + 2S & B_m^T A^T \bar{Q} B_m - S & \cdots & B_m^T A^{T^{N-1}} \bar{Q} B_m \\ B_m^T \bar{Q} A B_m - S & B_m^T \bar{Q} B_m + 2S & \cdots & B_m^T A^{T^{N-2}} \bar{Q} B_m \\ \vdots & \vdots & \ddots & \vdots \\ B_m^T \bar{Q} A^{N-1} B_m & B_m^T \bar{Q} A^{N-2} B_m & \cdots & B_m^T \bar{Q} B_m + 2S \end{bmatrix} . \tag{5.134}$$

$$G = \begin{bmatrix} B_m^T \bar{Q} A \\ B_m^T \bar{Q} A^2 \\ \vdots \\ B_m^T \bar{Q} A^N \end{bmatrix}, \qquad F = \begin{bmatrix} S \\ 0 \\ \vdots \\ 0 \end{bmatrix}$$

For the stable plant model, $\bar{Q}$ is the solution of the following discrete Lyapunov-equation

$$\bar{Q} = C^T Q C + A^T \bar{Q} A . \tag{5.135}$$

This can be solved with the MATLAB command `dlyap`.

The matrices D and W from the inequality constraint (5.133) are computed as shown below with

$$D = \begin{bmatrix} CIB_m & 0 & \cdots & 0 \\ CAB_m & CIB_m & \cdots & 0 \\ \vdots & \ddots & \ddots & \vdots \\ CA^{N-1} B_m & CA^{N-2} B_m & \cdots & CIB_m \end{bmatrix}, \quad W = \begin{bmatrix} I & 0 & \cdots & 0 \\ -I & I & \cdots & 0 \\ \vdots & \ddots & \ddots & \vdots \\ 0 & \cdots & -I & I \\ 0 & \cdots & 0 & -I \end{bmatrix}. \tag{5.136}$$

The values of the right-hand side vectors in equation (5.133) are the following:

$$i_1 = \begin{bmatrix} v_{m,max} \\ \vdots \\ v_{m,max} \end{bmatrix}, \quad i_2 = \begin{bmatrix} -v_{m,min} \\ \vdots \\ -v_{m,min} \end{bmatrix},$$

$$d_1 = \begin{bmatrix} z_{max} - CAw_k \\ \vdots \\ z_{max} - CA^N w_k \end{bmatrix}, \quad d_2 = \begin{bmatrix} -z_{min} + CAw_k \\ \vdots \\ -z_{min} + CA^N w_k \end{bmatrix}, \tag{5.137}$$

$$w_1 = \begin{bmatrix} \Delta v_{m,max} + v_{m,k-1} \\ \Delta v_{m,max} \\ \vdots \\ \Delta v_{m,max} \end{bmatrix}, \quad w_2 = \begin{bmatrix} \Delta v_{m,min} - v_{m,k-1} \\ \Delta v_{m,min} \\ \vdots \\ \Delta v_{m,min} \end{bmatrix}.$$

The following restrictions are imposed on the constraints to ensure consistence and feasibility of the origin

$$\begin{bmatrix} v_{m,max} \\ -v_{m,min} \\ z_{max} \\ -z_{min} \\ \Delta v_{m,max} \\ \Delta v_{m,min} \end{bmatrix} > \begin{bmatrix} 0 \\ 0 \\ 0 \\ 0 \\ 0 \\ 0 \end{bmatrix}. \tag{5.138}$$

Figure 5.8 shows the receding horizon regulator as a block with inputs and outputs.

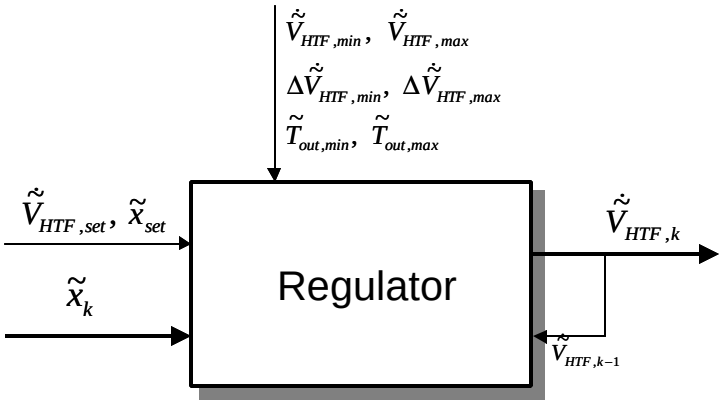

Figure 5.8: The receding horizon regulator as a block with inputs and outputs

5.4.2 Target Calculation

The target is the collector outlet temperature that the controller tries to maintain and was earlier called the collector outlet temperature set point. Since no external output disturbances are considered, the target is indeed identical with the temperature set point $\tilde{y}_{set} = \tilde{y}_{Target}$ and stays constant throughout the entire control procedure. In addition, $\tilde{y}_{set}$ is dependent on the two equations (5.119) and (5.120). When changes in the non-manipulable inputs $\tilde{u}_{d,k}$ occur or in the input step disturbance d_k, then the two equations (5.119) and (5.120) must still be satisfied for the constant target $\tilde{y}_{set}$. Thus, for every change in these variables, a recalculation of the state set point, $\tilde{x}_{set}$, and the input set point, $\tilde{u}_{m,set}$, must guarantee that the equations (5.119) and (5.120) are fulfilled and $\tilde{y}_{set}$ remains the target value. The two equations are the

equality constraints of the following quadratic program from Rawlings and Muske (1993) that calculates the required $\tilde{x}_{set}$ and $\tilde{u}_{m,set}$

$$\min_{[\tilde{x}_{set} \;\; \tilde{u}_{m,set}]^T} \Psi = \frac{1}{2}\left(\tilde{u}_{m,set} - \bar{u}\right)^T R_{set}\left(\tilde{u}_{m,set} - \bar{u}\right) \tag{5.139}$$

subject to:

$$\begin{bmatrix} I - A & -B_m \\ C & 0 \end{bmatrix}\begin{bmatrix} \tilde{x}_{set} \\ \tilde{u}_{m,set} \end{bmatrix} = \begin{bmatrix} B_m\, d + B_d\, \tilde{u}_d \\ \tilde{y}_{Target} \end{bmatrix}, \tag{5.140}$$

$$\tilde{u}_{m,min} \le \tilde{u}_{m,set} \le \tilde{u}_{m,max}. \tag{5.141}$$

In this quadratic program, $\bar{u}$ is the desired value of the input vector at steady state and R_{set} is a positive definite weighting matrix for the deviation of the input vector from $\bar{u}$.

Figure 5.9 shows the target calculation as a block with inputs and outputs.

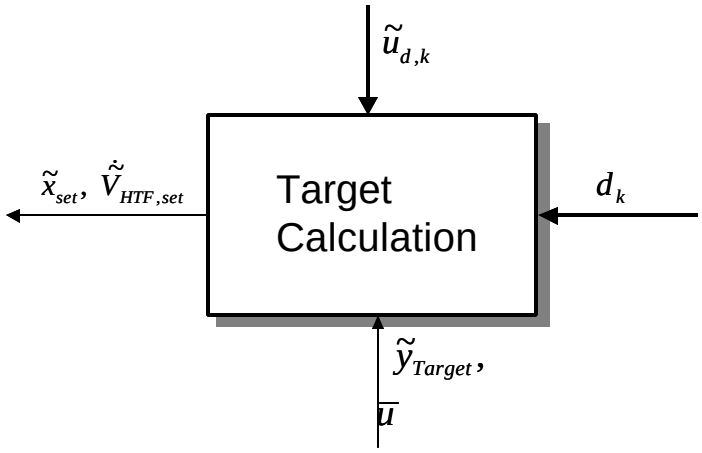

Figure 5.9: The Target Calculation as a block with inputs and outputs

5.4.3 State Estimator

In the section about the regulator, it was assumed that the states $\tilde{x}_k$ are measured. In fact, from the states only the collector outlet temperature $T_{out,k}$ is measured. Thus a method is sought to estimate the entire state $\tilde{x}_k$ from the known collector outlet temperature. In addition to the collector outlet temperature, both the manipulable and the non-manipulable inputs are known or measured. From these given information, the states are estimated through an optimal linear observer, called discrete Kalman filter, constructed for the system

$$\tilde{x}_{k+1} = A\tilde{x}_k + B_m\left(\tilde{u}_{m,k} + d_k\right) + B_d\,\tilde{u}_{d,k} + G_x\,x_k \qquad ,k = 0,\,1,\,2,... \tag{5.142}$$

$$d_{k+1} = d_k + w_k \tag{5.143}$$

$$\tilde{y}_k = C\tilde{x}_k + n_k\,. \tag{5.144}$$

In this representation, x_k, w_k and n_k are zero-mean, uncorrelated, normally distributed, stochastic variables with covariance matrices Q_x, Q_w and R_n respectively.

It was already mentioned that the input step disturbance d_k is used for integral action: in order to obtain offset-free control, it is assumed that the difference between the Kalman-filter-predicted output and the measured output is caused by an input step disturbance d_k. The input step disturbance can be estimated by the Kalman filter as well if it is treated as an additional state of the system, accounted by equation (5.143). The estimated input step disturbance is then used in the target calculation to compensate the offset.

The system can be rewritten with the following augmented matrices

$$\tilde{A}=\begin{bmatrix} A & B_m \\ 0 & 1 \end{bmatrix}, \qquad \tilde{B}_m=\begin{bmatrix} B_m \\ 0 \end{bmatrix}, \qquad \tilde{B}_d=\begin{bmatrix} B_d \\ 0 \end{bmatrix}, \qquad \tilde{C}=\begin{bmatrix} C & 0 \end{bmatrix}, \qquad \tilde{G}_x=\begin{bmatrix} G_x & 0 \\ 0 & 1 \end{bmatrix} \tag{5.145}$$

thus

$$\begin{bmatrix} \tilde{x}_{k+1} \\ d_{k+1} \end{bmatrix}=\tilde{A}\begin{bmatrix} \tilde{x}_k \\ d_k \end{bmatrix}+\tilde{B}_m\,\tilde{u}_{m,k}+\tilde{B}_d\,\tilde{u}_{d,k}+\tilde{G}_x\begin{bmatrix} x_k \\ w_k \end{bmatrix}, \tag{5.146}$$

$$\tilde{y}_k=\tilde{C}\begin{bmatrix} \tilde{x}_k \\ d_k \end{bmatrix}+n_k\ . \tag{5.147}$$

A full-order linear observer for the augmented system (5.146) and (5.147) is

$$\begin{bmatrix} \hat{x}_{k+1|k} \\ \hat{d}_{k+1|k} \end{bmatrix}=\tilde{A}\begin{bmatrix} \hat{x}_{k|k-1} \\ \hat{d}_{k|k-1} \end{bmatrix}+\tilde{B}_m\,\tilde{u}_{m,k|k-1}+\tilde{B}_d\,\tilde{u}_{d,k|k-1}+L\left(\tilde{y}_k-\tilde{C}\begin{bmatrix} \hat{x}_{k|k-1} \\ \hat{d}_{k|k-1} \end{bmatrix}\right), \tag{5.148}$$

where $\hat{x}_{k+1|k}$ and $\hat{d}_{k+1|k}$ is the estimate of the states for time $k+1$ given output and input measurements up to time k. The difference between the measured collector outlet temperature $\tilde{y}_k$ and the reconstructed output is multiplied by the observer gain L and fed back to minimize the estimation error, that is, the difference between the real states and the estimated ones. The stability and the asymptotic behavior of the estimation error are determined by the choice of L. The observer gain L that minimizes the mean square estimation error was first solved by Kalman and Bucy and is computed from the solution of the following discrete filterting steady-state Riccati equation

$$P=\tilde{A}\left[P-P\tilde{C}^T\left(\tilde{C}P\tilde{C}^T+R_n\right)^{-1}\tilde{C}P\right]\tilde{A}^T+\tilde{G}_x\tilde{Q}_x\tilde{G}_x^T, \tag{5.149}$$

$$L=\tilde{A}\,P\,\tilde{C}^T\left(\tilde{C}\,P\,\tilde{C}^T+R_n\right)^{-1}. \tag{5.150}$$

Here, the following augmented covariance matrix is used

$$\tilde{Q}_x = \begin{bmatrix} Q_x & 0 \\ 0 & Q_w \end{bmatrix}. \tag{5.151}$$

The derivation of equation (5.149) and (5.150) is not shown here, it can be found in Kwakernaak & Sivan (1972). Discrete steady-state Riccati equations can be solved with MATLAB using the command `dare`.

Figure 5.10 shows the estimator as a block with inputs and outputs

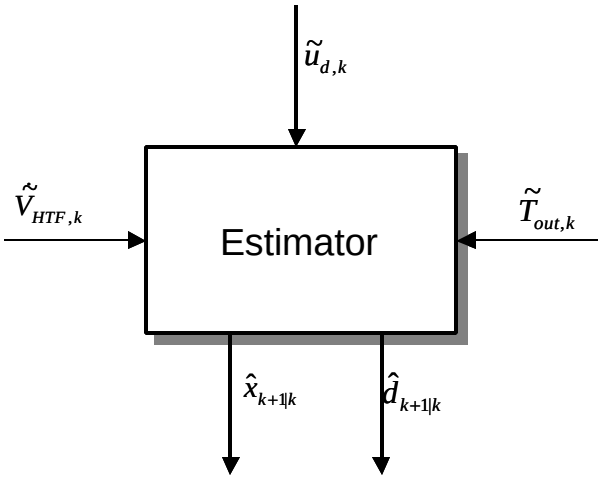

Figure 5.10: The Estimator as a block with inputs and outputs

5.5 Controller Implementation and Results

The receding horizon regulator, the target calculation and the state estimator are appropriately linked together to form the MPC controller as shown in Figure 5.11. The MPC controller was implemented in MATLAB following the structure of the flow chart in Figure 5.11. MATLAB was chosen as the controller language since its control and optimization toolboxes provide the procedures (e.g. the quadratic program) needed to calculate the adjustment (MathWorks, 2001). The plant model, however, was implemented in EES using

its great feature of inbuilt thermodynamic fluid property functions. No defined interface exists between MATLAB and EES. Thus a communication between these two programs was established through Dynamic Data Exchange (DDE) under the Windows operating system. MATLAB as the client initiates the DDE communication and requests EES, the server, to solve the plant model equations. The actual data (e.g. the collector outlet temperature) is transferred through data files between the two communicating processes.

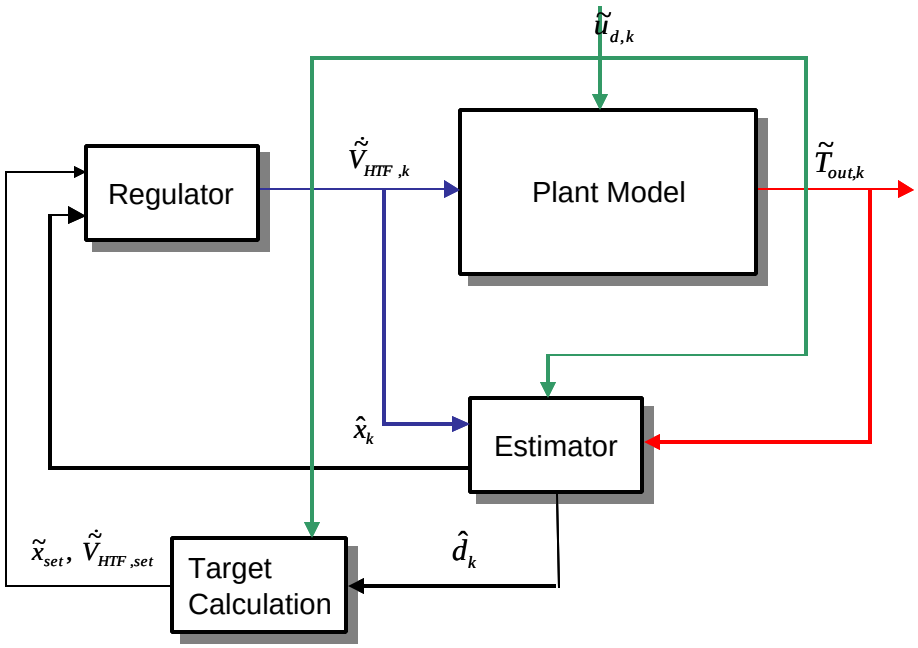

Figure 5.11: MPC controller for the plant model

The performance of the controller is evaluated for four different days in 1998, shown in Figures 5.12, 5.13, 5.14 and 5.15. Figure 5.12 shows the collector outlet temperature, the HTF volume flow rate and the gross output for June 20, 1998. For the HTF volume flow rate, the dashed line represents the adjustment made by a human controller on that day.

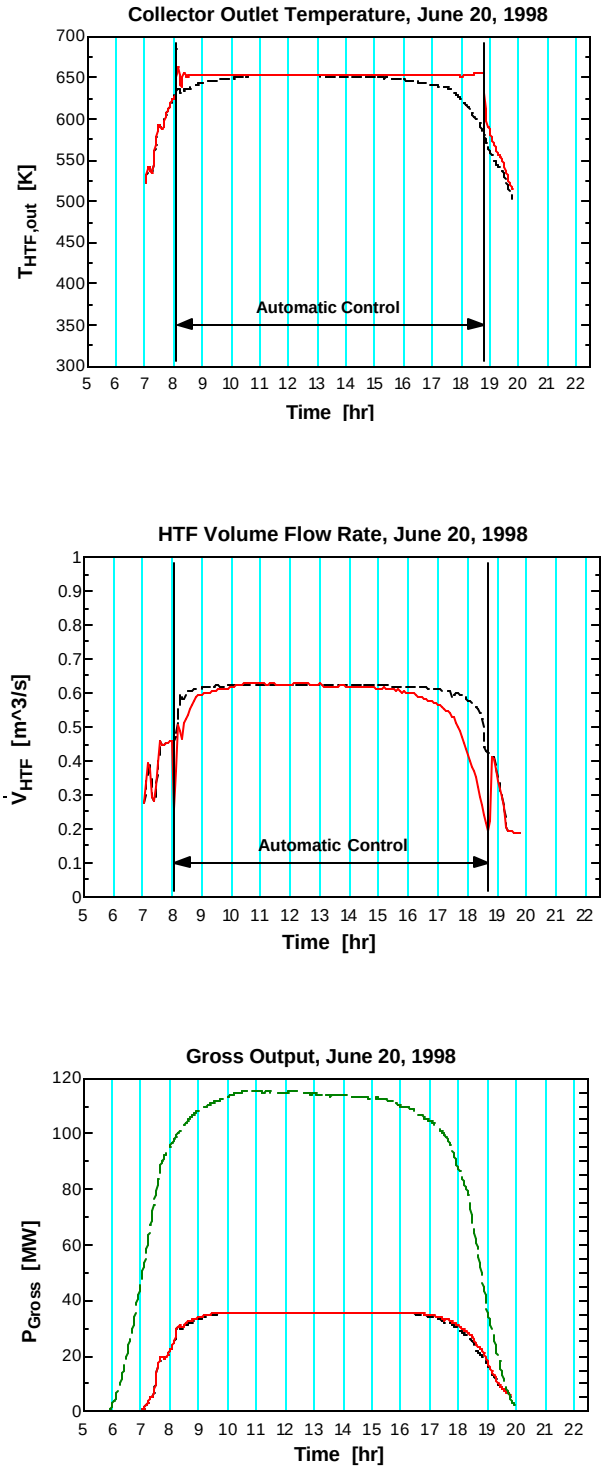

Figure 5.12: Collector outlet temperature, HTF volume flow rate and gross output for June 20, 1998. The collector outlet temperature and the gross output are simulated. For the HTF volume flow rate, the dashed line represents the measured input for a human controller on that day and the solid line represents the input generated through MPC control. For the gross output, the long-dashed line shows the absorbed energy.

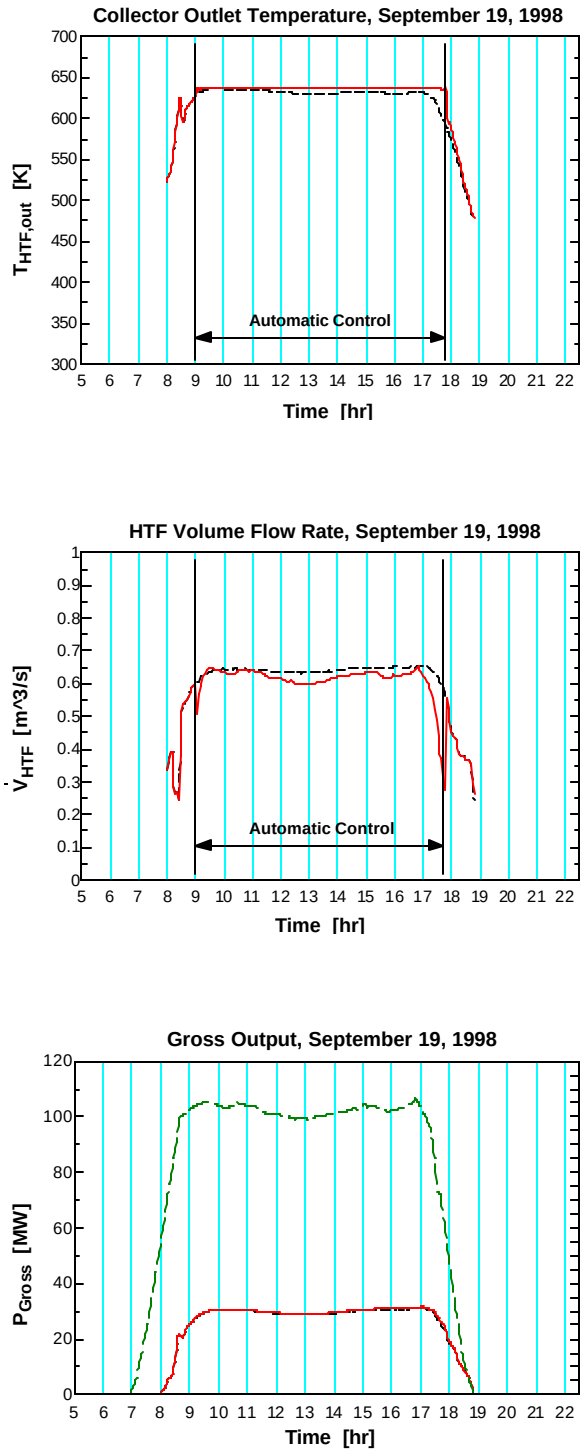

Figure 5.13: Collector outlet temperature, HTF volume flow rate and gross output for September 19, 1998. The collector outlet temperature and the gross output are simulated. For the HTF volume flow rate, the dashed line represents the measured input for a human controller on that day and the solid line represents the input generated through MPC control. For the gross output, the long-dashed line shows the absorbed energy.

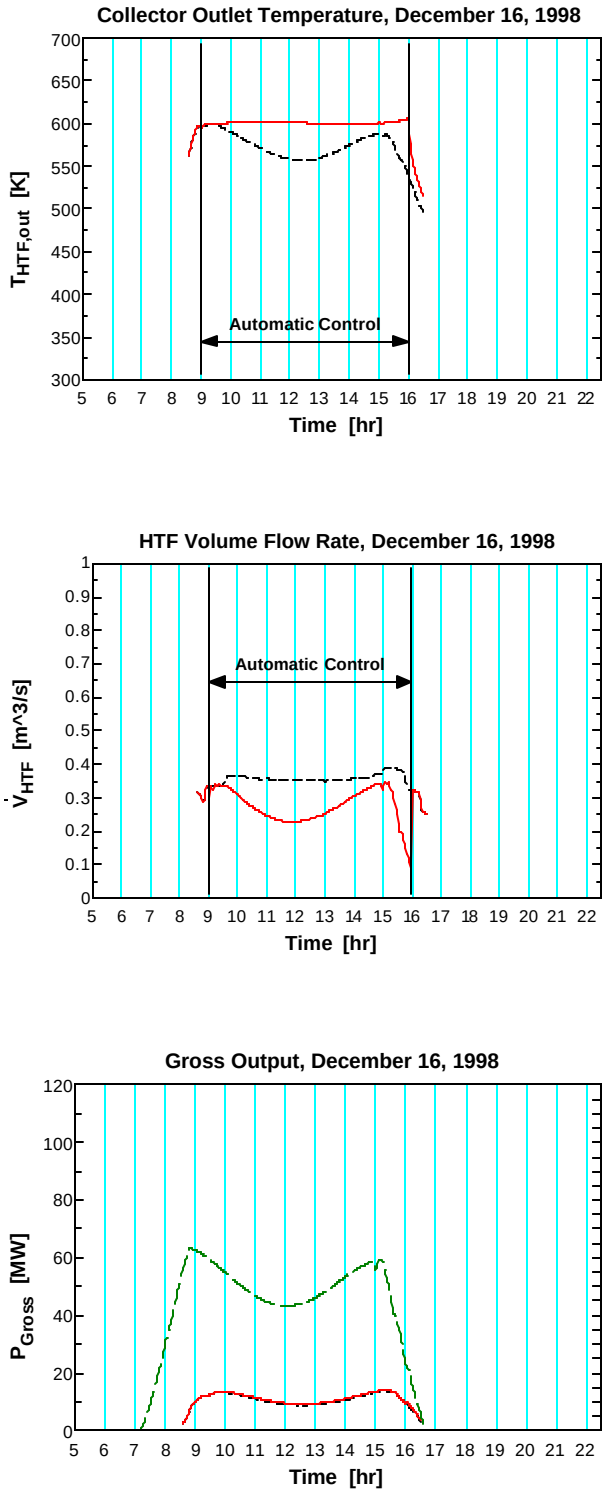

Figure 5.14: Collector outlet temperature, HTF volume flow rate and gross output for December 16, 1998. The collector outlet temperature and the gross output are simulated. For the HTF volume flow rate, the dashed line represents the measured input for a human controller on that day and the solid line represents the input generated through MPC control. For the gross output, the long-dashed line shows the absorbed energy.

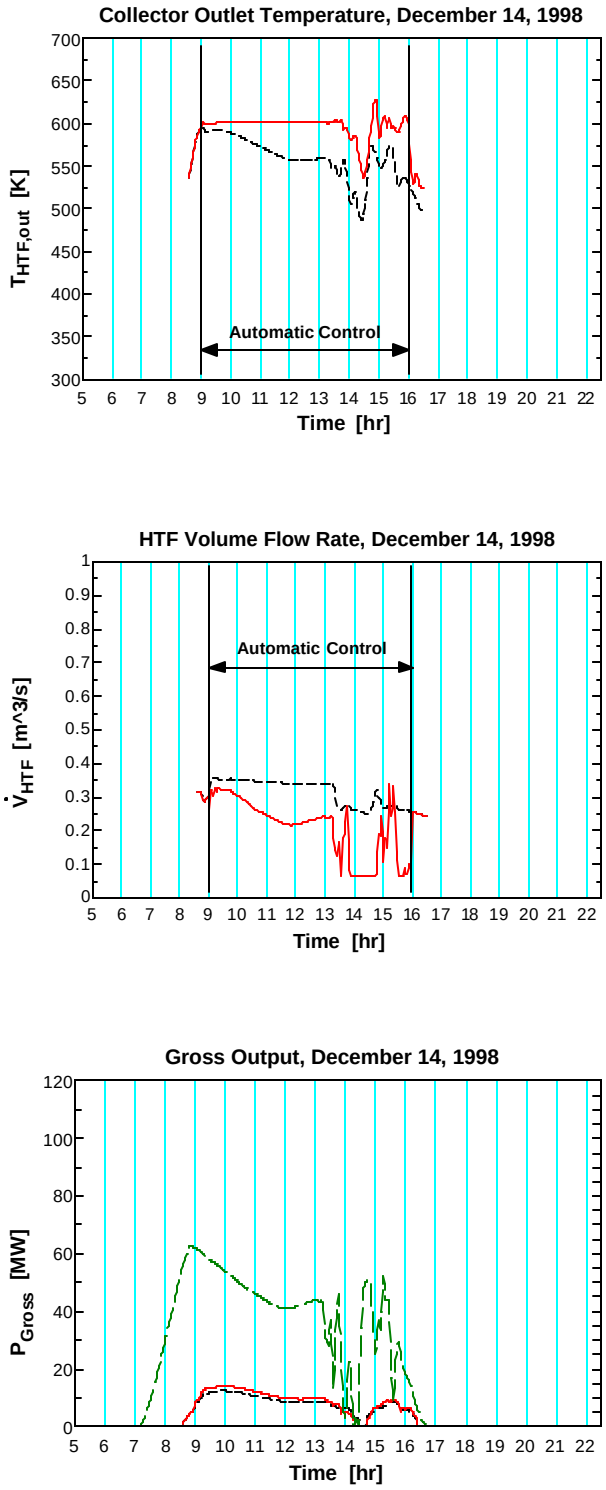

Figure 5.15: Collector outlet temperature, HTF volume flow rate and gross output for December 14, 1998. The collector outlet temperature and the gross output are simulated. For the HTF volume flow rate, the dashed line represents the measured input for a human controller on that day and the solid line represents the input generated through MPC control. For the gross output, the long-dashed line shows the absorbed energy.

The related collector outlet temperature and the gross output, calculated through simulation with the complex plant model, are the dashed lines in the top figure and in the bottom figure respectively. The HTF volume flow rate shown as solid line represents the input calculated through model predictive control. The solid lines in the top and the bottom figure are the corresponding collector outlet temperature and gross output. The automatic controller is turned on at 8.05 hr in the morning and turned off at 18.8 hr. The start up and shut down are assumed to be done by a human. The MPC controller obtains the ability to hold the collector outlet temperature at a constant set point (653.9 K) for a long time throughout the day. For a damping of oscillations, the regulator parameters are $N = 20$, $Q = 50$ and $S = 1000$ for a sample period of $\Delta = 100\,\mathrm{s}$. A noise free control is assumed and the variances of the stochastic variables in the estimator are chosen very small. The performance of the automatic controller is better than the performance of the human controller. However, oscillations occur when starting the automatic control and when the controlled plant reaches the transient. Although different regulator parameters were tested, it was not possible to reject these oscillations. The fact that the MPC controller shows a better performance than the human controller in generating a constant set point collector outlet temperature, does not improve the gross output remarkably, as can be seen from the bottom Figure. As an illustration of efficiency, the absorbed energy is plotted in the graph as well.

In Figure 5.13, the collector outlet temperature and the HTF volume flow rate are shown for September 19, 1998. Again, dashed lines represent human control and solid lines represent automatic control. The linear model used to control on that day is different from the linear model used to control on June 20, 1998 since it was linearized around a different steady-state solution of the nonlinear model. The MPC controller is turned on at 9.00 hr and

turned off at 17.8 hr. The regulator parameters are the same as for June 20, 1998. The set point temperature is 637.2 K. The MPC control action results in a collector outlet temperature that is held constantly in the set point. Slight oscillations occur before the automatic controller is turned off. Also in this case, there is no remarkable improvement in the gross output through automatic control.

In Figure 5.14, the results are shown for December 16, 1998. Again, a different linear model is applied for MPC control compared to the ones used for the control on a summer or early fall day. The automatic controller is turned on at 9.00 hr and turned off at 16.00 hr. The collector outlet temperature set point is 597.3 K, the regulator parameters are the same as above. The automatic control performance is much better than the human one. The controlled temperature slightly rises before the controller is turned off. The gross output doesn't change much when either human or automatic control is applied.

Finally, a partially cloudy day is considered in Figure 5.15. Since December 14, 1998 was two days before December 16, 1998, considered above in Figure 5.14, the same linear model and the same controller parameters and set point temperature are taken. The MPC controller is turned on at 9.00 hr and turned off at 16.00 hr. The automatic controlled collector outlet temperature is in the set point until the solar energy goes down. The automatic controller tries to compensate the occurring drop in the collector outlet temperature through the adjustment of the HTF volume flow rate while reaching its lower bound $\dot{V}_{HTF,min} = 0.0682\ \mathrm{m}^3/\mathrm{s}$. Since the MPC controller is now constraint in its control action, it cannot hold the collector outlet temperature in its set point and the temperature decreases. However, the control action of the automatic controller results in a collector outlet

temperature much closer to the set point compared to the human controlled one. There is no remarkable improvement in the gross output due to automatic controls.

Chapter 6

Conclusions and Recommendations

6.1 Conclusions

A nonlinear model of the 30 MWe SEGS VI parabolic trough plant has been established. The model consists of a dynamic model for the collector field and a steady-state model for the power plant.

First, the collector field model was presented as coupled partial differential equations for energy. For the implementation in digital machines, a set of ordinary differential equations was obtained through dicretization of the governing energy PDEs. The calculation of the absorbed solar energy from the direct normal solar radiation was presented. The performance of this model was evaluated through a comparison between predicted and measured data. The model calculations matched the measurement very well.

A steady-state model for the power plant Clausius-Rankine cycle was developed from measured power plant data and from a report by Lippke (1995) on the power plant design conditions. Good agreement between the power plant model predictions and measured data was achieved.

The collector field model and the power plant model were combined to an entire plant model that was implemented in EES. This plant model was also evaluated through a comparison between predicted and measured data. It proved to be a useful model for SEGS VI.

A model predictive controller was developed for the SEGS VI plant model. Its task is to maintain a constant collector outlet temperature on different days of a year by adjusting the heat transfer fluid volume flow rate while solar radiation changes. The control algorithmic, which is based on Rawlings and Muske (1993), was introduced on the example of a simplified model. The automatic controller was implemented in MATLAB. The control performance was evaluated through simulations for four different days in 1998. The MPC controller showed the capability to hold the collector outlet temperature close around the specified set point for a long time during the day. The automatic controller demonstrated a better control of the collector outlet temperature than the human control. However, the improvement in the predicted gross output of the power plant due to the better control of the collector outlet temperature is small.

6.2 Recommendations

Further studies should include the model predictive control strategy with the objective to maximize the gross output. Controlling both, the HTF volume flow rate and the steam mass flow rate in the power plant could help improving the daily gross output of the parabolic trough plant.

Appendix A

Collector Dimensions

$Length$	=	753.6 m	, collector mirror length
$D_{ABS,i}$	=	0.066 m	, inside diameter of the absorber tube
$D_{ABS,o}$	=	0.07 m	, outside diameter of the absorber tube
$D_{ENV,i}$	=	0.112 m	, inside diameter of the glass envelope
$D_{ENV,o}$	=	0.115 m	, outside diameter of the glass envelope
$A_{ABS,i}$	=	0.003421 m^2	, crosssectional area inside the absorber tube
A_{ABS}	=	0.0004273 m^2	, crosssectional area of the absorber material
A_{ENV}	=	0.0005349 m^2	, crosssectional area of the glass envelope
$L_{Spacing}$	=	13 m	, distance between two collector rows
W	=	4.823 m	, collector mirror width
$n_{Collectors}$	=	50	, total number of collectors in the field

Appendix B

Nomenclature

A	area, m if surface per length or m^2 if cross-sectional; state-space model matrix
a_A, a_B	HTF flow fraction for heat exchanger train A or B
B	state-space model matrix
b_A, b_B	HTF flow fraction for reheater A or B
C	state-space model matrix
c	specific heat, J/kg
c_p	specific heat at constant pressure, J/kg·K
D	diameter, m; state-space model matrix; quadratic program constraint matrix
d	input step disturbance
d_n	day number
E_t	equation of time
F	flow fraction; quadratic program matrix
G	irradiance, W/m^2; quadratic program matrix
G_x	state noise dynamics matrix
g	gravitational acceleration, m/s^2
H	quadratic program matrix
h	specific enthalpy, J/kg; convection heat transfer coefficient, $W/m^2 \cdot K$
J_x, J_u	Jacobian matrix
k	thermal conductivity, W/m·K
L	length, m; filter gain matrix
L_{st}, L_{loc}	standard and local longitude, deg
$Length$	collector mirror length
$\dot{m}$	mass flow rate, kg/s
Nu	Nusselt number
n	number
P	steady-state discrete filtering Riccati matrix
P_{Gross}	gross output, W
Pr	Prandtl number
p	Pressure, N/m^2
Q	energy transfer, J; output penalty matrix
Q_x, Q_w	convariance matrix of x and w

$\dot{Q}$	heat transfer rate, W
q	heat transfer rate per unit length, W/m
Ra	Rayleigh number
Re	Reynolds number
$R_{\dot{m}}$	mass ratio
R_p	pressure ratio
R_n	covariance matrix of n
S	input rate of change penalty matrix
s	specific entropy, J/kg-K
T	temperature, K
t	time, s
UA	overall heat transfer coefficient and area product, W/K
u	input vector
V	volume , m^3
$\dot{V}$	volume flow rate, m^3/s
v	input vector substitute
v^N	vector of N future input vectors
W	collector mirror width, m; quadratic program constraint matrix
w	state vector substitute
x	model state vector; shading
y	output vector
z	coordinate, m; output vector substitute

Greek Letters

a	thermal diffusivity, m^2/s; absorptance
a_p	profile angle, deg
b	volumetric thermal expansion coefficient, K^{-1}
g	fudge factor
Δ	sampling period, s
Δp	pressure drop ratio
Δp_{HE}, Δp_{RH}	pressure drop, N/m^2
ΔQ	change in the energy transfer, J
$\Delta \dot{V}$	rate of change in the volume flow rate
Δz	length of discrete collector element, m
d	declination, deg
e	effectiveness, emissivity
h	efficiency
q	angle of incidence, deg

q_z	zenith angle, deg
m	viscosity, kg/s·m
n	kinematic viscosity, m^2/s; zero-mean, normal output noise vector
x	zero-mean, normal state noise vector; component of state vector
r	Mass density, kg/m^3; specular reflectance; feedback
s	Stefan-Boltzmann constant
Φ_k	regulator objective function value at time k
f	latitude, deg
Ψ	target tracking objective function value
t	time constant, s; transmittance
(ta)	transmittance-absorptance product
w	hour angle, deg; zero-mean, normal state step disturbance noise vector

Subscripts

ABS	absorber
Air	air
Annulus	in the annulus
absorbed	absorbed solar energy
amb, ambient	ambient, in the environment
atm	atmospheric
bn	direct normal beam
Col	collector
Collectors	number of collectors
Cool	cooling water
CP	condensate pump
c	cross-sectional; cold fluid
convection	convection heat transfer
d	non-manipulable input; discrete-time system matrix
END	end time
ENV	envelope
Environment	environmental
Exp	expansion vessel
eff	effective
evac	evacuated
external	heat transfer to environment
FP	feedwater pump
gained	gained energy
Gross	gross output
HE	heat exchanger

HE A, HE B	heat exchanger trains A and B
HP	high pressure turbine part
HPFH	high pressure feedwater heater
HPT 1,2	high pressure turbine section 1 and 2
HTF	heat transfer fluid
h	hot fluid
i	incoming; inside
in	inlet
init	initial condition
inlet	inlet of the trough collector field
internal	heat transfer between absorber and glass envelope
is	isentropic
L	effective length
LP	low pressure turbine part
LPFH	low pressure feedwater heater
LPT 1,2,3	low pressure turbine section 1,2 and 3
m	manipulable input
min	minimum, lower bound
max	maximum, upper bound
nom	nominal solution
o	outside; outgoing
opt	optical
out	outlet
RH A, RH B	reheater A and B
radiation	radiation heat transfer
rev	reversible
Spacing	distance between two collector rows
Steam	steam condition
set	set point
sunrise, sunset	sunrise and sunset hour angle
surf	surface
TV1, TV2	throttle valve 1 and 2
Target	target value
Water	water condition
Wind	wind speed
z	zenith

Overbar, Tilde and Hat

$\bar{}$	surface average conditions; desired value at steady state
~	perturbation from nominal solution; augmented system matrix
^	estimated value

References

Duffie, J.A and Beckman, W.A. (1991), *Solar Engineering of Thermal Processes*, John Wiley & Sons, Inc., New York.

Iqbal, M. (1983), *An Introduction to Solar Radiation*, Academic Press Canada, Ontario.

Incropera, F.P. and De Witt, D.P. (2002), *Introduction to Heat Transfer*, John Wiley & Sons, Inc., New York.

Pilkington (1996), *Status Report on Solar Thermal Power Plants*, Pilkington Solar International GmbH, Cologne, Germany.

Klein, S.A. (2001), *EES Engineering Equation Solver*, F-Chart Software, USA

Lippke, F. (1995), *Simulation of the part-load behavior of a 30 MWe SEGS plant*, SAND95-1293, Sandia National Laboratories, Albuquerque, NM.

El-Wakil, M.M. (1984), *Powerplant Technology*, McGraw-Hill, Inc., New York.

MathWorks (2001), *Using the Optimization Toolbox*, The Mathworks, Inc., Natick, MA

Kwakernaak, H. and Sivan, R. (1972), *Linear Optimal Control Systems*, John Wiley & Sons, Inc., New York.

Schindwolf, R. (1980), *Fluid Temperature Control of Parabolic Trough Solar Collectors*, presented at the Joint Automatic Control Conference, San Francisco, Calif., Aug. 13-15, 1980.

Rawlings, J.B. and Muske, K.R. (1993), *Model Predictive Control with Linear Models*, AIChE Journal, 39 (2), 262-287.

Rawlings, J.B. (2000), *Tutorial Overview of Model Predictive Control*, IEEE Control Systems Magazine, 38-52.